*Technical Memorandum No. 33-187*

# *Environmental Dynamic and Acoustic Data Report of the Ranger 6 Flight*

*M. C. Trummel*
*D. B. Wiksten*

N68 86038 (ACCESSION NUMBER) 59 (PAGES) CR 94742 (NASA CR OR TMX OR AD NUMBER) (THRU) NONE (CODE) (CATEGORY) FACILITY FORM 602

jpl
JET PROPULSION LABORATORY
CALIFORNIA INSTITUTE OF TECHNOLOGY
PASADENA, CALIFORNIA

October 19, 1964

JUN 1968 RECEIVED NASA STI FACILITY INPUT BRANCH

JUN 1968 RECEIVED NASA STI FACILITY INPUT BRANCH

RQ7-5160

*Technical Memorandum No. 33-187*

# *Environmental Dynamic and Acoustic Data Report of the Ranger 6 Flight*

*M. C. Trummel*
*D. B. Wiksten*

W. Shipley

W. Shipley, *Chief*
*Environmental Requirements Section*

JET PROPULSION LABORATORY
CALIFORNIA INSTITUTE OF TECHNOLOGY
PASADENA, CALIFORNIA

October 15, 1964

Copyright © 1964
Jet Propulsion Laboratory
California Institute of Technology

Prepared Under Contract No. NAS 7-100
National Aeronautics & Space Administration

# CONTENTS


**I. Introduction and Summary** . . . . . 1

**II. Instrumentation** . . . . . 2
A. Vibration . . . . . 2
B. Acoustics . . . . . 3

**III. Vibration Data** . . . . . 4
A. Wide-Band History . . . . . 4
B. Band-Pass Analysis . . . . . 4
C. Power Spectral-Density Analysis . . . . . 5
D. Oscillograph Records of Events of Interest . . . . . 5
E. Shock Spectra . . . . . 5

**IV. Acoustic Data** . . . . . 37
A. Flight Microphone . . . . . 37
B. Umbilical-Tower Microphones . . . . . 37

**V. Discussion** . . . . . 44
A. High-Frequency Vibration . . . . . 44
B. Low-Frequency Vibration . . . . . 48
1. Booster Engine Cut-Off Transient . . . . . 48
2. Radial Vibration . . . . . 49
C. Acoustic Data . . . . . 49
1. Internal Sound-Field Measurement . . . . . 49
2. Umbilical-Tower Microphone Data . . . . . 50

**VI. Conclusions** . . . . . 51
A. Wide-Band Vibration . . . . . 51
B. TV Subsystem Turn-On . . . . . 51
C. BECO Transient . . . . . 51
D. Acoustic Measurements . . . . . 52

**References** . . . . . 52


# TABLES


**1. *Ranger-6* dynamic and acoustic instrumentation** . . . . . 2

**2. Summary of transient data *RA-6* vibration and acoustics** . . . . . 6

## FIGURES


1. Amplifier frequency response for Channel 17 . . . . . 3
2. System frequency response for Channel 18 at 130 db . . . . . 3
3. Dynamic instrumentation locations for *RA-6* spacecraft and umbilical tower . . . . . 3
4. Accelerometer mounting block for Channels 10, 12, and 17 . . . . . 4
5. Flight microphone . . . . . 4
6. *RA-6* flight data, wide-band level vs time . . . . . 5
7. Acceleration spectral density for Channel 10 at −8 to −6 sec . . . . 7
8. Acceleration spectral density for Channel 10 at lift-off . . . . . 7
9. Acceleration spectral density for Channel 10 at 380-cps vibration . . . 8
10. Acceleration spectral density for Channel 10 at transonic flight . . . . 8
11. Acceleration spectral density for Channel 10 at 135.5–137.5 sec . . . 9
12. Acceleration spectral density for Channel 10 at 139–141 sec . . . . . 9
13. Acceleration spectral density for Channel 11 at −8 to −6 sec . . . . 10
14. Acceleration spectral density for Channel 11 at −1 to +1 sec . . . . 10
15. Acceleration spectral density for Channel 11 at lift-off . . . . . 11
16. Acceleration spectral density for Channel 11 at transonic flight . . . . 11
17. Acceleration spectral density for Channel 11 at 136.5–138.5 sec . . . 12
18. Acceleration spectral density for Channel 11 at 139–141 sec . . . . . 12
19. Acceleration spectral density for Channel 12 at −8 to −6 sec . . . . 13
20. Acceleration spectral density for Channel 12 at lift-off . . . . . 13
21. Acceleration spectral density for Channel 12 at 380-cps vibration . . . 14
22. Acceleration spectral density for Channel 12 at transonic flight . . . . 14
23. Acceleration spectral density for Channel 12 at 136.5–138.5 sec . . . 15
24. Acceleration spectral density for Channel 12 at 139–141 sec . . . . . 15
25. Acceleration spectral density for Channel 17 at −8 to −6 sec . . . . 16
26. Acceleration spectral density for Channel 17 at lift-off . . . . . 16
27. Acceleration spectral density for Channel 17 at 380-cps vibration . . . 17
28. Acceleration spectral density for Channel 17 at transonic flight . . . . 17
29. Acceleration spectral density for Channel 17 at 113.5–115.5 sec . . . 18
30. Oscillogram at lift-off . . . . . 19
31. Oscillogram at transonic flight . . . . . 20
32. Oscillogram at BECO . . . . . 21

## FIGURES (Cont'd)

33. Oscillogram for Channel 8 on at booster jettison . . . . . 22
34. Oscillogram for Channel 8 off . . . . . 23
35. Oscillogram for SECO . . . . . 24
36. Oscillogram for shroud jettison . . . . . 25
37. Oscillogram for *Atlas–Agena* separation . . . . . 26
38. Oscillogram for first *Agena* ignition . . . . . 27
39. Shock spectra for Channel 12 at lift-off . . . . . 28
40. Shock spectra for Channel 17 at lift-off . . . . . 29
41. Shock spectra for Channel 10 at BECO . . . . . 30
42. Shock spectra for Channel 11 at BECO . . . . . 30
43. Shock spectra for Channel 12 at BECO . . . . . 31
44. Shock spectra for Channel 11 at booster jettison . . . . . 31
45. Shock spectra for Channel 12 at booster jettison . . . . . 32
46. Shock spectra for Channel 10 at jettison of horizon sensor fairings . . . 32
47. Shock spectra for Channel 11 at jettison of horizon sensor fairings . . . 33
48. Shock spectra for Channel 12 at jettison of horizon sensor fairings . . . 34
49. Shock spectra for Channel 17 at jettison of horizon sensor fairings . . . 34
50. Shock spectra for Channel 10 at shroud ejection . . . . . 35
51. Shock spectra for Channel 17 at shroud ejection . . . . . 35
52. Shock spectra for Channel 12 at *Atlas–Agena* separation . . . . . 36
53. Pressure spectral density for flight microphone at pre-flight quiet time . . . . . 37
54. Pressure spectral density for flight microphone at lift-off . . . . . 38
55. Pressure spectral density for flight microphone at 380-cps vibration . . . . . 38
56. Pressure spectral density for flight microphone at transonic flight . . . 39
57. Pressure spectral density for flight microphone at 87.5–89.5 sec . . . 39
58. Pressure spectral density for flight microphone at 113.5–115.5 sec . . . . . 40
59. Sound-pressure spectrum level for flight microphone at pre-flight quiet time . . . . . 41
60. Sound-pressure spectrum level for flight microphone at lift-off . . . . 41
61. Sound-pressure spectrum level for flight microphone at 380-cps vibration . . . . . 41

## FIGURES (Cont'd)

62. Sound-pressure spectrum level for flight microphone at transonic flight . . . . . 42

63. Sound-pressure spectrum level for flight microphone at 87.5–89.5 sec . . . . . 42

64. Sound-pressure spectrum level for flight microphone at 113.5–115.5 sec . . . . . 42

65. Pressure spectral density for umbilical-tower microphone No. 1 at lift-off . . . . . 43

66. Pressure spectral density for umbilical-tower microphone No. 2 at lift-off . . . . . 43

67. Sound-pressure spectrum level for umbilical-tower microphone No. 1 at lift-off . . . . . 44

68. Sound-pressure spectrum level for umbilical-tower microphone No. 2 at lift-off . . . . . 44

69. Uncorrected *RA-6* flight-vibration data compared with *RA 1–4* flight-vibration data at lift-off . . . . . 45

70. Uncorrected *RA-6* flight-vibration data compared with *RA 1–4* flight-vibration data at transonic flight . . . . . 45

71. *RA 1–4* flight-accelerometer mounting block . . . . . 46

72. Ratio of flight-accelerometer acoustic susceptances, *RA 1–4* to *RA-6* . . . . . 46

73. Measured *RA-6* flight vibration corrected to *RA 1–4* flight accelerometer at lift-off . . . . . 47

74. Measured *RA-6* flight vibration corrected to *RA 1–4* flight accelerometer at transonic flight . . . . . 47

75. Transonic flight vibration adjusted to spacecraft feet . . . . . 47

76. *RA-6* specified flight-acceptance test spectrum compared with actual test spectra . . . . . 48

77. Shock spectra of BECO transient for *RA-2, 3, 4, 5, 6* . . . . . 48

78. Internal acoustic-pressure data at lift-off in 1/3-octave bands compared with reverberant chamber test levels . . . . . 49

79. Umbilical-tower microphone data at lift-off in 1/3-octave bands . . . 50

80. Ratio of internal to external sound pressure at lift-off compared with a ground test . . . . . 50

## ABSTRACT

This Report presents and analyzes dynamic-environmental data measured during the launch of the *Ranger 6* (*RA-6*) spacecraft. Included are acoustic data measured internal to the spacecraft shroud, acoustic data measured on the umbilical tower, and low- and high-frequency vibration data measured near the spacecraft-*Agena* interface. Several forms of data are presented and discussed. These are oscillograph records, wide-band analyses, band-pass filter analyses, power spectral-density (PSD) analyses, and shock-spectrum analyses. The data are shown to be compatible with data from previous *Ranger* flights and with spacecraft acoustic and vibration-test levels.


## I. INTRODUCTION AND SUMMARY

This Report presents an analysis of all vibration and acoustic data pertinent to the *Ranger*-spacecraft dynamic environment which were measured during the *Ranger 6* (*RA-6*) flight. Six *Agena* telemetry channels were utilized: four low-frequency accelerometers, one high-frequency accelerometer, and one high-frequency flight microphone. Valid data were recovered from prior to launch to spacecraft injection into lunar trajectory.

Data analyses and varieties of presentation are included. These are oscillograph records, wide-band analyses, band-pass filter analyses, power spectral-density (PSD) analyses, and shock-spectrum analyses. Measured levels are compared with previously predicted levels and with environmental test levels.

The first *Ranger* spacecraft incorporating a spacecraft cavity microphone in the flight instrumentation was *RA-6*. The measured noise field was somewhat lower than anticipated, and, therefore, the acoustic tests were more than adequate to qualify the spacecraft for the measured *RA-6* flight environment. The external sound field at lift-off as measured by the umbilical-tower microphones also appeared lower than expected; however, comparing attenuation as measured by the external and internal measurements showed reasonable agreement with ground tests. The spacecraft cavity sound-pressure level at transonic flight was 6 db lower than at lift-off as opposed to the increase in measured vibration. This phenomenon may be explained by a localized aerodynamic buffet in the adapter area at transonic flight.

Conclusions drawn from a review of the vibration data indicate that vibration levels were nominal, or within the anticipated ranges. It is also concluded that present vibration-test levels were adequate to qualify the spacecraft for the dynamic environment observed on the *RA-6* flight. The torsional transient motion occurring at booster engine cut-off (BECO) was observed to be at a lower level than on any previous flight.

Wide-band random vibration is of most significance during the launch and the transonic periods of flight. The

measurement of higher levels of vibration than previously seen during these periods has been, at least in a large part, attributed to a new accelerometer mount rather than to a more severe dynamic environment. When observed levels are adjusted to compare with previous flight data, reasonable statistical agreement is found.

The turn-on of the TV subsystem during launch has been a topic of investigation because it resulted in the ultimate failure of the TV system. No direct contribution of the dynamic environment to the turn-on or turn-off of the TV subsystem has been established. No abnormal shock or vibration was observed at any time in the flight.

## II. INSTRUMENTATION

### A. Vibration

Flight vibration instrumentation pertinent to the *RA-6* spacecraft consisted of five accelerometers located in or near the spacecraft adapter. The four accelerometers in the adapter provided two radial measurements (one high-frequency 7–2,000 cps, and one low-frequency 0–150 cps) and two tangential measurements (0–320 cps). The tangential measurements were made on opposite sides of the adapter so that torsional motion could be detected. The fifth accelerometer (0–150 cps) was located slightly below the adapter in the *Agena* and it measured acceleration in an axial direction. Data pertaining to the acceleration measurement and calibration characteristics are tabulated in Table 1 (Ref. 1).

**Table 1. *Ranger-6* dynamic and acoustic instrumentation[a]**

| IRIG channel LMSC measurement number | Orientation | IRIG 7.5% calibration levels | Transducer frequency response[b] and natural frequency, cps | Amplifier frequency response,[c] cps | IRIG frequency response,[d] cps | Valid frequency range, cps |
|---|---|---|---|---|---|---|
| 9<br>PL 34 | Axial | +12.9 to −4.9 *g* | 400<br>980 | 0–2,000 | 300 | 0–150 |
| 10<br>PL 32 | Radial | ±1.67 *g* | 150<br>375 | 0–2,000 | 400 | 0–150 |
| 11<br>PL 31 | Tangential | ±5.5 *g* | 320<br>805 | 0–2,000 | 550 | 0–320 |
| 12<br>PL 33 | Tangential | ±5.5 *g* | 320<br>805 | 0–2,000 | 800 | 0–320 |
| 17<br>PL 23 | Radial | ±16.7 *g* | 7–8,000 | Cut-off at 2,000<br>(See Fig. 1) | 3950 | 7–2,000 |
| 18<br>PL 6 | Omnidirectional<br>(Microphone) | 145.8 db (ref.)<br>0.0002 μbar | | 0–2,000<br>(See Fig. 2) | 5250 | 100–2,000 |

[a]Reference: LMSC Drawing Numbers 1359964 and 1360819.
[b]Frequency response is flat over given range ±5% (ref: LMSC Drawing Numbers 1615367 and 1613071).
[c]Frequency response is flat over given range ±4% (ref: LMSC Drawing Numbers 1616462 and 16164779).
[d]Assuming Modulation Index of 1.

Figures 1 and 2 show amplifier frequency-response curves for Channels 17 and 18, as obtained from the Lockheed Missile Systems Company (LMSC) calibration report. Accelerometer locations are shown in Fig. 3. Figure 4 shows the mounting block for Channels 10, 12, and 17.

A valid frequency range is indicated in Table 1. These ranges were estimated by considering transducer frequency response, amplifier frequency response, and Inter-Range Instrumentation Group (IRIG) frequency response for the various telemetry channels. The IRIG frequency response is given for a modulation index of 1.0, rather than the usual 5.0, because vibration data is observed on these channels to these frequencies. The valid frequency ranges stated are ones which are being used for data reduction purposes. The degree of validity cannot be precisely determined, however, because sufficient calibration data is not available.

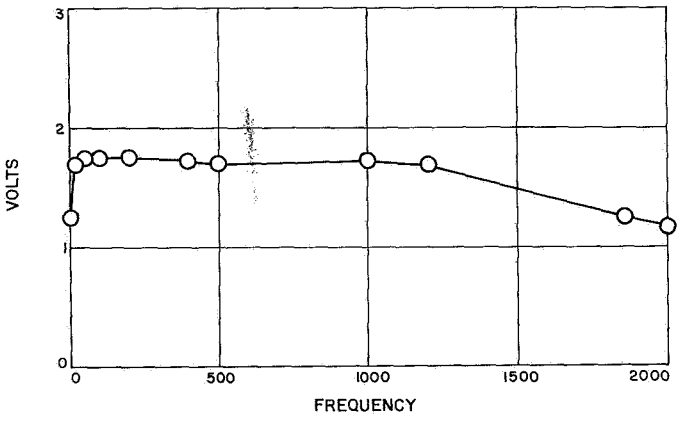


**Fig. 1. Amplifier frequency response for Channel 17**

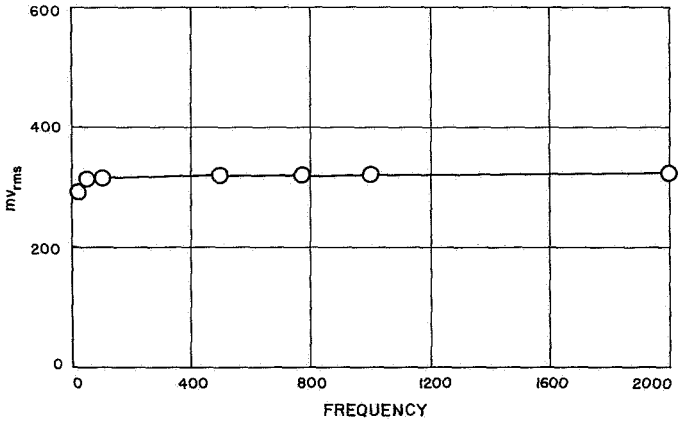


**Fig. 2. System frequency response for Channel 18 at 130 db**

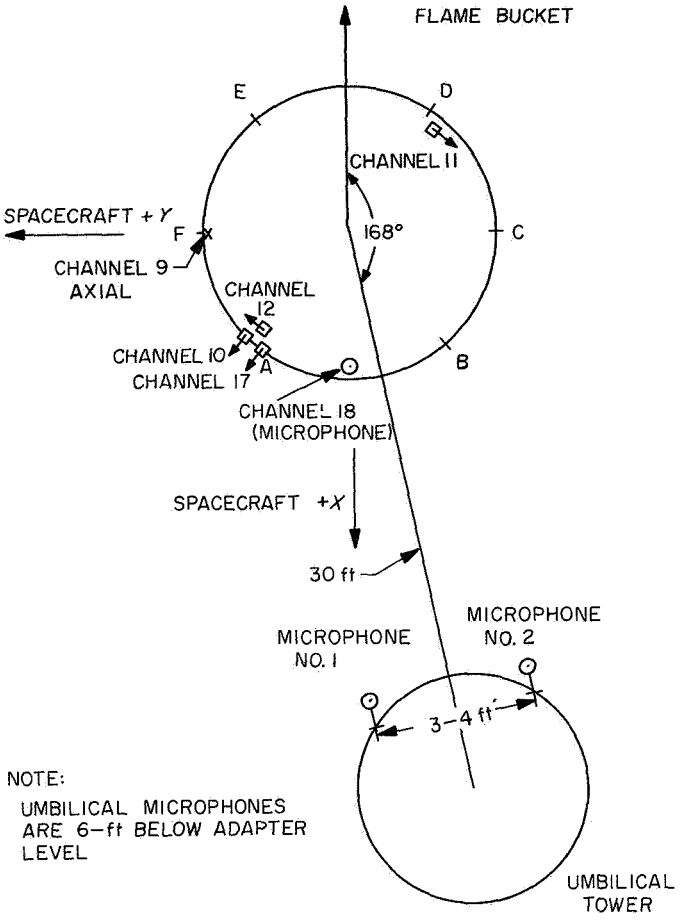


APPROXIMATE STATION NO.

| CHANNEL | AGENA STATION | RANGER STATION |
|---|---|---|
| 9 | 245 | 513 |
| 10 | 237 | 505 |
| 11 | 234 | 502 |
| 12 | 237 | 505 |
| 17 | 238 | 506 |
| 18 | 189 | 457 |

**Fig. 3. Dynamic instrumentation locations for *RA-6* spacecraft and umbilical tower**

## *B. Acoustics*

Acoustic measurements on *RA-6* were achieved with one microphone mounted in the spacecraft (Channel 18 in Fig. 3) and two microphones mounted on the umbilical tower. The flight microphone is shown in Fig. 5. Frequency-response data for the flight microphone are included in Table 1.

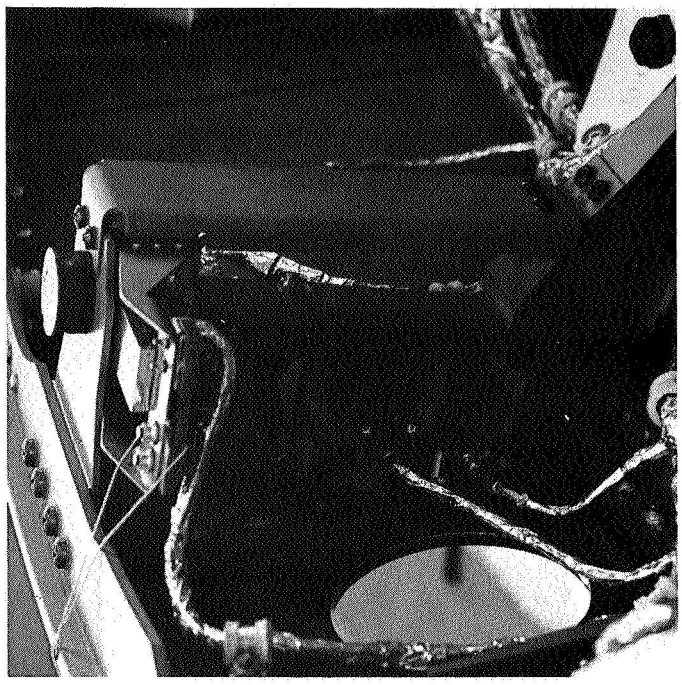

**Fig. 4. Accelerometer mounting block for Channels 10, 12, and 17**

**Fig. 5. Flight microphone**

## III. VIBRATION DATA

The continuous, telemetered accelerometer signals are recorded in FM-multiplex on magnetic tape. The following various types of data reduction were then performed on the recorded data.

### *A. Wide-Band History*

The wide-band average acceleration is shown in Fig. 6 for Channels 10, 11, 12, and 17 for the high-level vibration portion of flight. Also shown is the wide-band acoustic-noise level monitored on Channel 18. The two most severe wide-band vibration periods are the launch and transonic portions of flight. It is noted that Channels 12 and 17 show the data signal out-of-FM-band during the transonic period of flight and, consequently, vibration levels are actually somewhat higher than shown for these channels during this period.

### *B. Band-Pass Analysis*

Band-pass analysis of the raw flight data was made. For Channels 9, 10, 11, and 12, the frequency range covered was 10–1,000 cps, while for Channels 17 and 18 the range was 10–2,000 cps. In each case, 100-cps bands were used.

It was observed that a relatively high-level vibration appeared in the 300–400-cps band of Channels 10, 12, and 17. Filtering of Channel 17 with a narrow-band filter centered at 380 cps indicates a quasi-sinusoidal wave form. *Ranger 6* was the first flight in which such a signal was observed. Channels 10, 12, and 17 are located near each other. The absence of the 380-cps motion on either Channel 9 or 11 indicates that this vibration was probably a local effect. The wide-band vibration during this portion

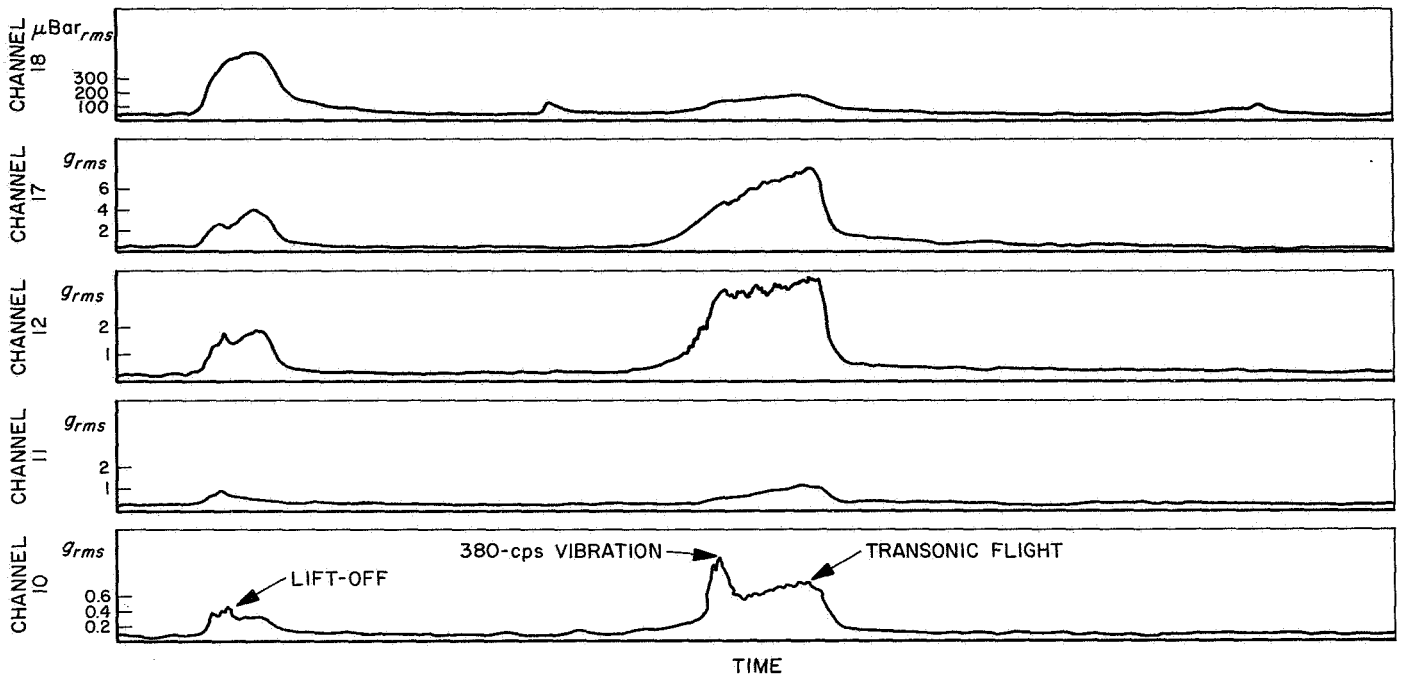


**Fig. 6. *RA-6* flight data, wide-band level vs time**

of flight was excited primarily by aerodynamic turbulence. No mechanical source of such motion is known to have been present.

### C. Power Spectral-Density Analysis

Two-second portions of data from each of Channels 10, 11, 12, and 17 were reduced to PSD plots. The portions of interest were selected from areas where the band-pass analysis indicated high levels.

The analysis bandwidth used was either 13.5 or 13.8 cps, depending on the analyzer used. The PSD plots for each of the above-mentioned channels and times are shown in Figs. 7 through 29. A comparison of test levels and the highest environmental levels of *RA-6* is made in Section V of this Report.

### D. Oscillograph Records of Events of Interest

Portions of the oscillograph record for specific events are shown in Figs. 30 through 38. The discriminator low-pass filter frequencies used to recover the data are as follows:

| *Channel* | *Frequency* |
|---|---|
| 9 | 45 cps |
| 10 | 110 cps |
| 11 | 110 cps |
| 12 | 160 cps |
| 17 | 3 kc cps |
| 18 | 6 kc cps |

Selected events have been summarized in Table 2. The data in columns headed "shock" generally represent short duration oscillations. Where a frequency is given, it is the predominant frequency apparent in the waveform.

### E. Shock Spectra

The shock spectra for selected events were computed and are shown in Figs. 39 through 52. The shock spectrum presents the maximum response of a single degree-of-freedom system to the observed acceleration as a function of system natural frequency. Spectra are shown for systems having damping factors ($\zeta$) of both 0 and 2.5% of critical damping.

An event of special interest is the torsional oscillation at BECO. The tangential acceleration, measured on Channels 11 and 12, and the corresponding shock spectra are shown in Figs. 42 and 43. A comparison of the *RA-6* BECO pulse with previously observed BECO pulses is presented in Section V of this Report.

## Table 2. Summary of transient data *RA-6* vibration and acoustics

| Event | Channel 9 | | Channel 10 | | Channel 11 | | Channel 12 | | Channel 17 | | Channel 18[a] |
|---|---|---|---|---|---|---|---|---|---|---|---|
| | dc shift | Vibration | Shock | Wide-band vibration | Shock | Wide-band vibration | Shock | Wide-band vibration | Shock | Wide-band vibration | |
| Launch | — | ±1 *g* | ±0.8 *g* @ 180 cps | 0.21 $g_{rms}$ | — | 0.21 $g_{rms}$ | ±2 *g* | 1.87 $g_{rms}$ | ±24 *g* @ 800 cps | 3.7 $g_{rms}$ | 126 db |
| Transonic flight | — | ±2 *g* | — | 1.03 $g_{rms}$ | — | 0.72 $g_{rms}$ | — | 3.6 $g_{rms}$ | — | 8.2 $g_{rms}$ | 120 db |
| BECO | 5.2 *g* to 1 *g* | — | ±0.5 *g* @ 65 cps | — | ±1.4 *g* @ 65 cps | — | ±1.4 *g* @ 65 cps | — | — | — | |
| Booster jettison | — | ±1 *g* @ 50 cps | ±0.3 *g* @ 35 cps | — | ±0.5 *g* @ 35 cps | — | ±0.7 *g* @ 35 cps | — | — | 0.6 $g_{rms}$ | |
| SECO | −1 *g* | ±1 *g* | ± 0.2 *g* @ 100 cps | — | ±0.4 *g* @ 40 cps | — | ±0.5 *g* @ 110 cps | — | — | — | |
| Jettison horizon sensor fairings | Triangular pulse 1 *g* × 0.02 sec | — | ±0.5 *g* | — | ±1.5 *g* | — | ±1.5 *g* | — | ±20 *g* @ 1100 cps | — | |
| Shroud ejection | — | O.B.[b] | ±1.3 *g* | — | Loss of valid data | Loss of valid data | O.B.[b] | — | ±25 *g* | | |
| *Atlas-Agena* | — | — | ±0.2 *g* @ 100 cps | — | Invalid | Invalid | ±1.5 *g* @ 160 cps | — | ±8 *g* | — | |
| 1st *Agena* ignition | +1 *g* | ±0.5 *g* @ 45 cps | ±0.4 *g* @ 100 cps | — | Invalid | Invalid | ±1.2 *g* @ 100 cps | — | — | — | |
| 1st *Agena* cut-off | −2 *g* | — | ±0.8 *g* @ 80 cps | — | Invalid | Invalid | ±1.3 *g* @ 80 cps | — | — | — | |
| 2nd *Agena* ignition | +2.5 | — | ±1 *g* @ 50 cps | — | Invalid | Invalid | — | — | ±1 *g* @ 50 cps | — | |
| 2nd *Agena* cut-off | −6 *g* | — | ±2 *g* | — | Invalid | Invalid | ±2 *g* @ 70 cps | — | ±5 *g* @ 70 cps | — | |

[a]db (ref.) 0.0002 μbar

[b]O.B. = out-of-FM-band. Local effects only.

Notes: — means levels were negligible.
All *g* values are zero-to-peak unless otherwise noted.
rms values corrected for instrumentation noise measured prior to launch.

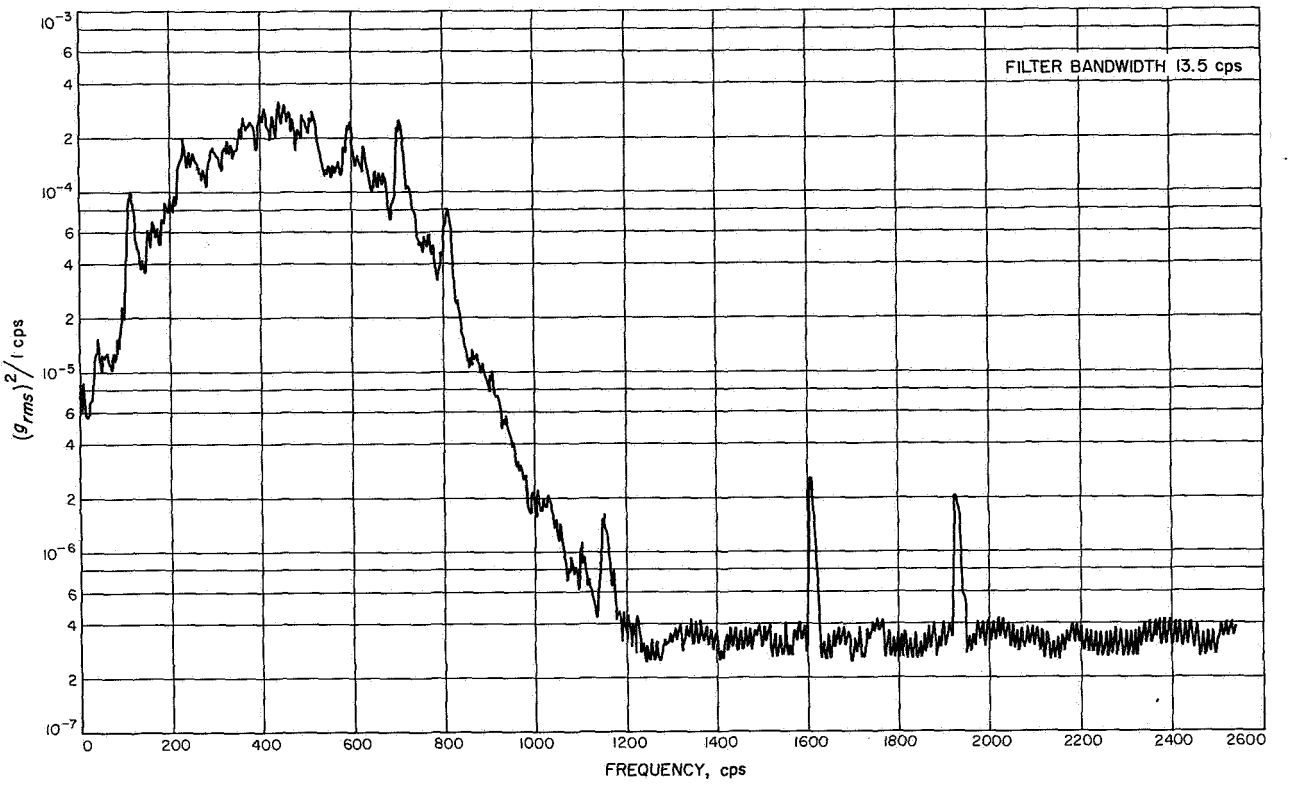


**Fig. 7. Acceleration spectral density for Channel 10 at −8 to −6 sec**

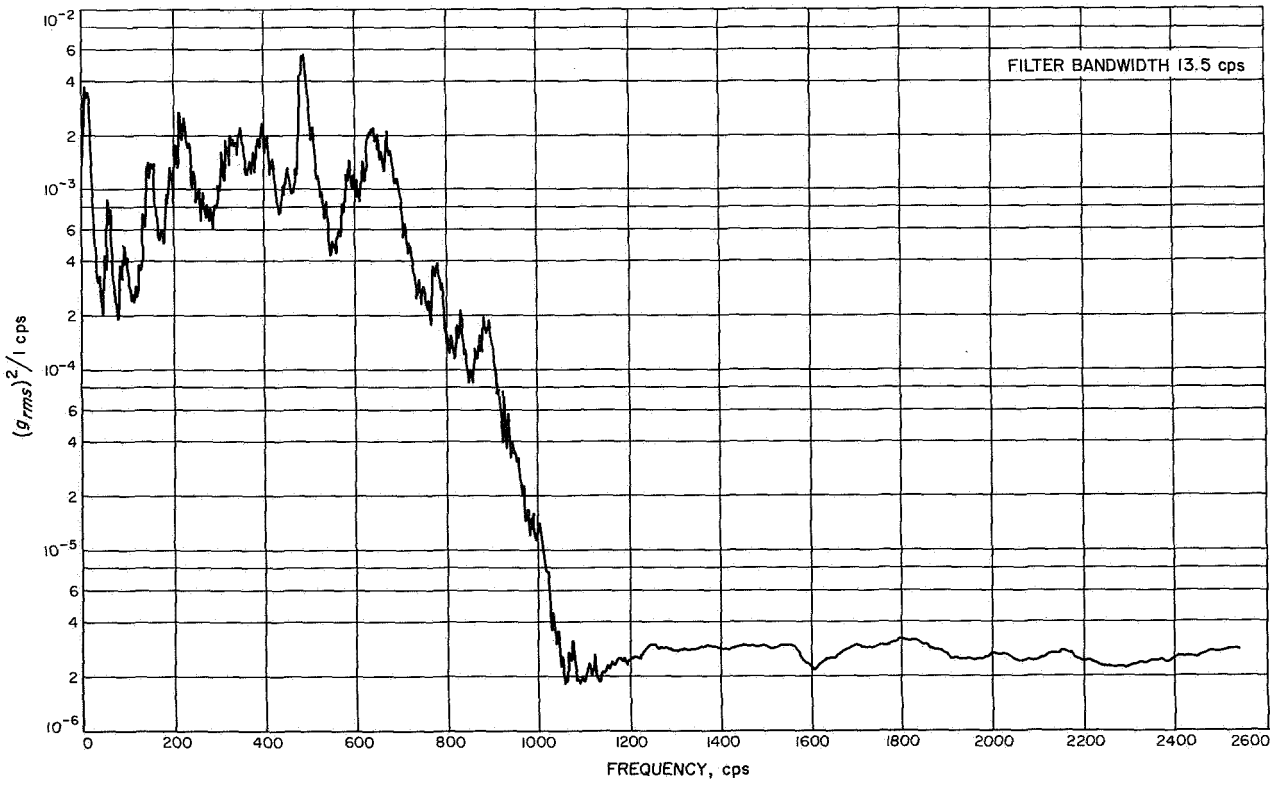


**Fig. 8. Acceleration spectral density for Channel 10 at lift-off**

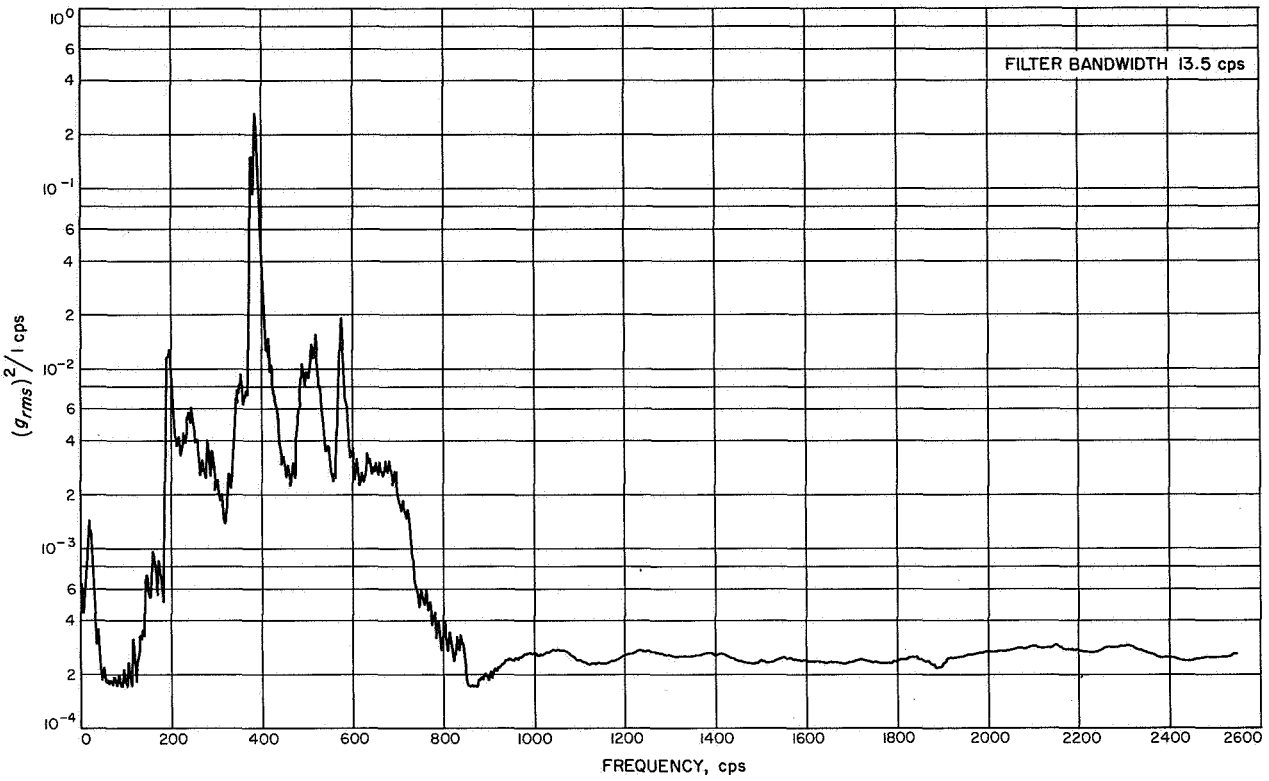


**Fig. 9. Acceleration spectral density for Channel 10 at 380-cps vibration**

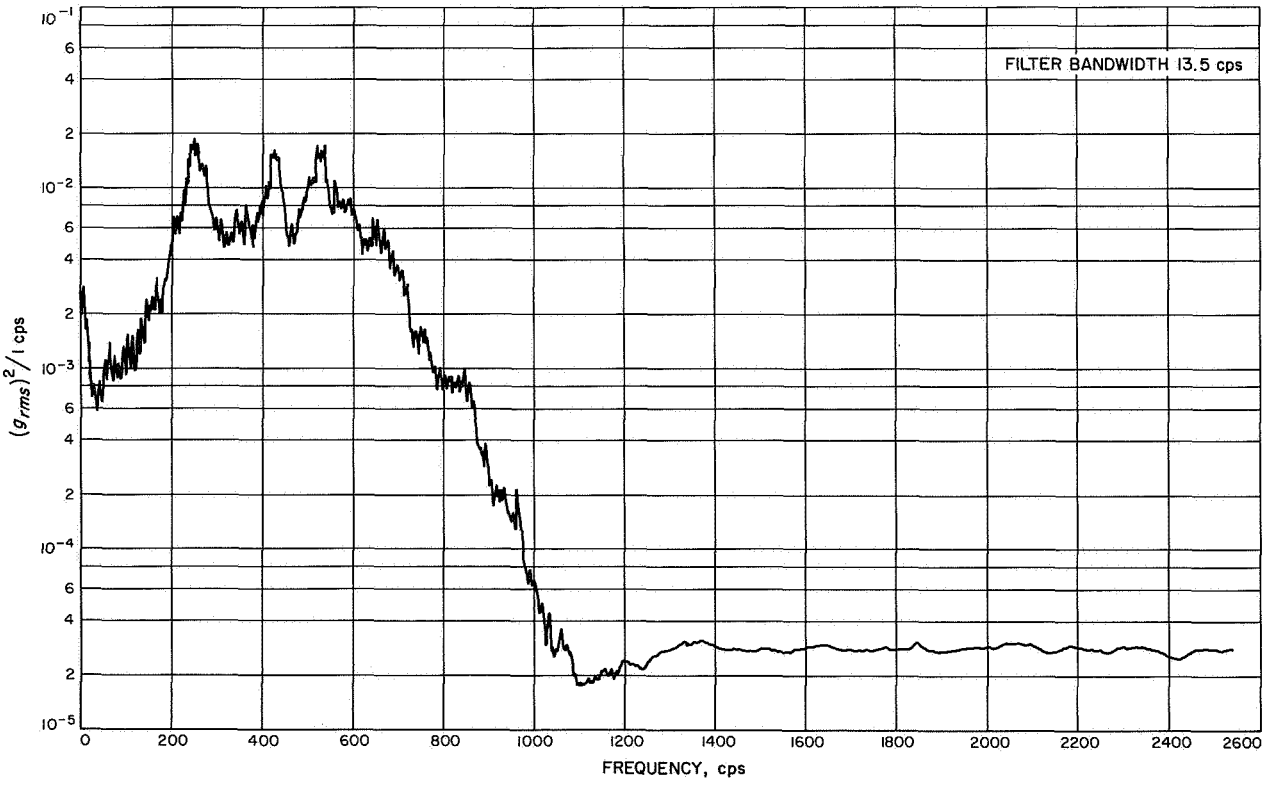


**Fig. 10. Acceleration spectral density for Channel 10 at transonic flight**

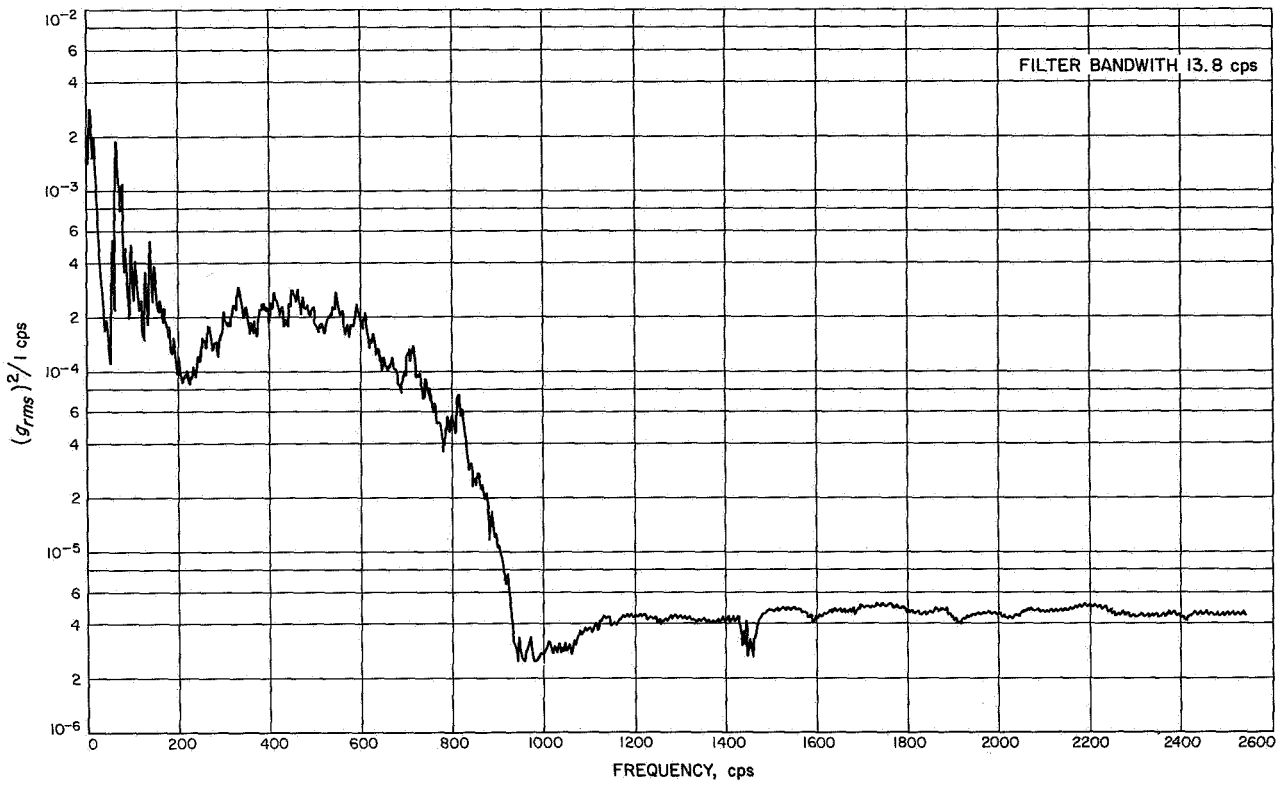


**Fig. 11. Acceleration spectral density for Channel 10 at 135.5–137.5 sec**

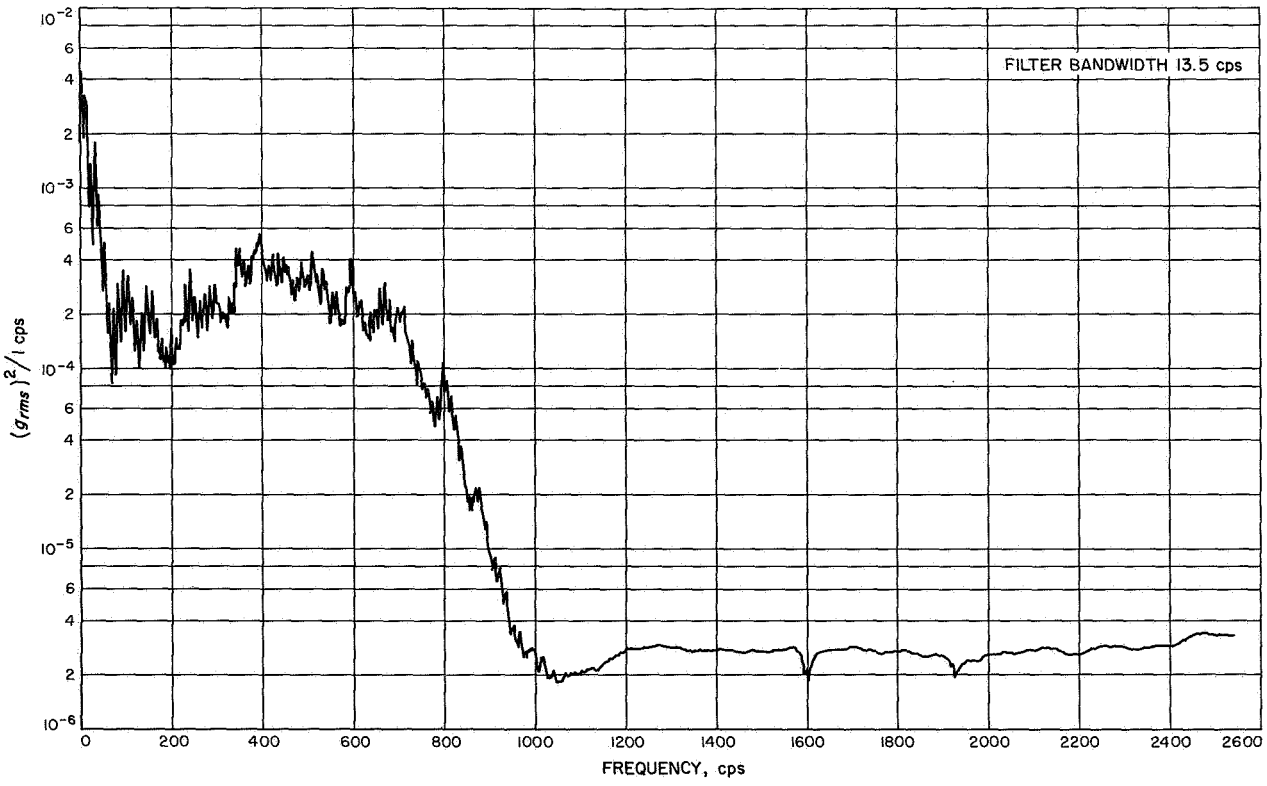


**Fig. 12. Acceleration spectral density for Channel 10 at 139–141 sec**

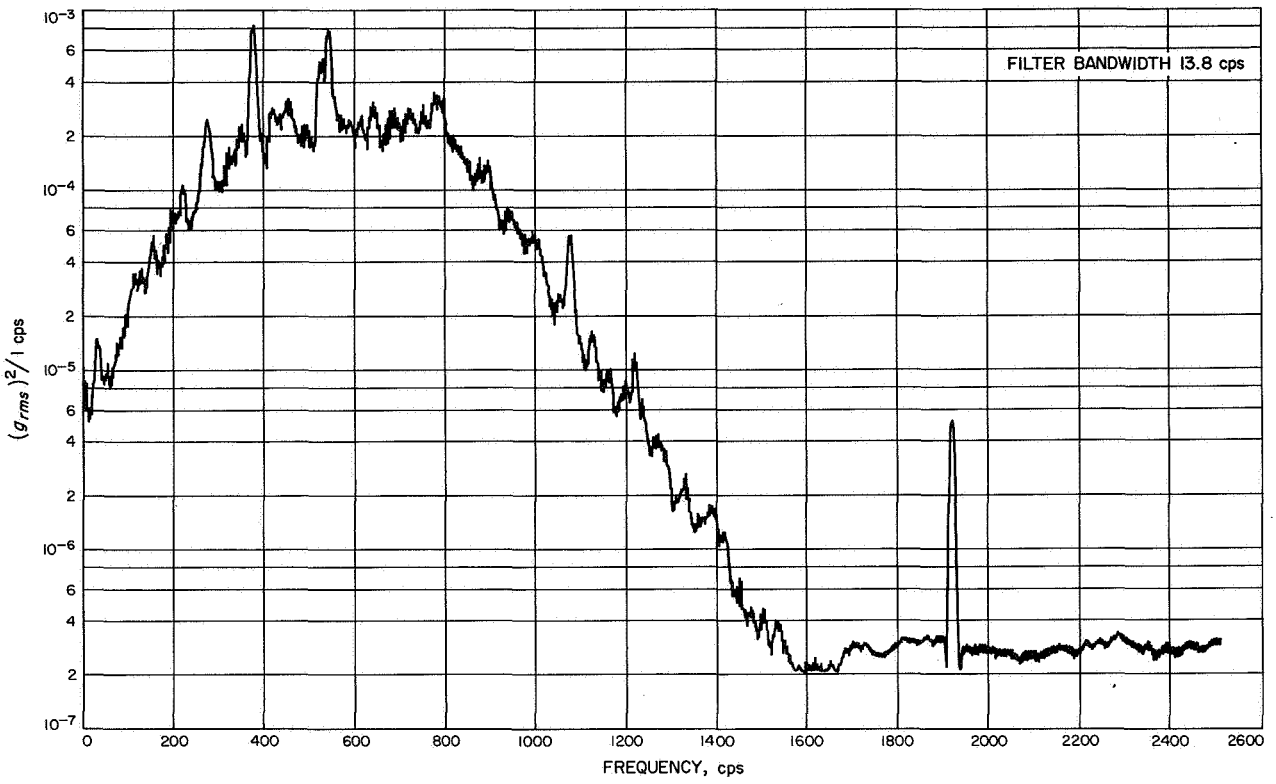


Fig. 13. Acceleration spectral density for Channel 11 at −8 to −6 sec

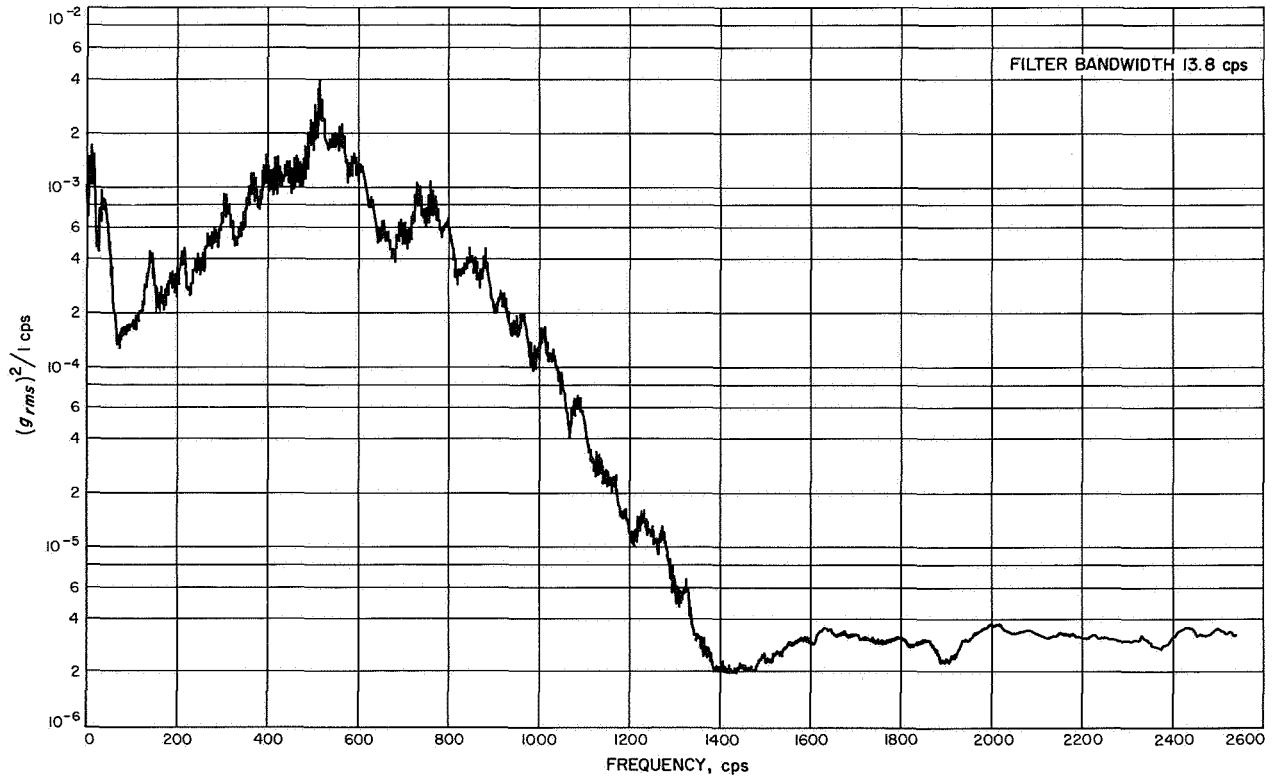


Fig. 14. Acceleration spectral density for Channel 11 at −1 to +1 sec

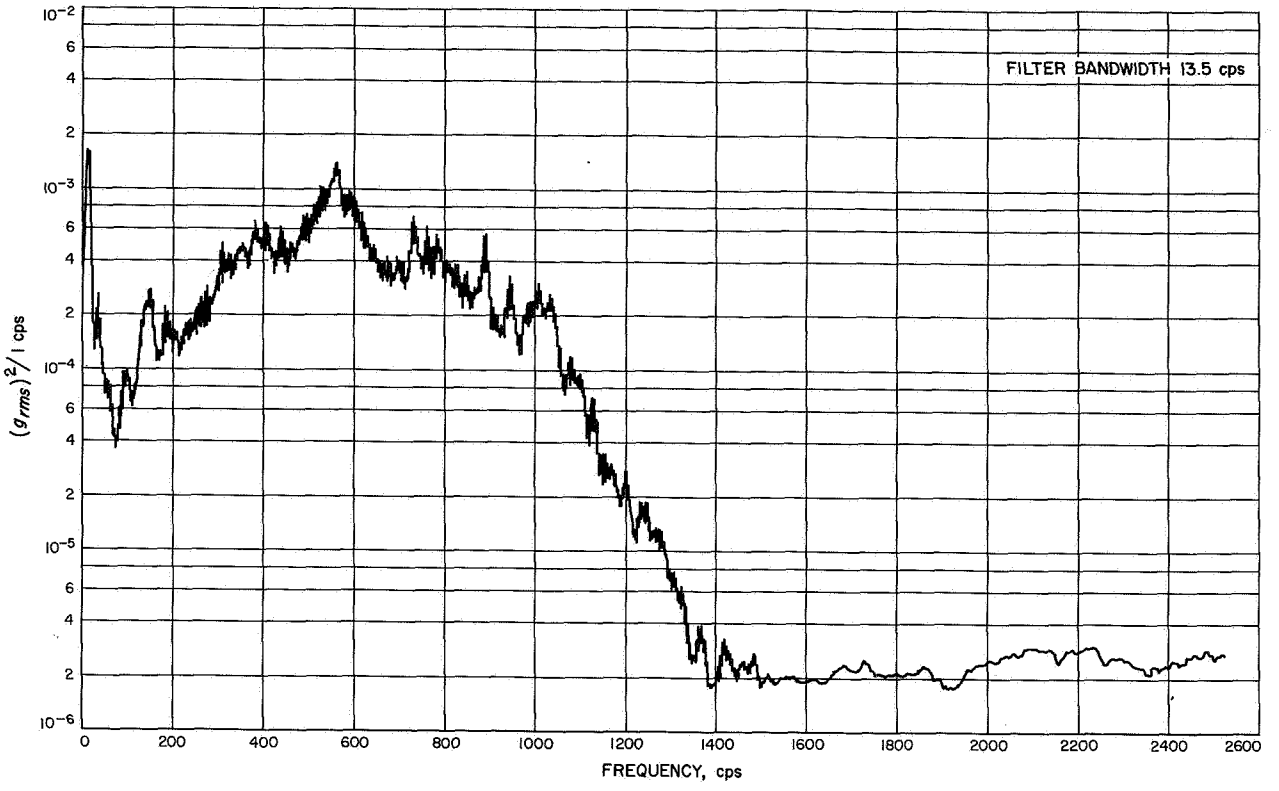


**Fig. 15. Acceleration spectral density for Channel 11 at lift-off**

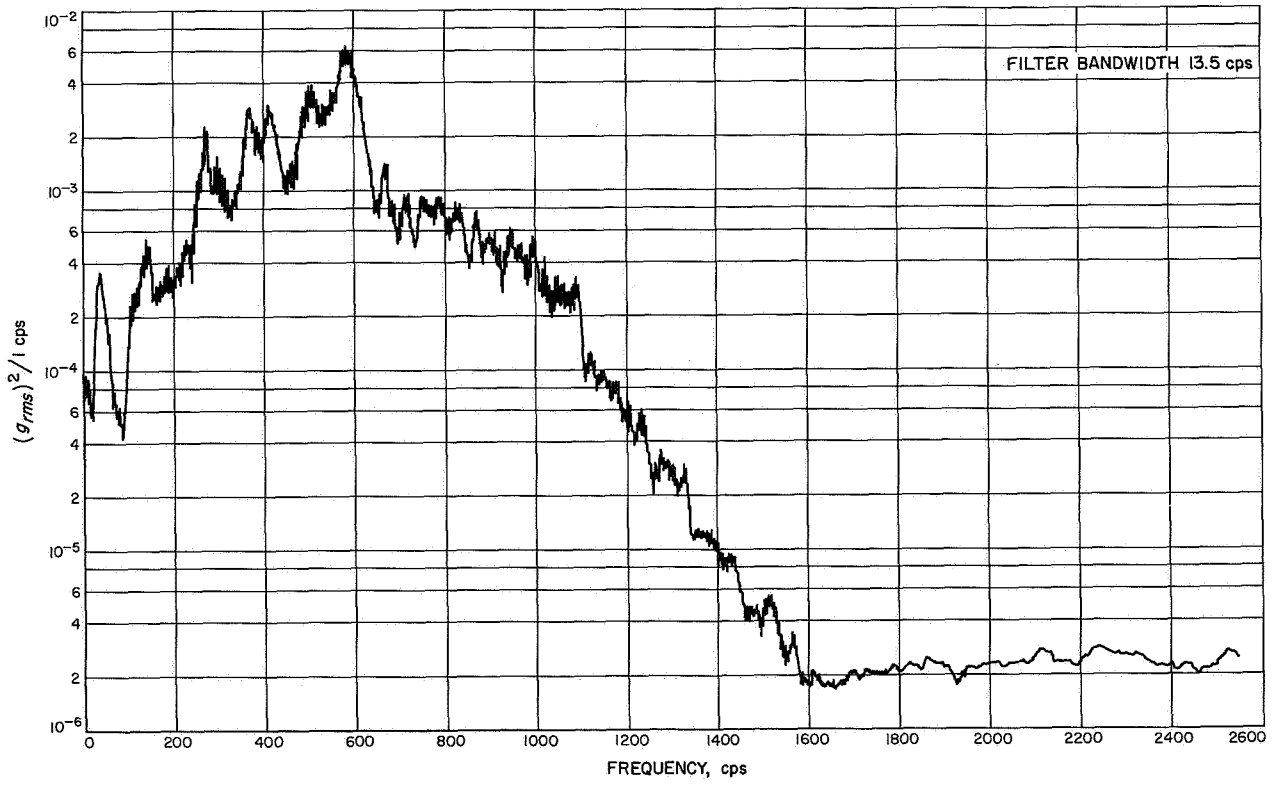


**Fig. 16. Acceleration spectral density for Channel 11 at transonic flight**

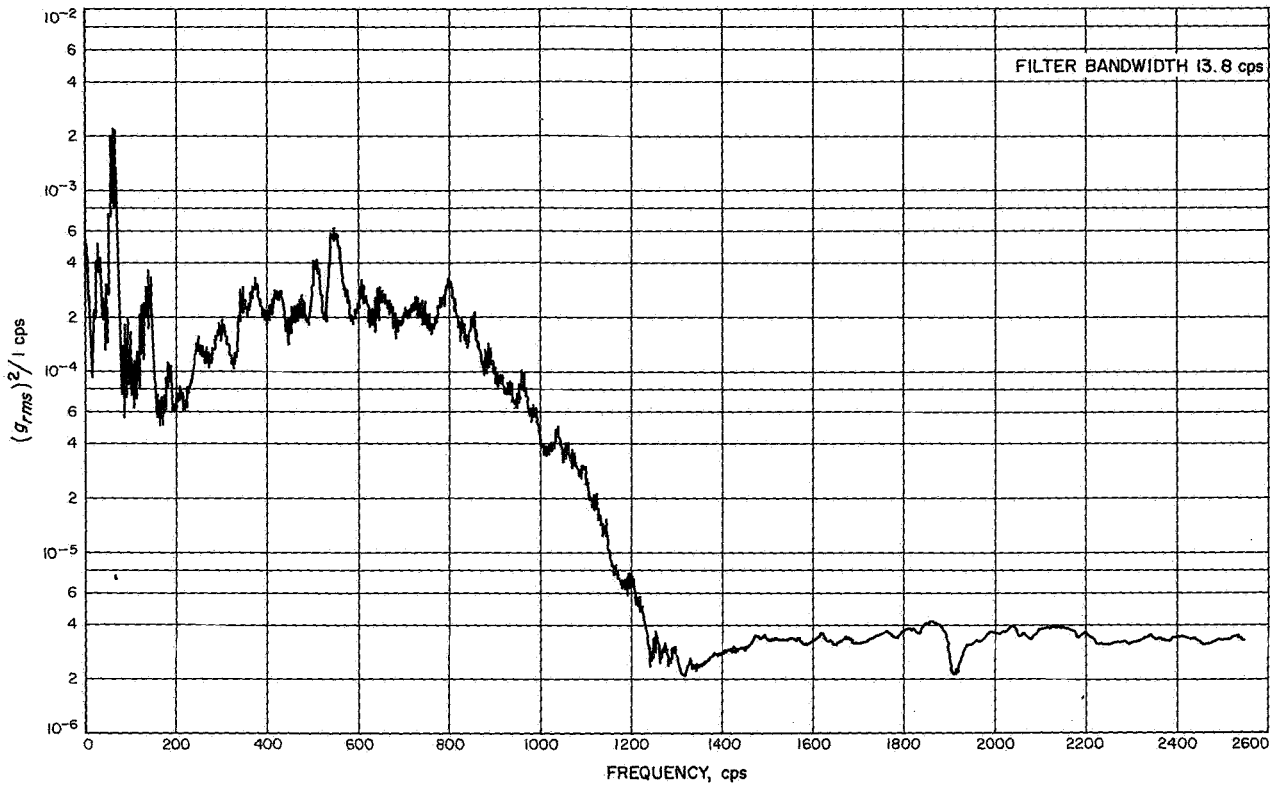


**Fig. 17. Acceleration spectral density for Channel 11 at 136.5–138.5 sec**

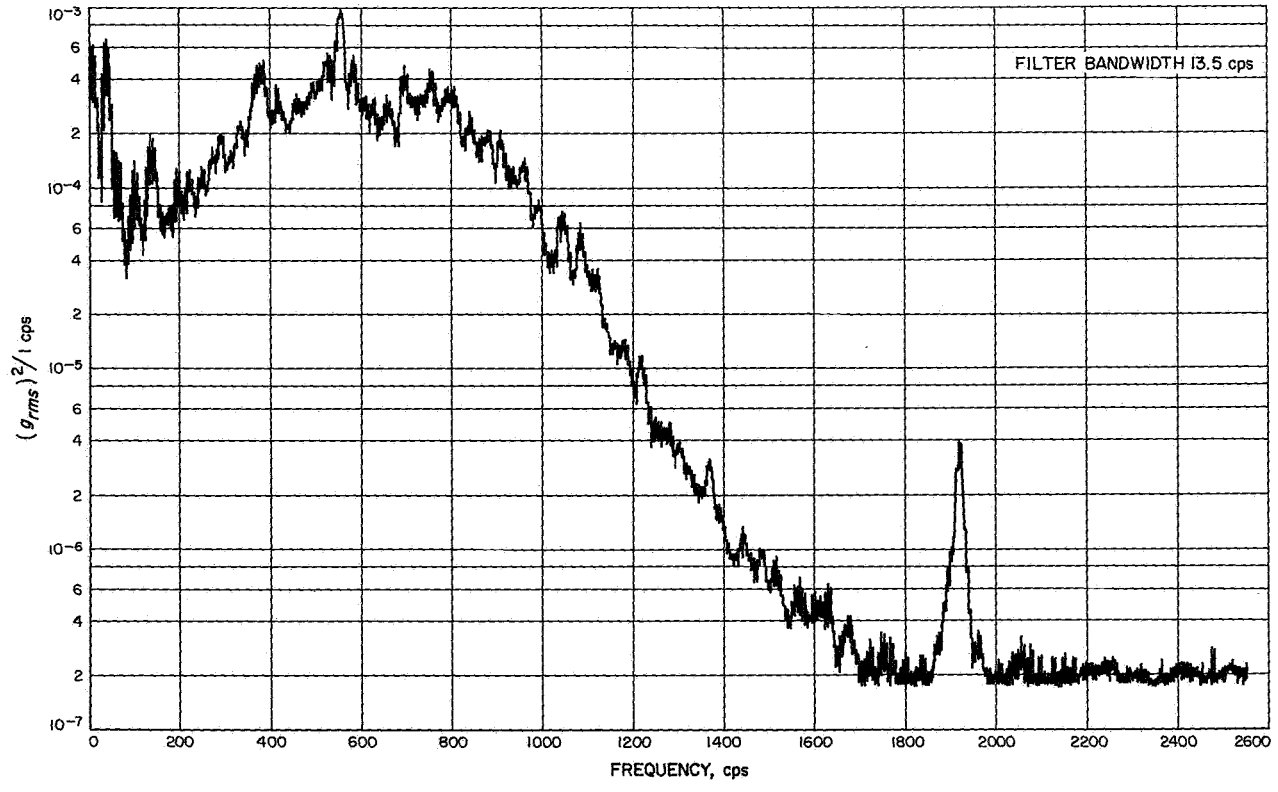


**Fig. 18. Acceleration spectral density for Channel 11 at 139–141 sec**

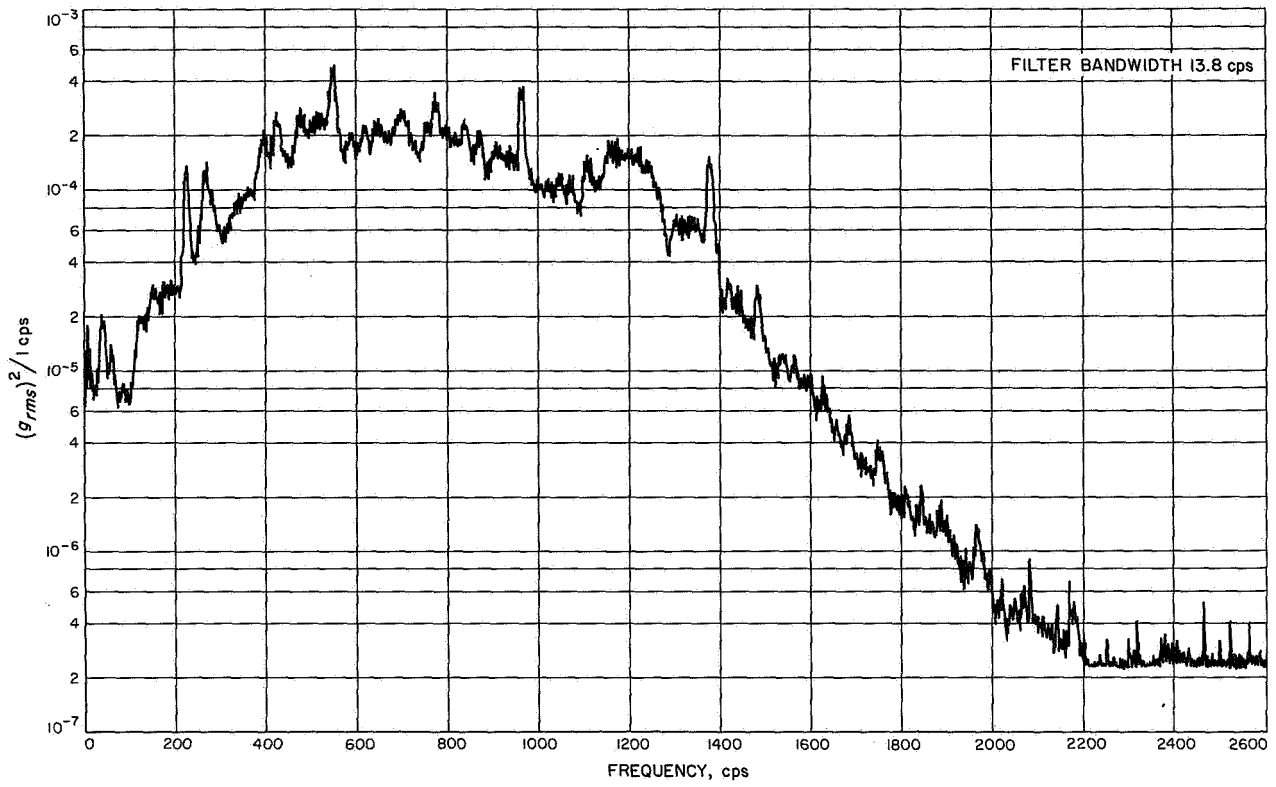


**Fig. 19. Acceleration spectral density for Channel 12 at −8 to −6 sec**

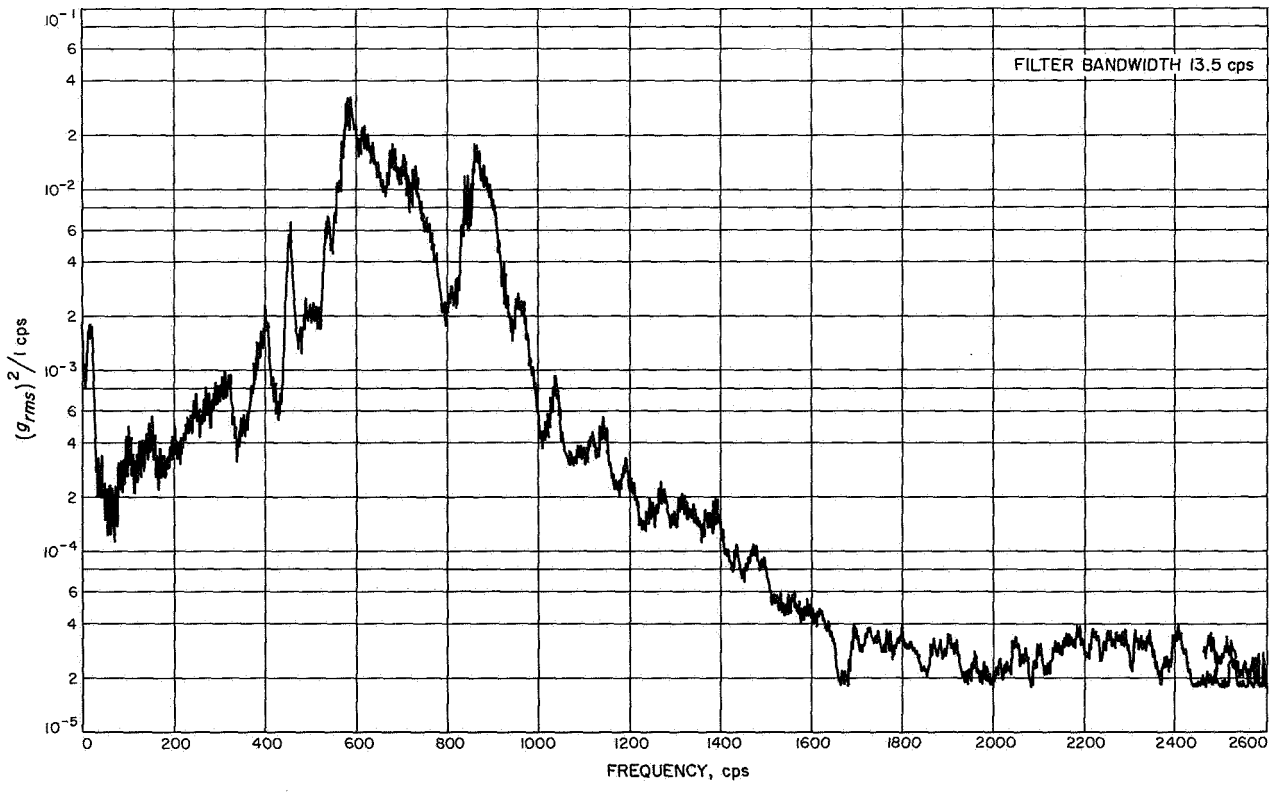


**Fig. 20. Acceleration spectral density for Channel 12 at lift-off**

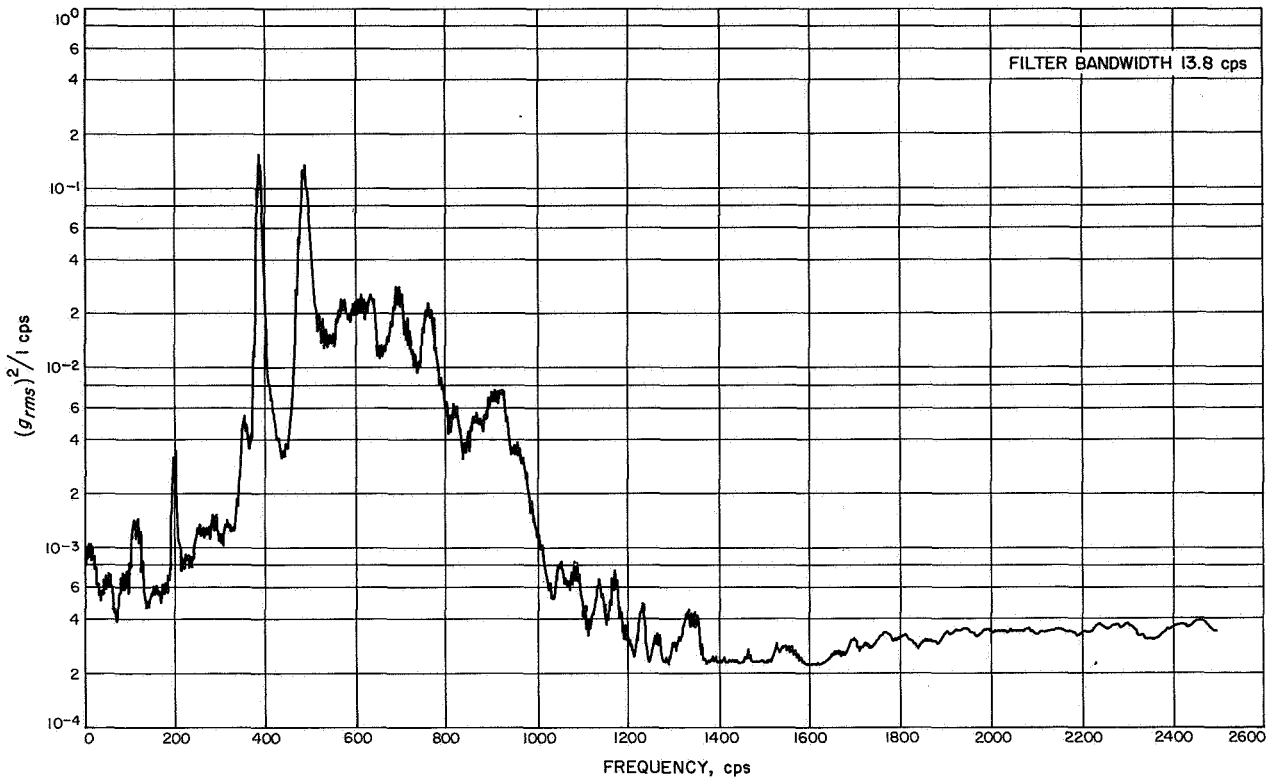


**Fig. 21. Acceleration spectral density for Channel 12 at 380-cps vibration**

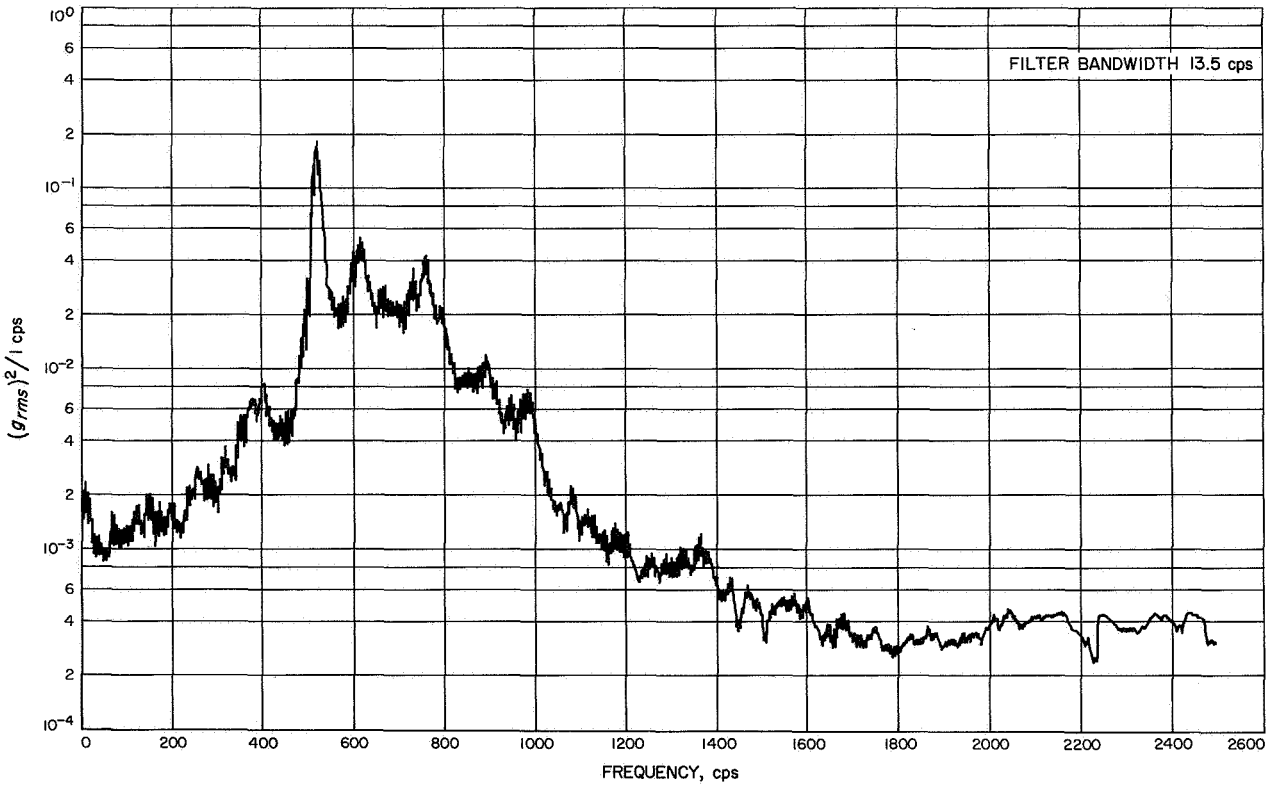


**Fig. 22. Acceleration spectral density for Channel 12 at transonic flight**

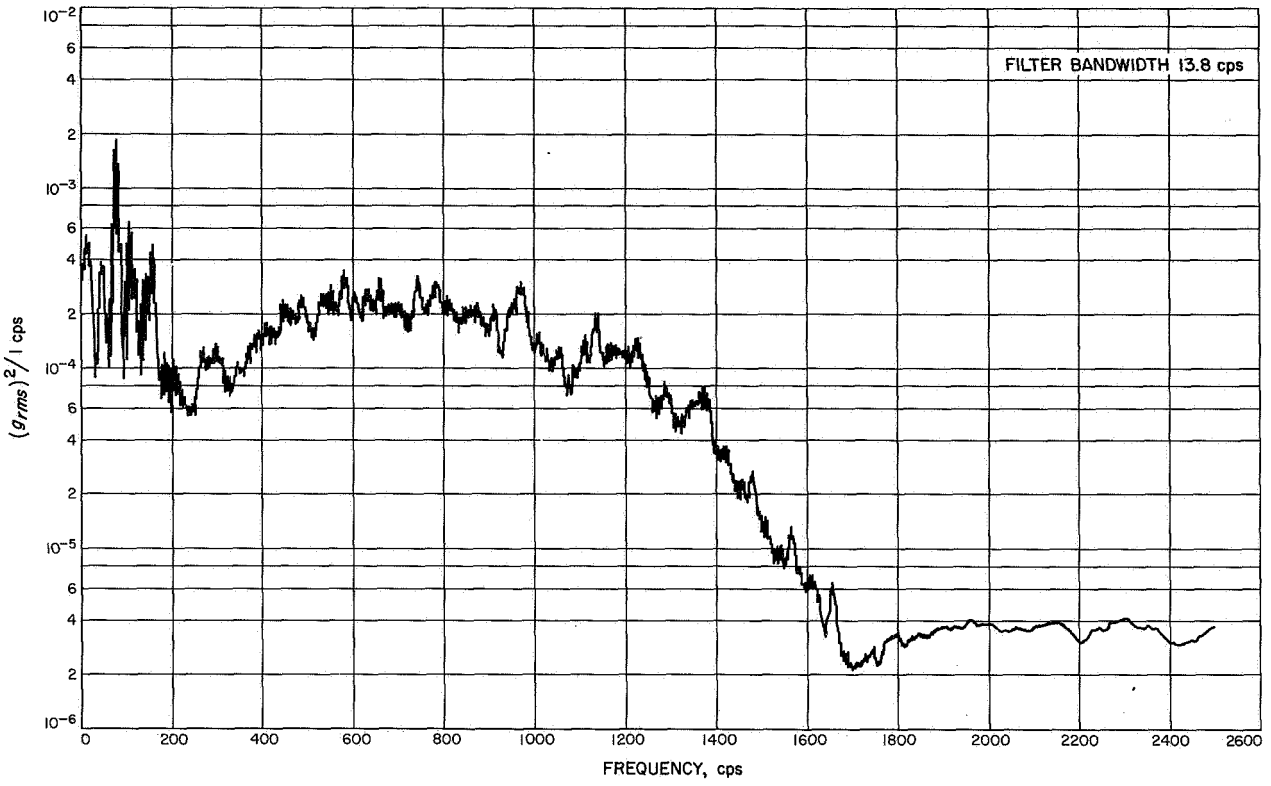


**Fig. 23. Acceleration spectral density for Channel 12 at 136.5–138.5 sec**

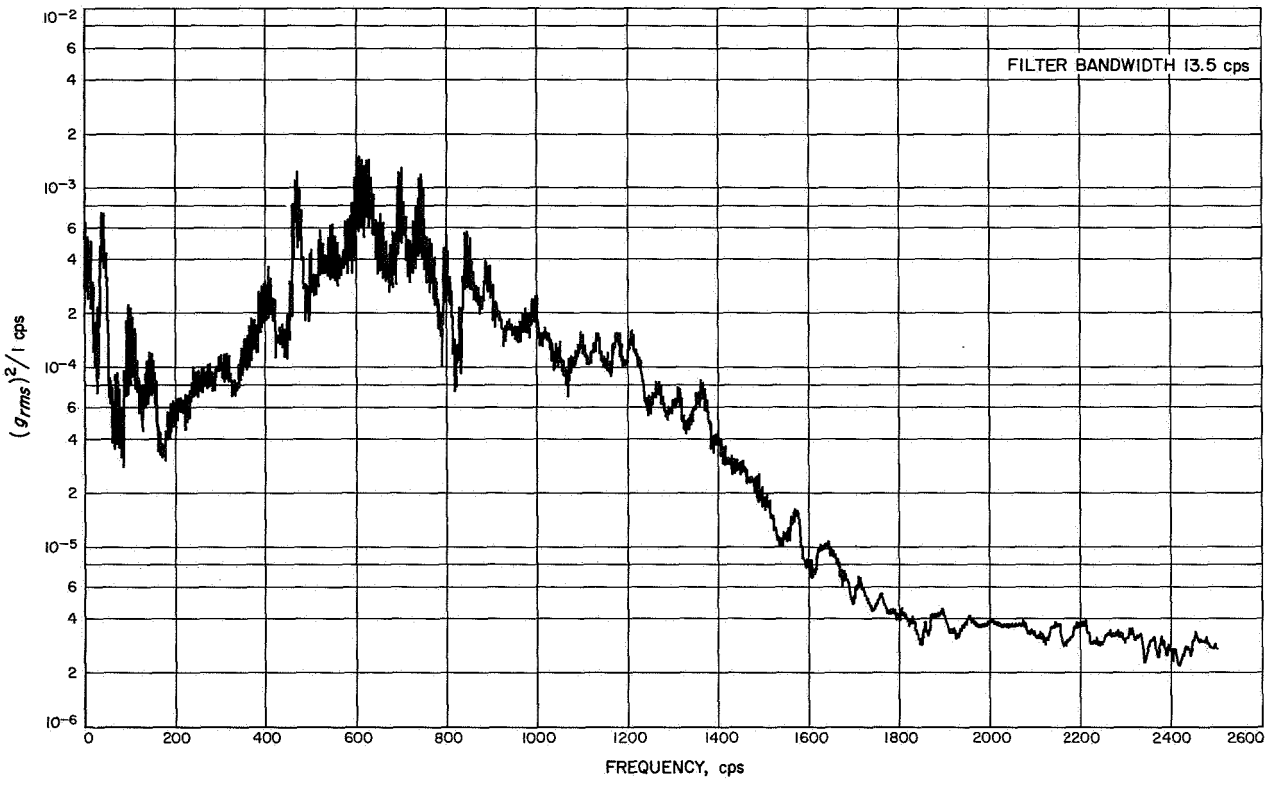


**Fig. 24. Acceleration spectral density for Channel 12 at 139–141 sec**

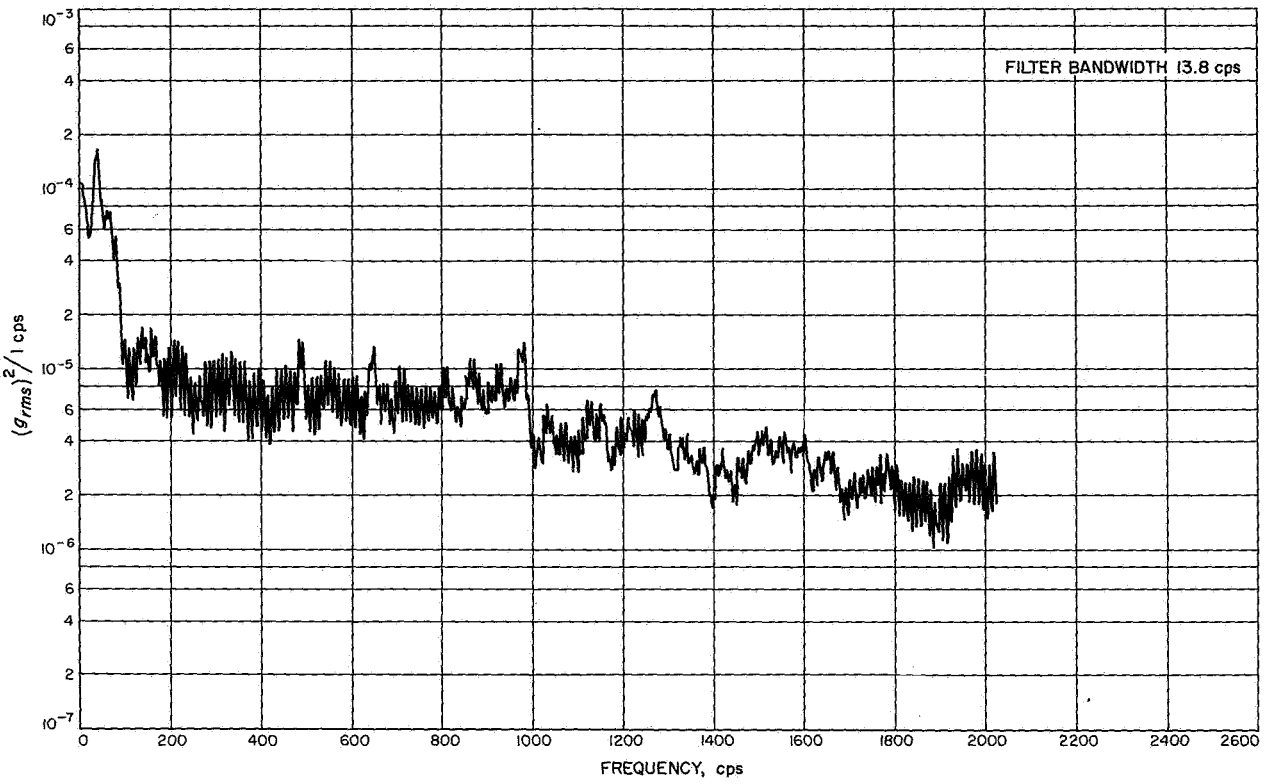


**Fig. 25. Acceleration spectral density for Channel 17 at −8 to −6 sec**

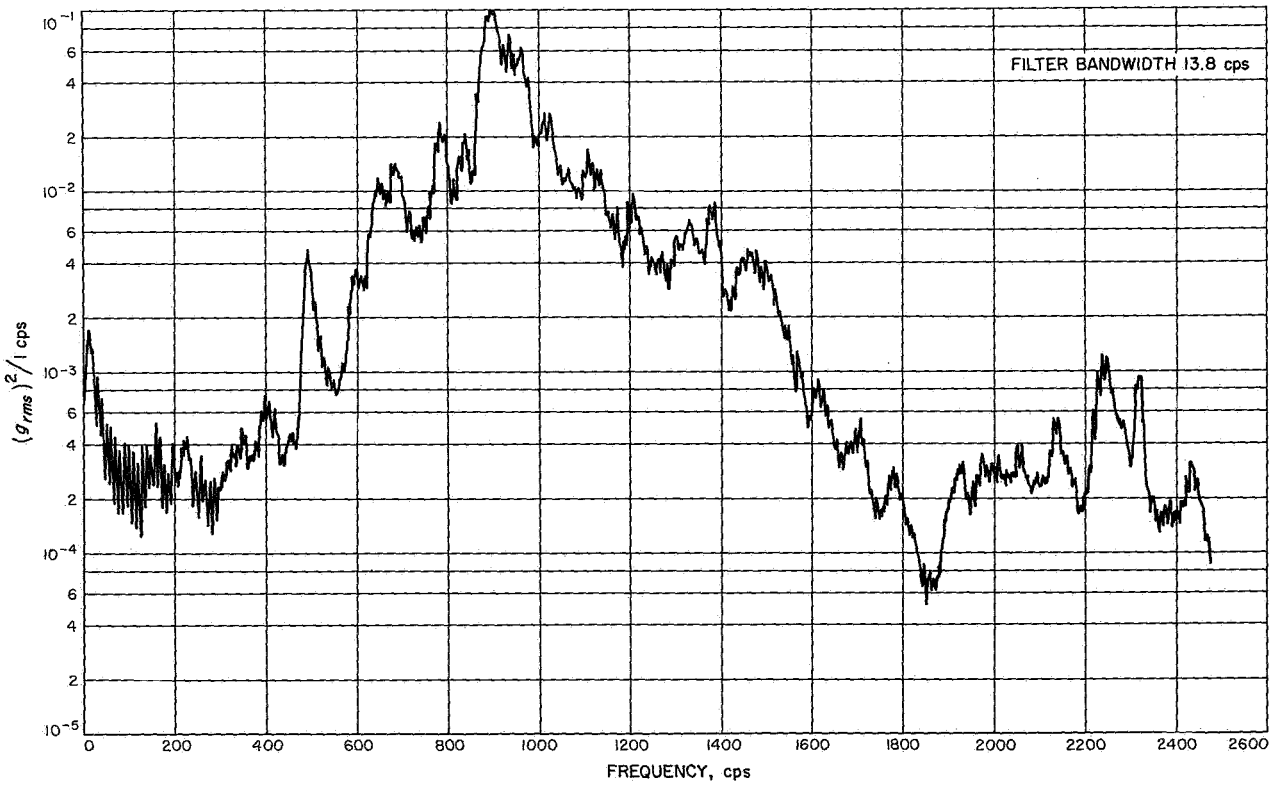


**Fig. 26. Acceleration spectral density for Channel 17 at lift-off**

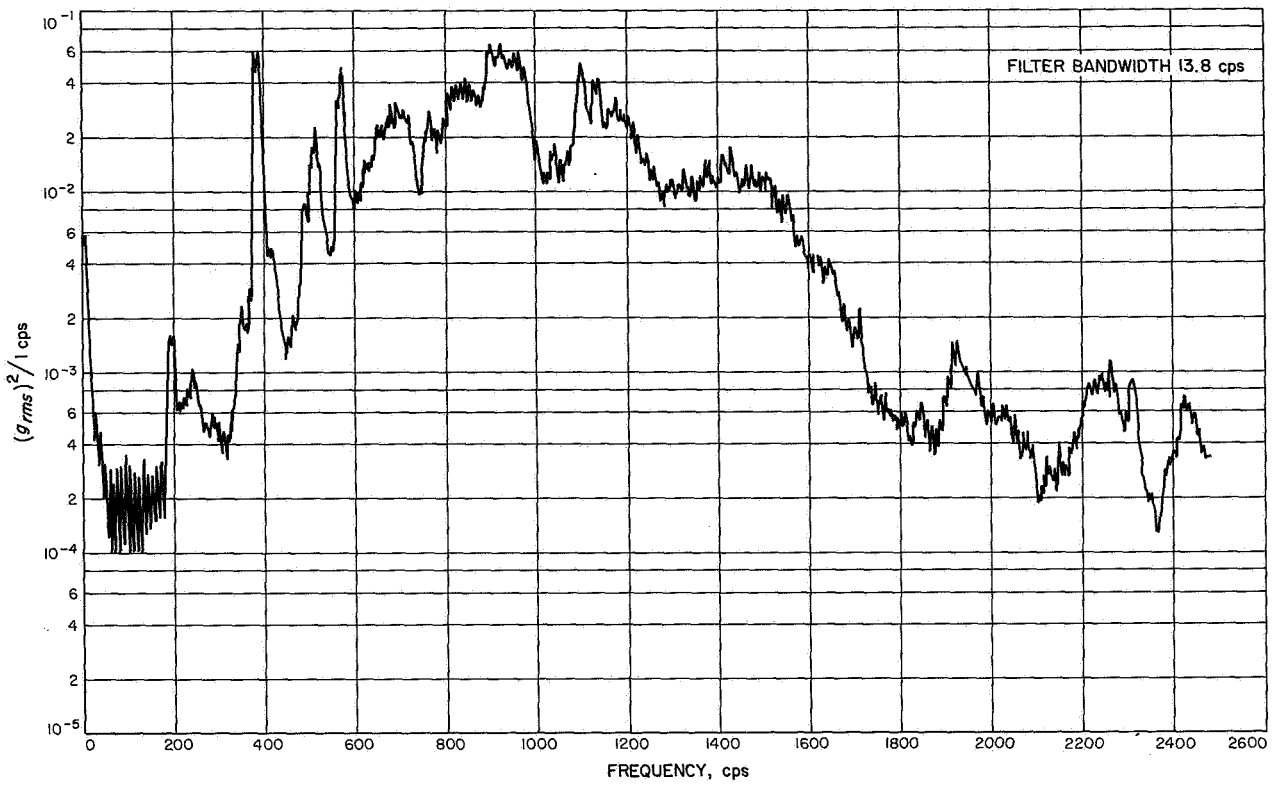


**Fig. 27. Acceleration spectral density for Channel 17 at 380-cps vibration**

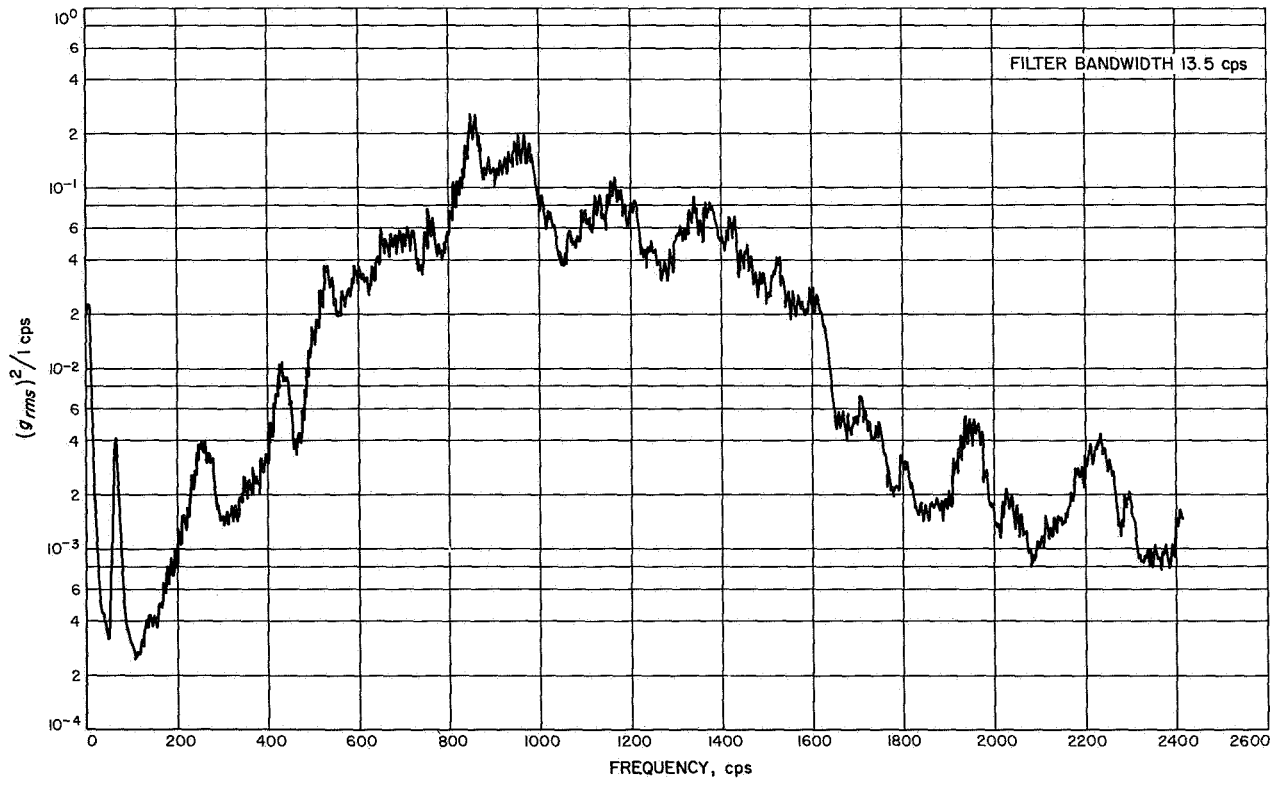


**Fig. 28. Acceleration spectral density for Channel 17 at transonic flight**

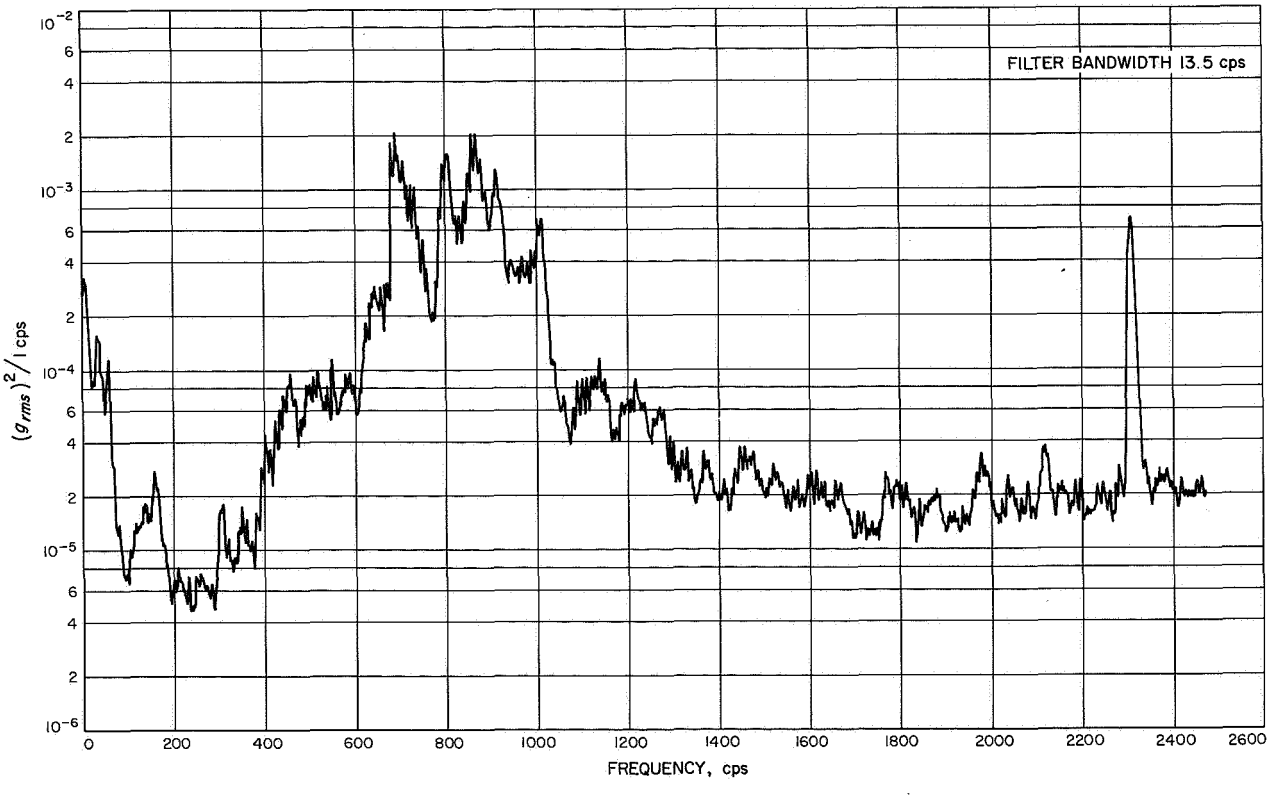


**Fig. 29. Acceleration spectral density for Channel 17 at 113.5–115.5 sec**

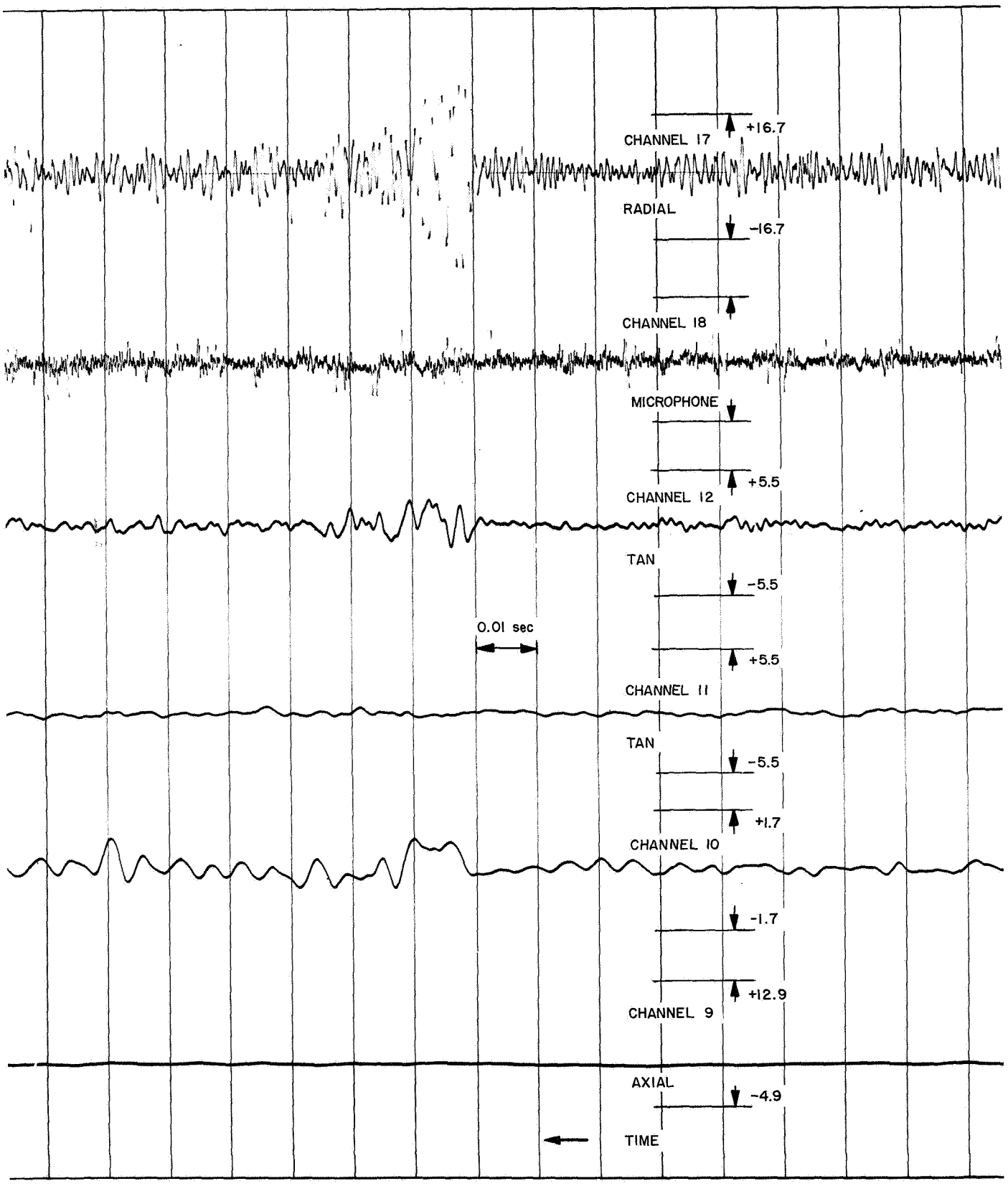


**Fig. 30. Oscillogram at lift-off**

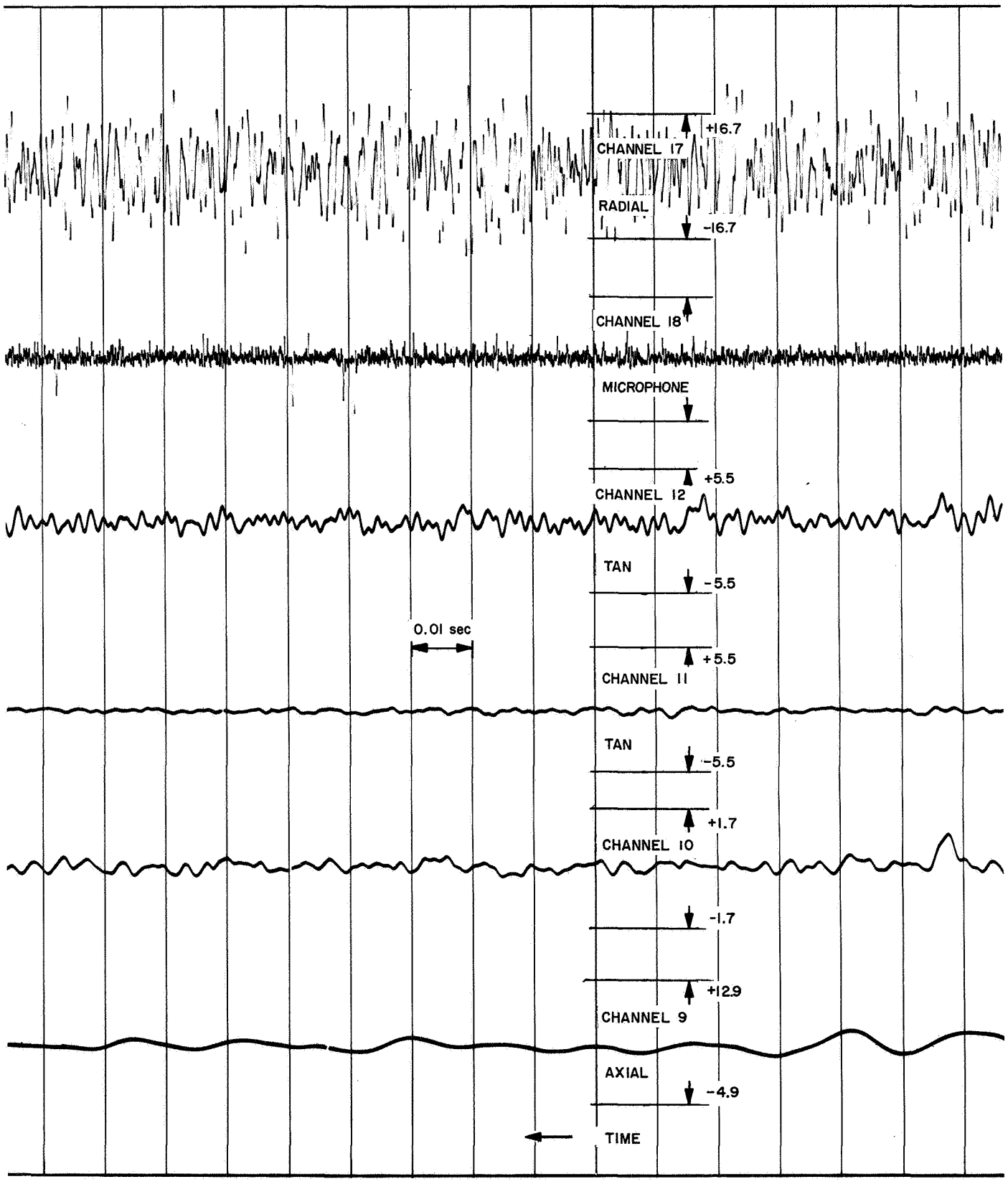


**Fig. 31. Oscillogram at transonic flight**

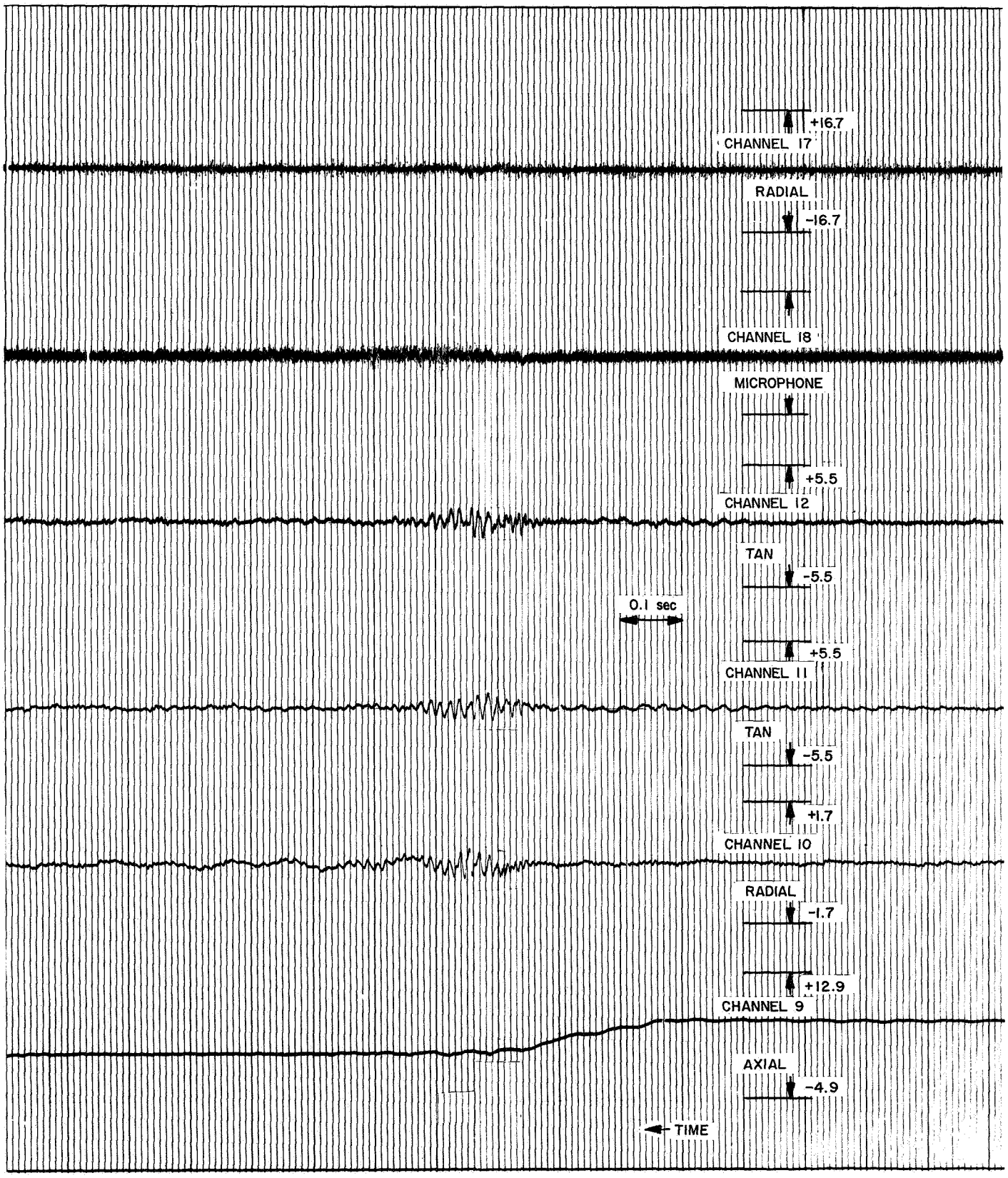


**Fig. 32. Oscillogram at BECO**

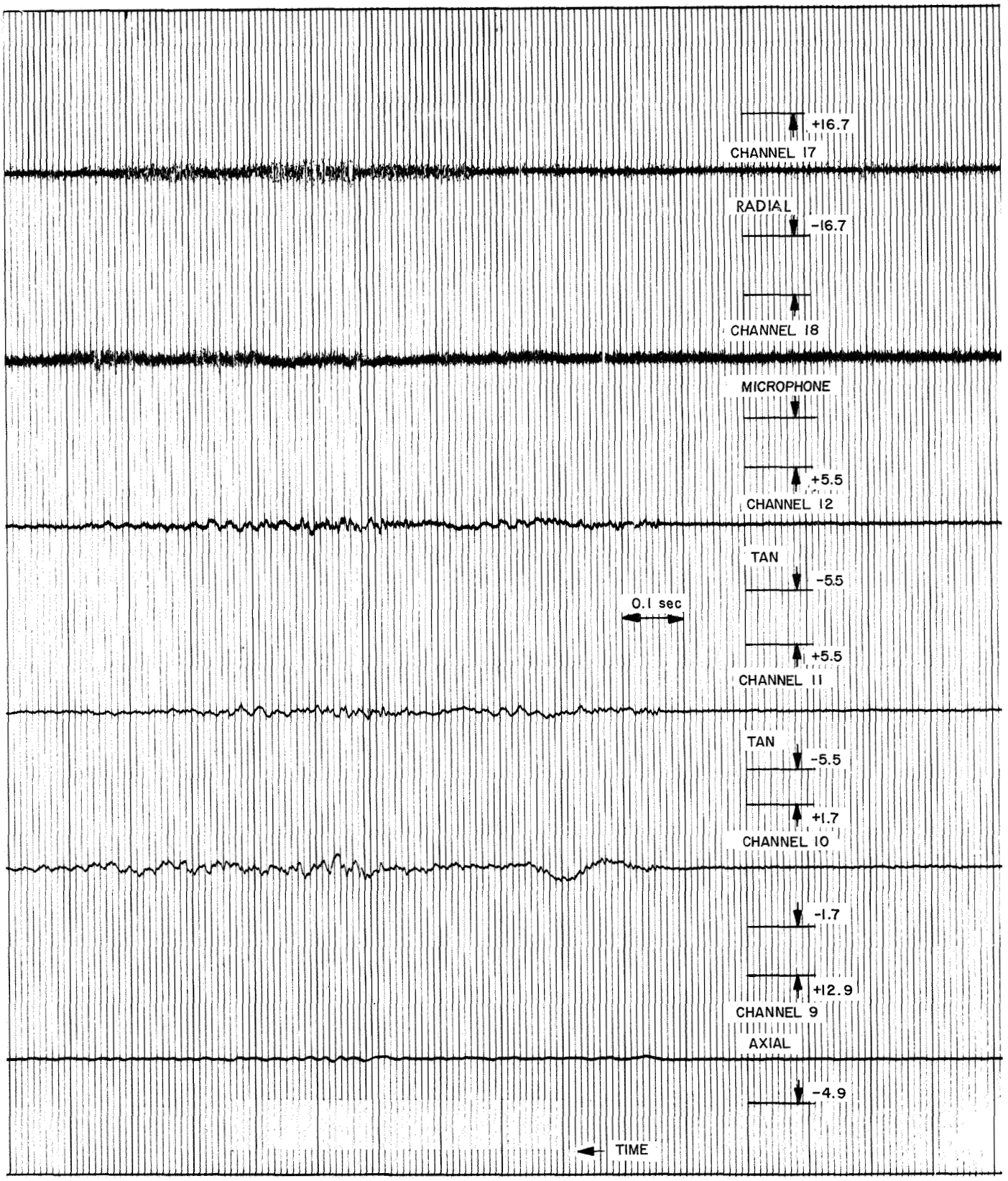


**Fig. 33. Oscillogram for Channel 8 on at booster jettison**

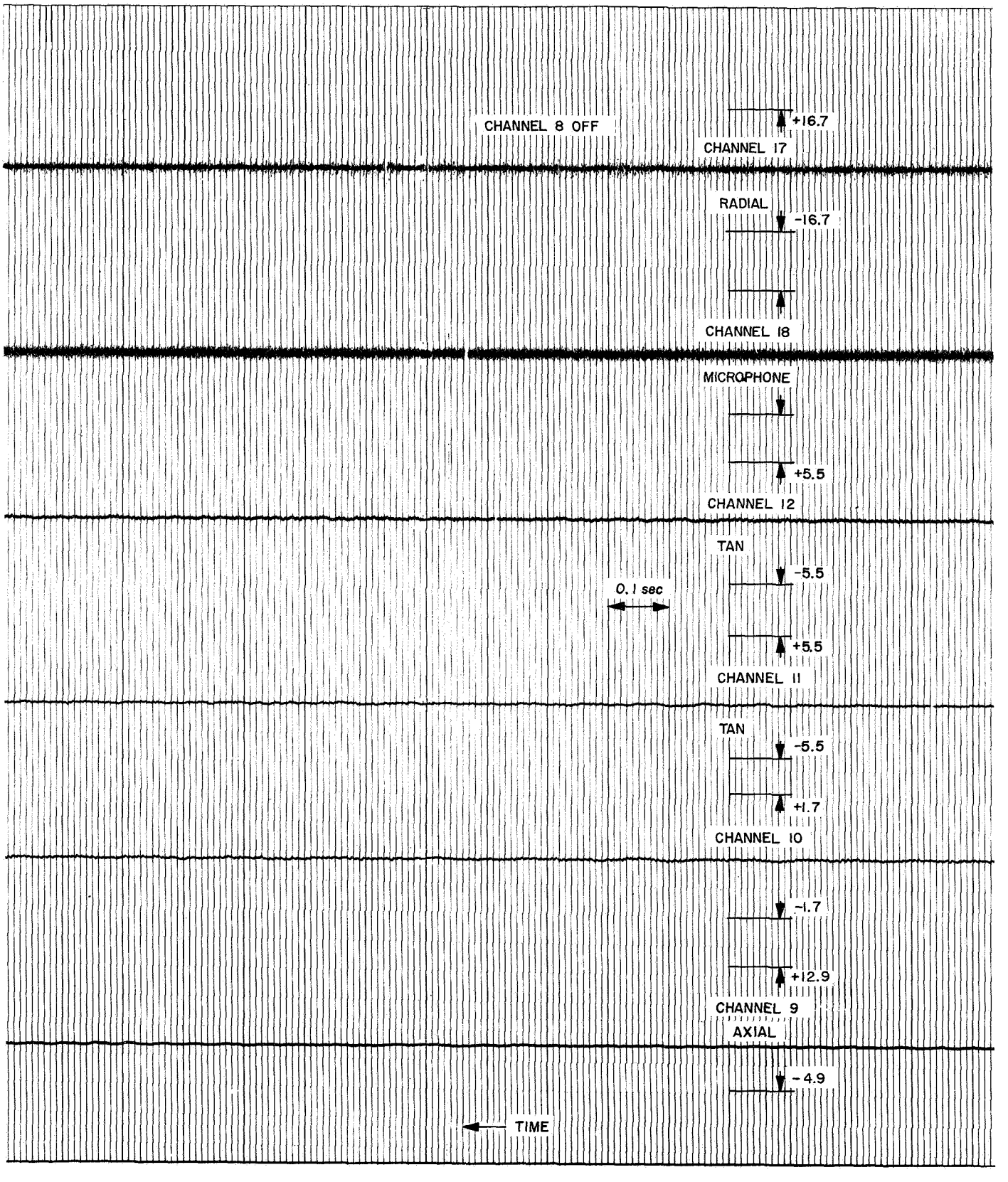


**Fig. 34. Oscillogram for Channel 8 off**

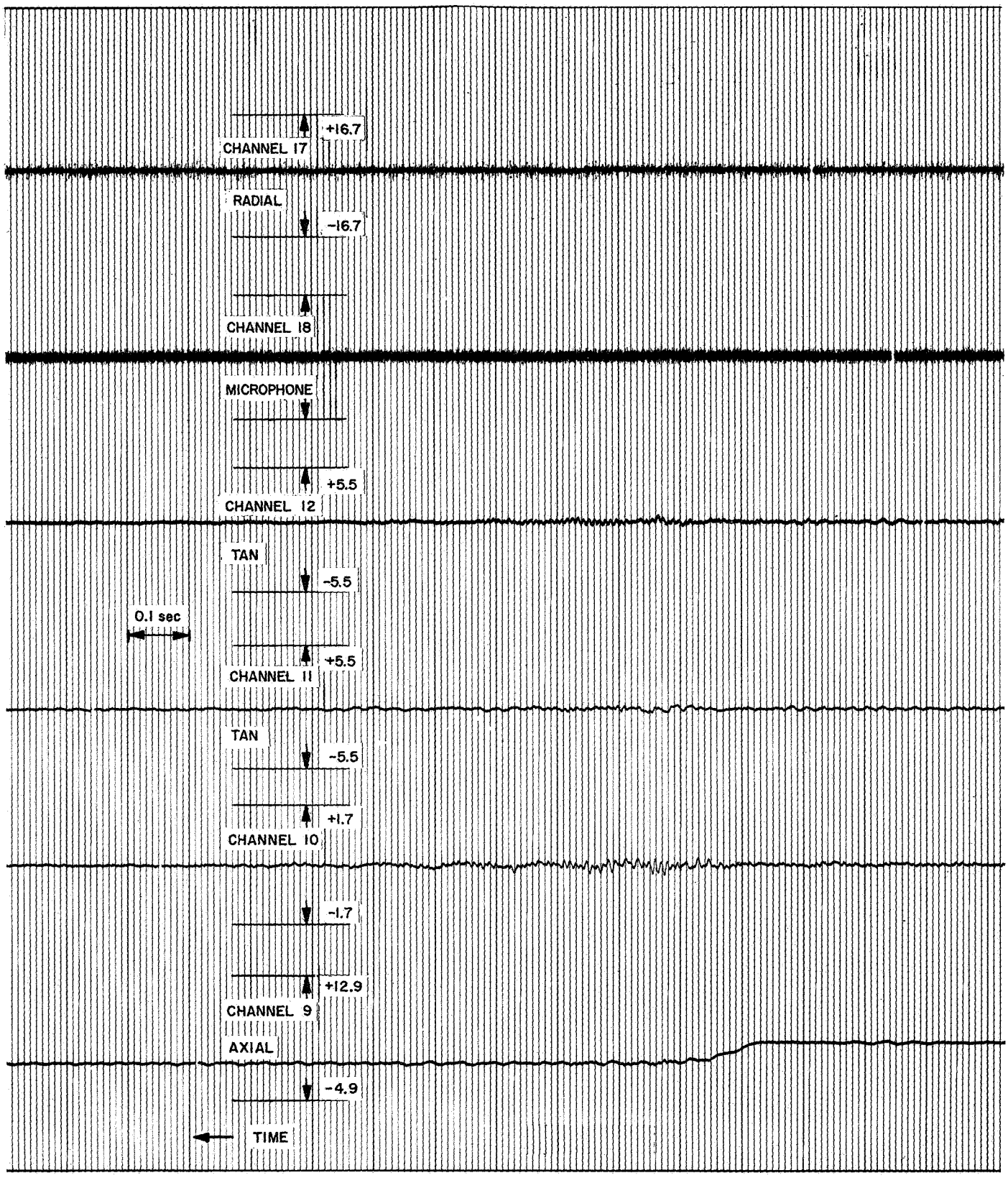


Fig. 35. Oscillogram for SECO

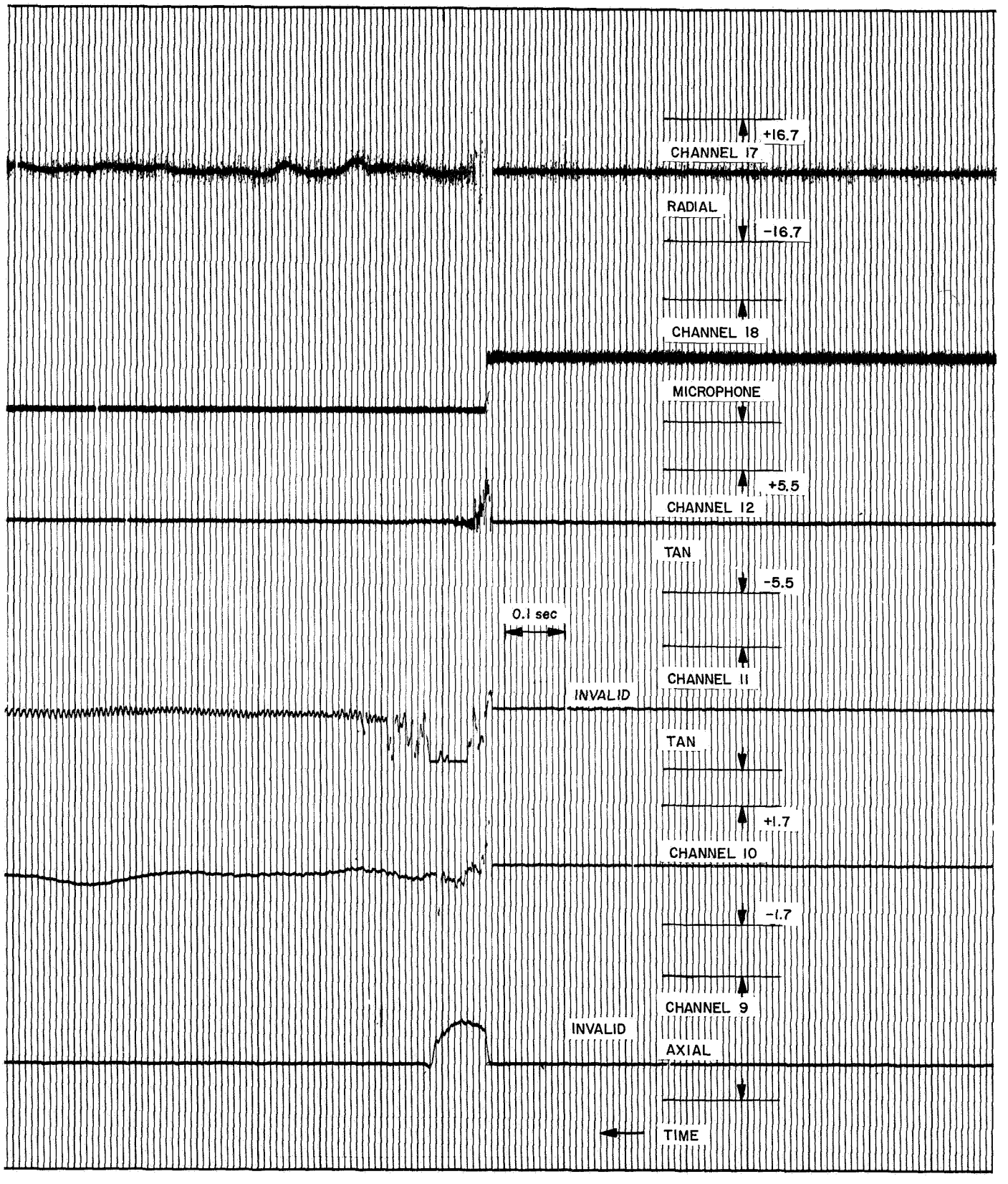


**Fig. 36. Oscillogram for shroud jettison**

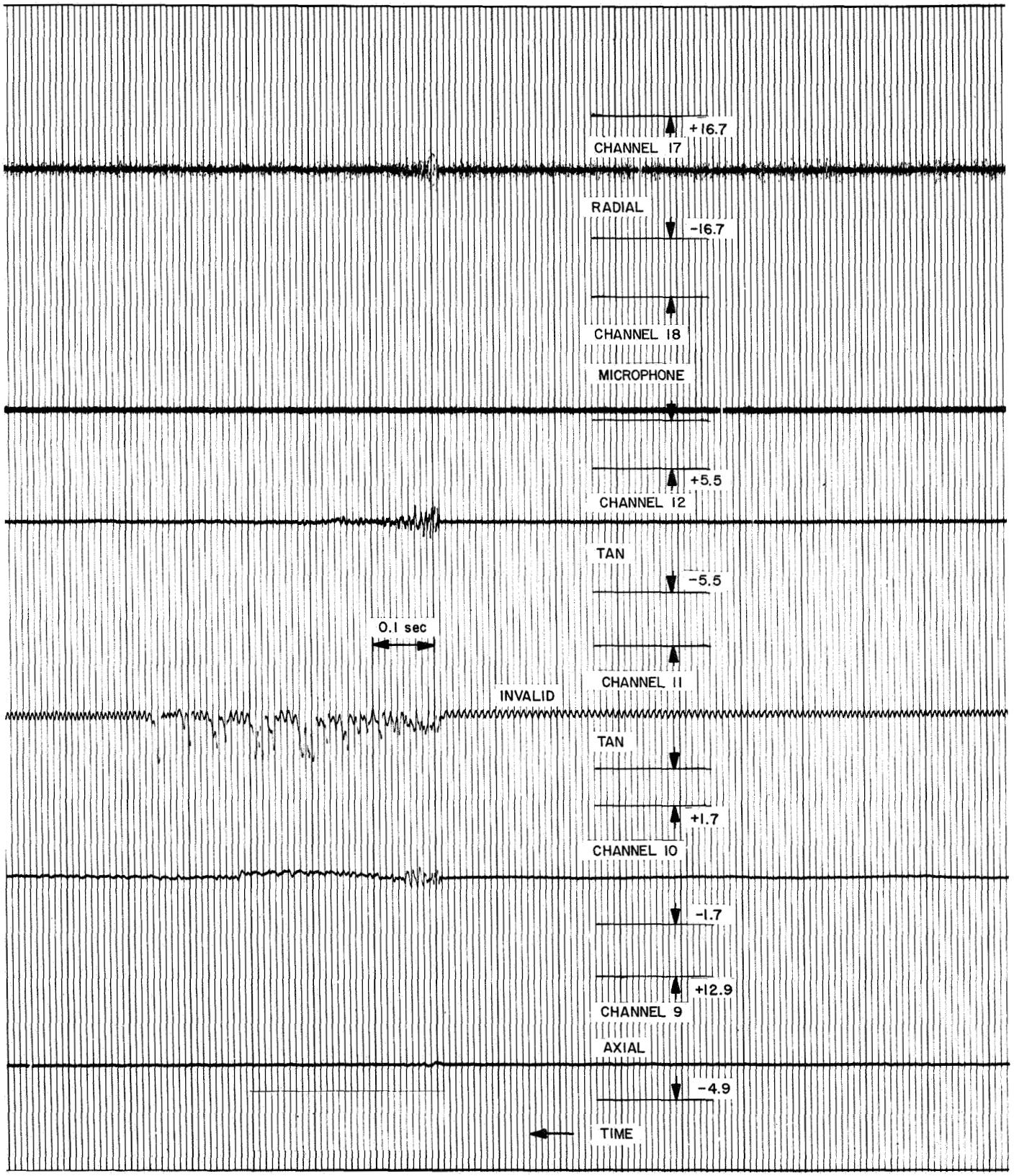


**Fig. 37. Oscillogram for *Atlas–Agena* separation**

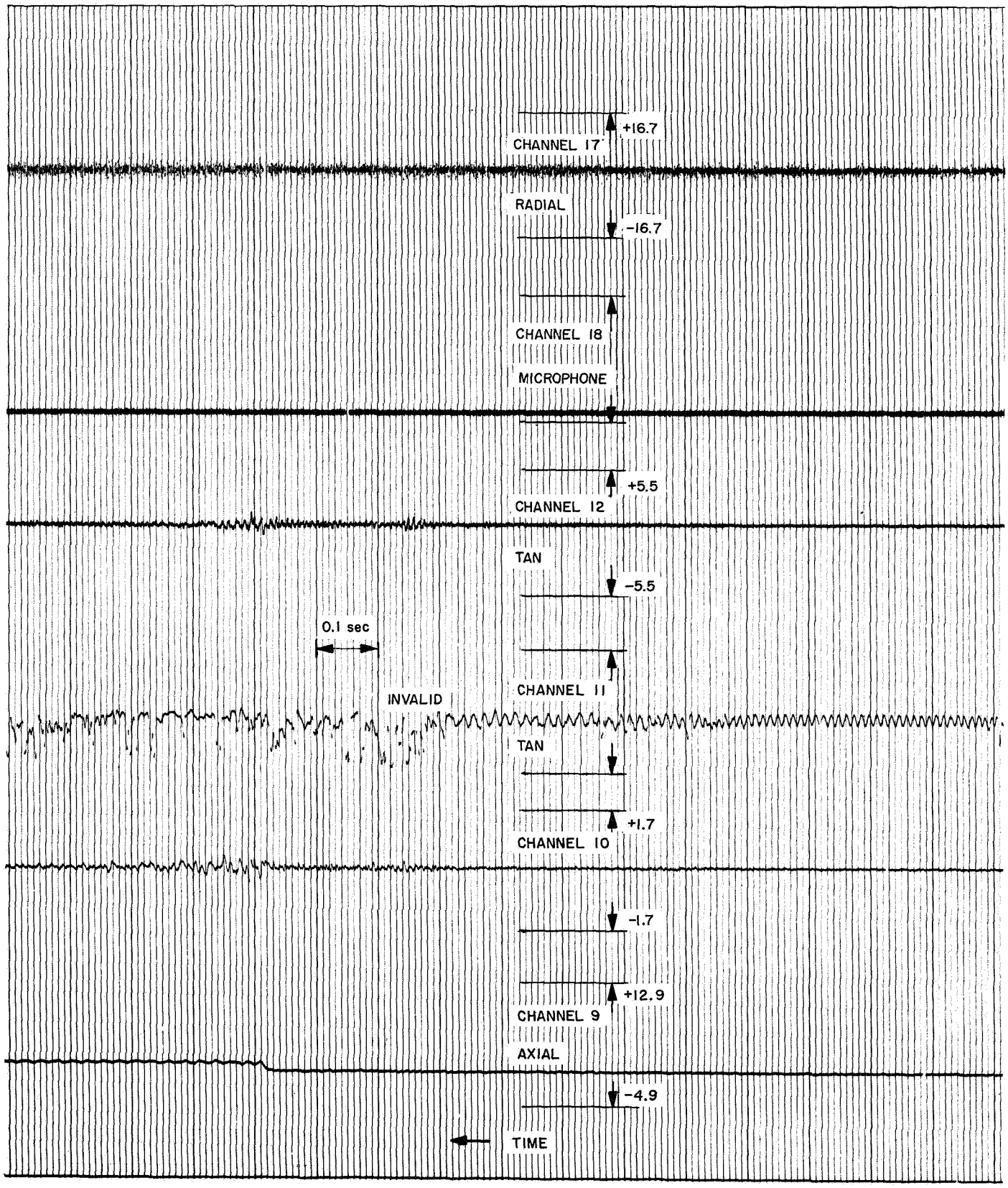


**Fig. 38. Oscillogram for first *Agena* ignition**

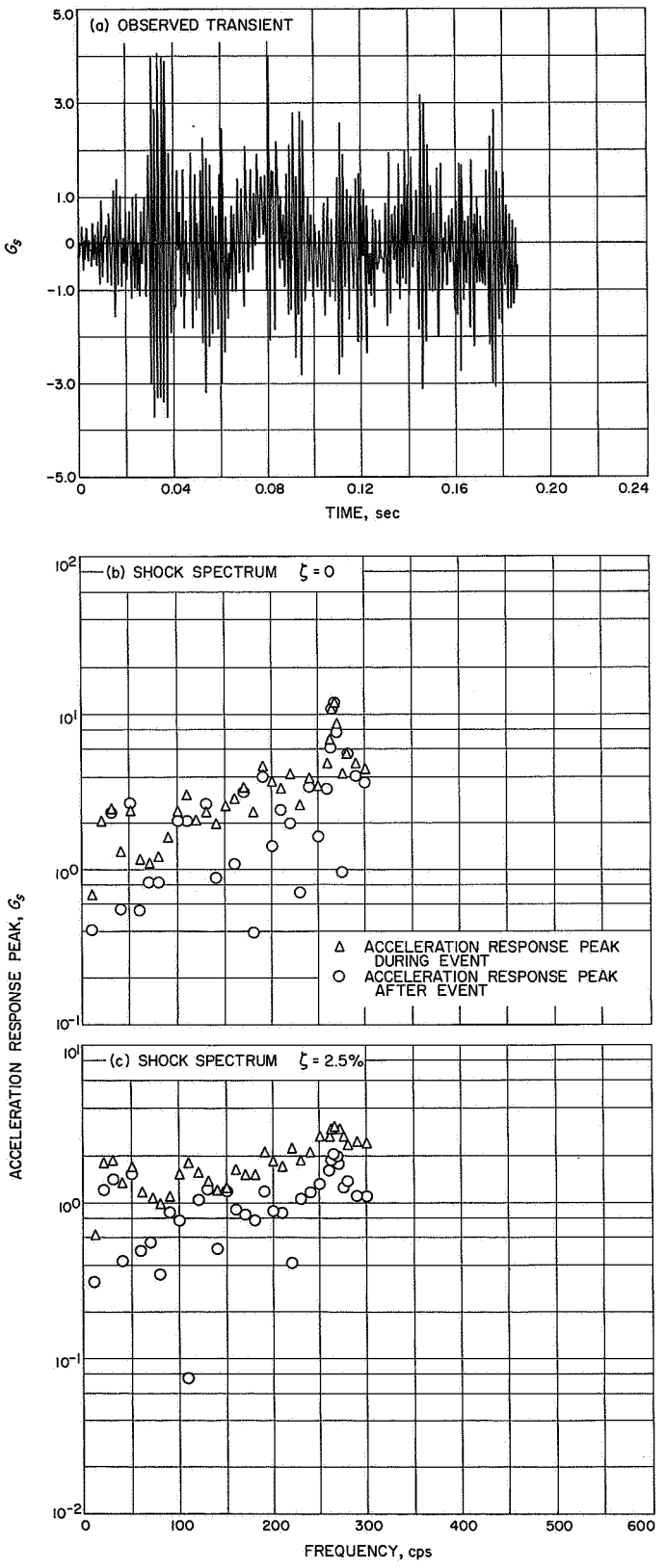


**Fig. 39. Shock spectra for Channel 12 at lift-off**

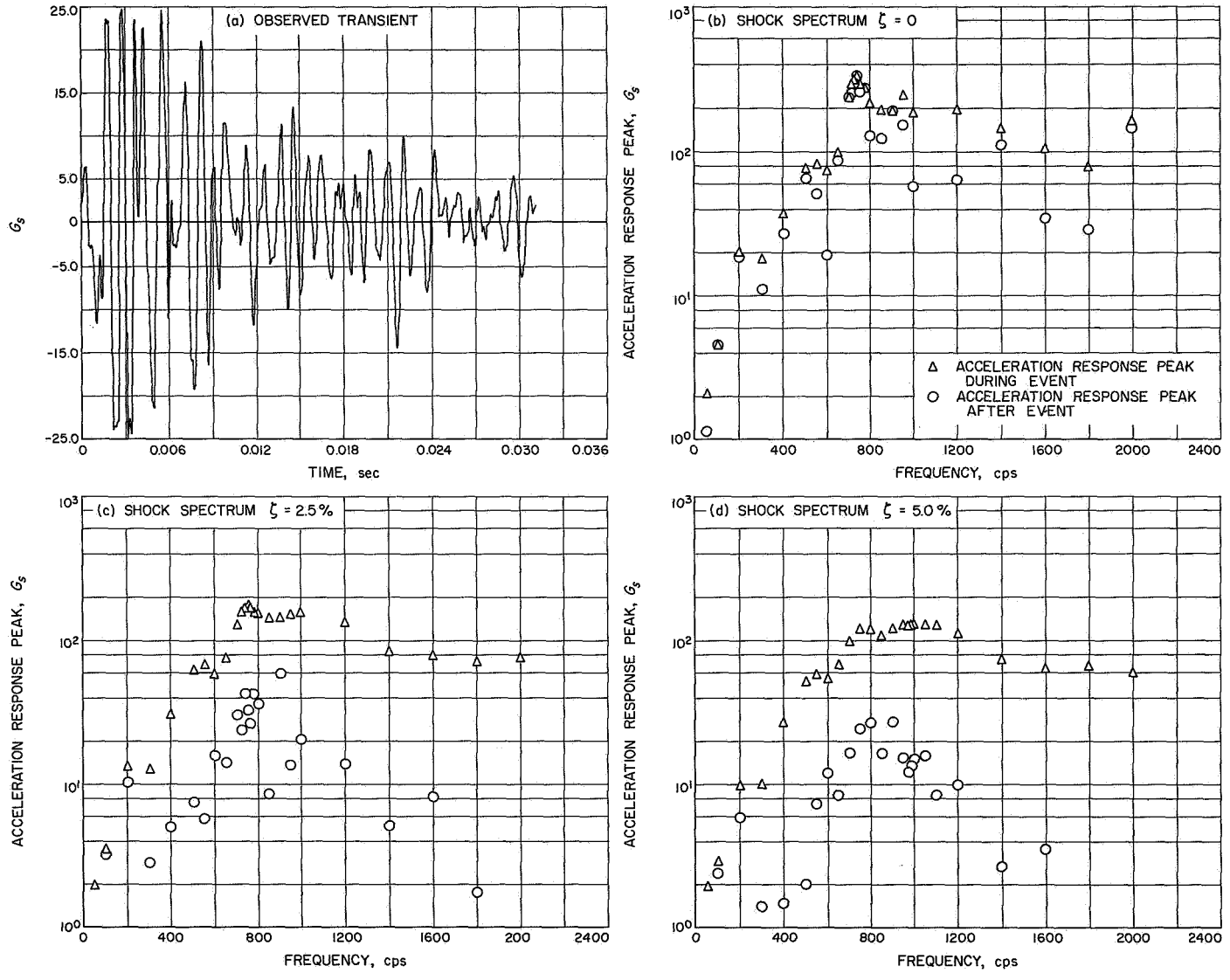


**Fig. 40. Shock spectra for Channel 17 at lift-off**

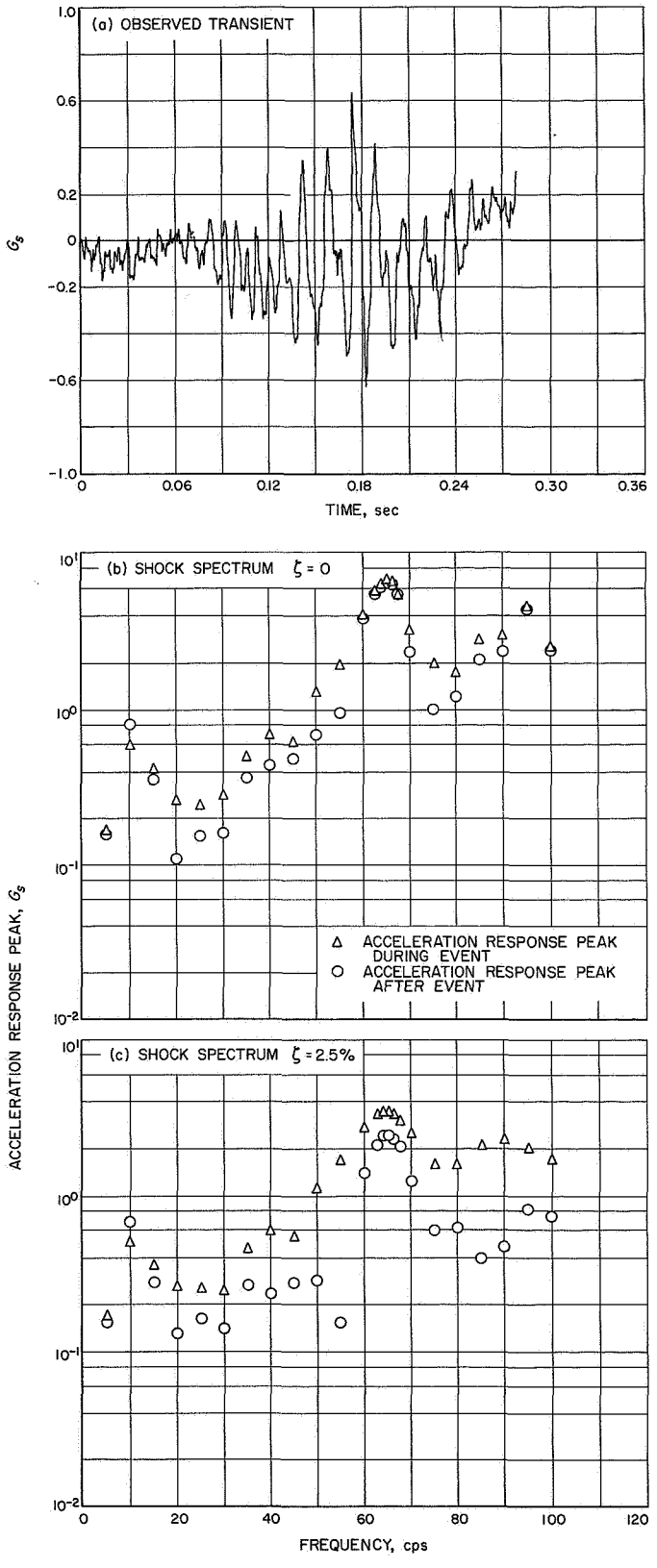
(a) OBSERVED TRANSIENT
$G_s$
TIME, sec
(b) SHOCK SPECTRUM $\zeta = 0$
(c) SHOCK SPECTRUM $\zeta = 2.5\%$
ACCELERATION RESPONSE PEAK, $G_s$
△ ACCELERATION RESPONSE PEAK DURING EVENT
○ ACCELERATION RESPONSE PEAK AFTER EVENT
FREQUENCY, cps

Fig. 41. Shock spectra for Channel 10 at BECO

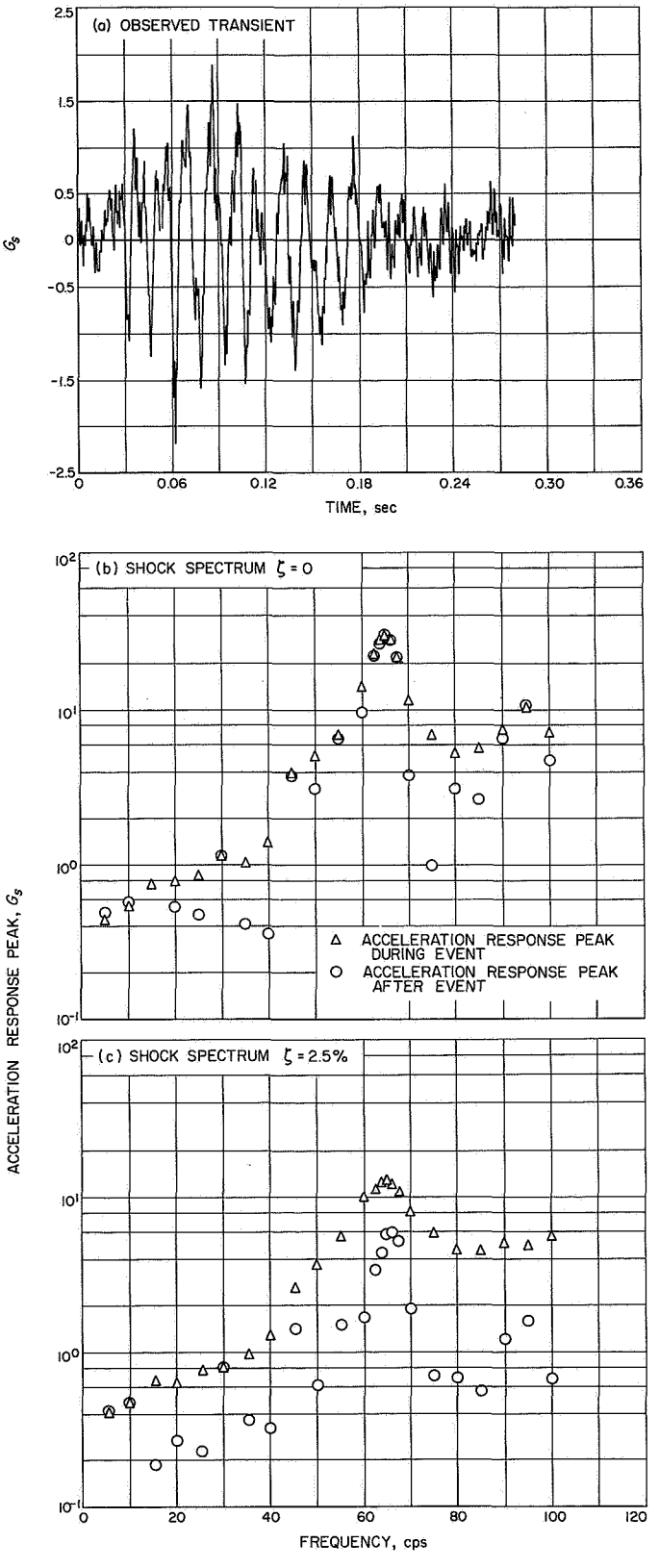
(a) OBSERVED TRANSIENT
$G_s$
TIME, sec
(b) SHOCK SPECTRUM $\zeta = 0$
(c) SHOCK SPECTRUM $\zeta = 2.5\%$
ACCELERATION RESPONSE PEAK, $G_s$
△ ACCELERATION RESPONSE PEAK DURING EVENT
○ ACCELERATION RESPONSE PEAK AFTER EVENT
FREQUENCY, cps

Fig. 42. Shock spectra for Channel 11 at BECO

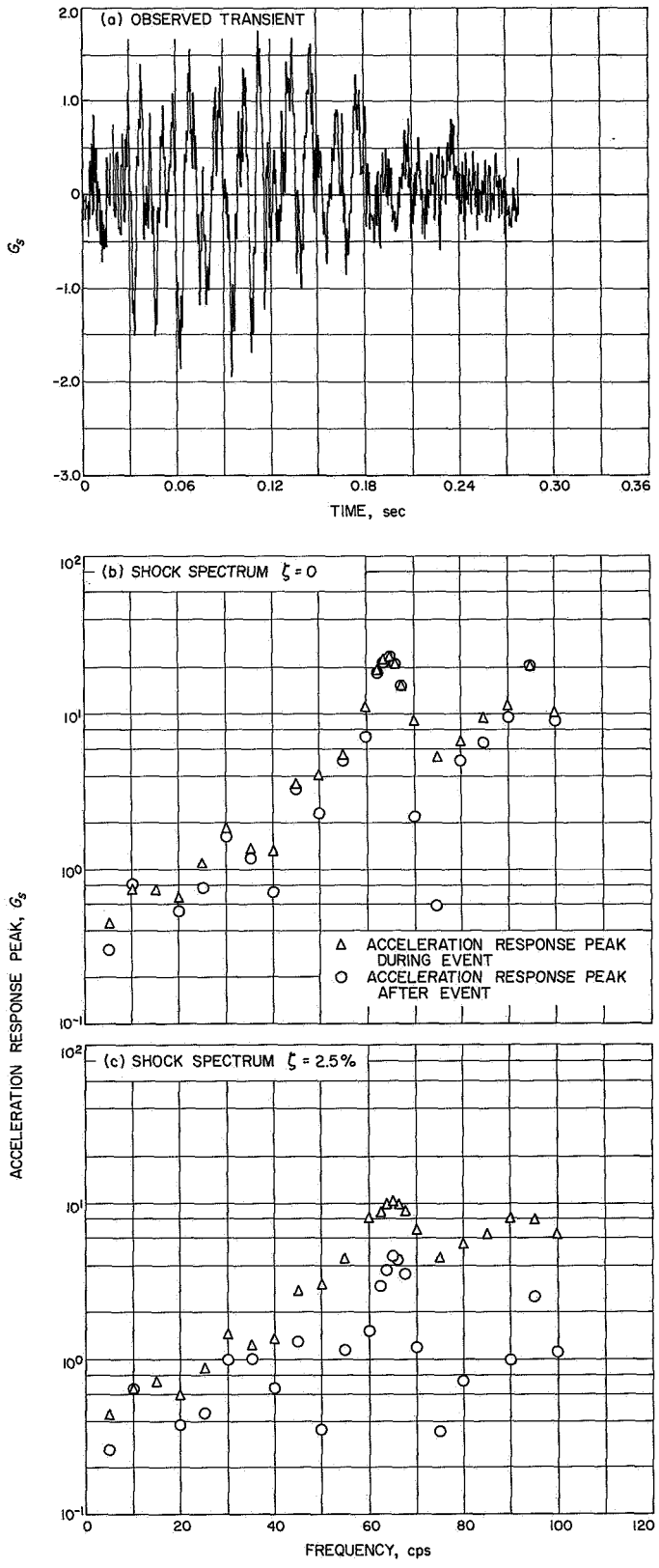


Fig. 43. Shock spectra for Channel 12 at BECO

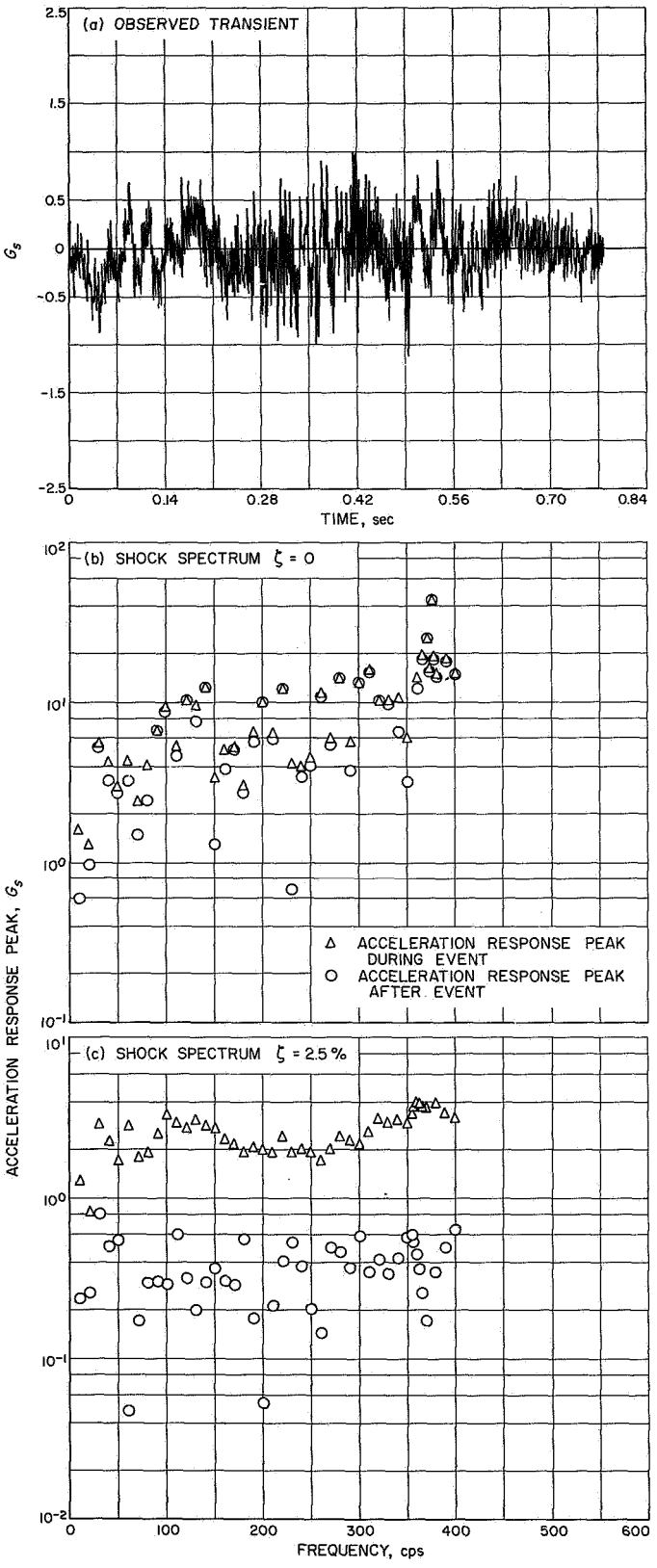


Fig. 44. Shock spectra for Channel 11 at booster jettison

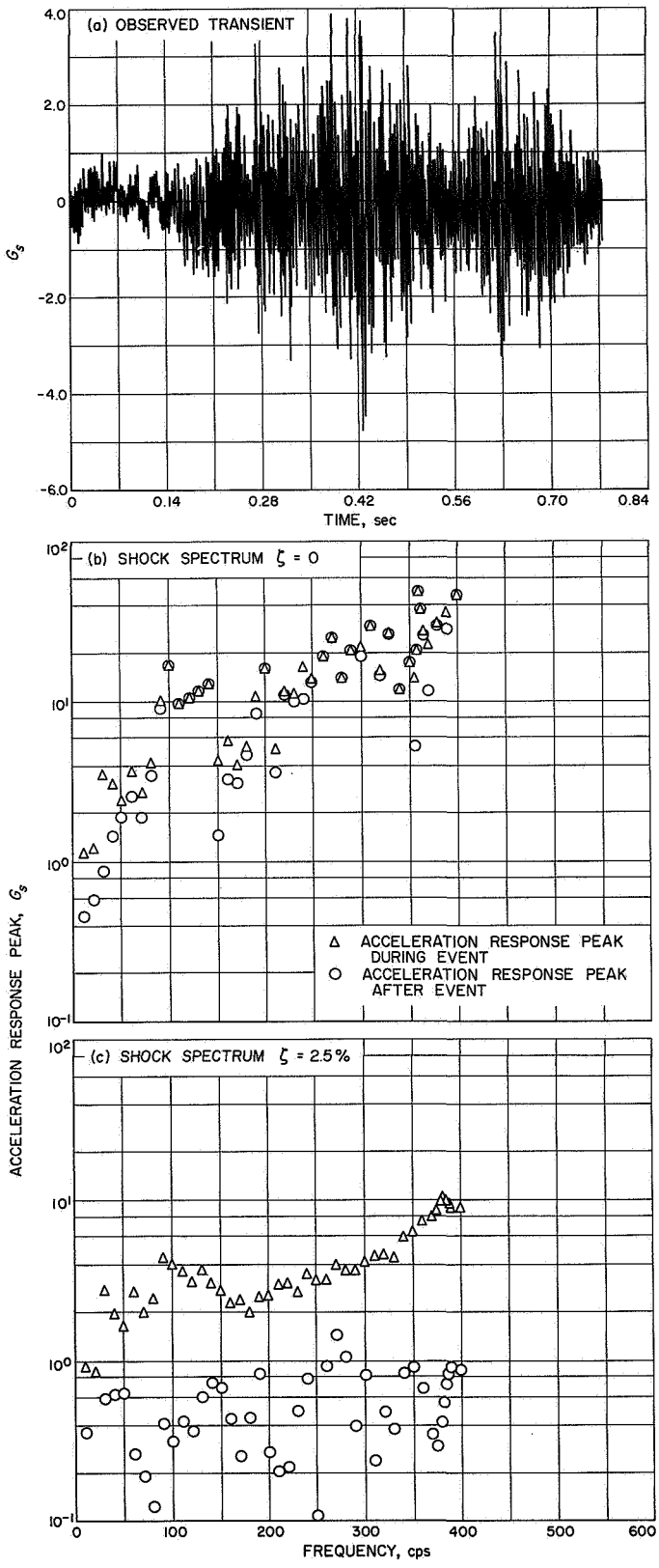


**Fig. 45. Shock spectra for Channel 12 at booster jettison**

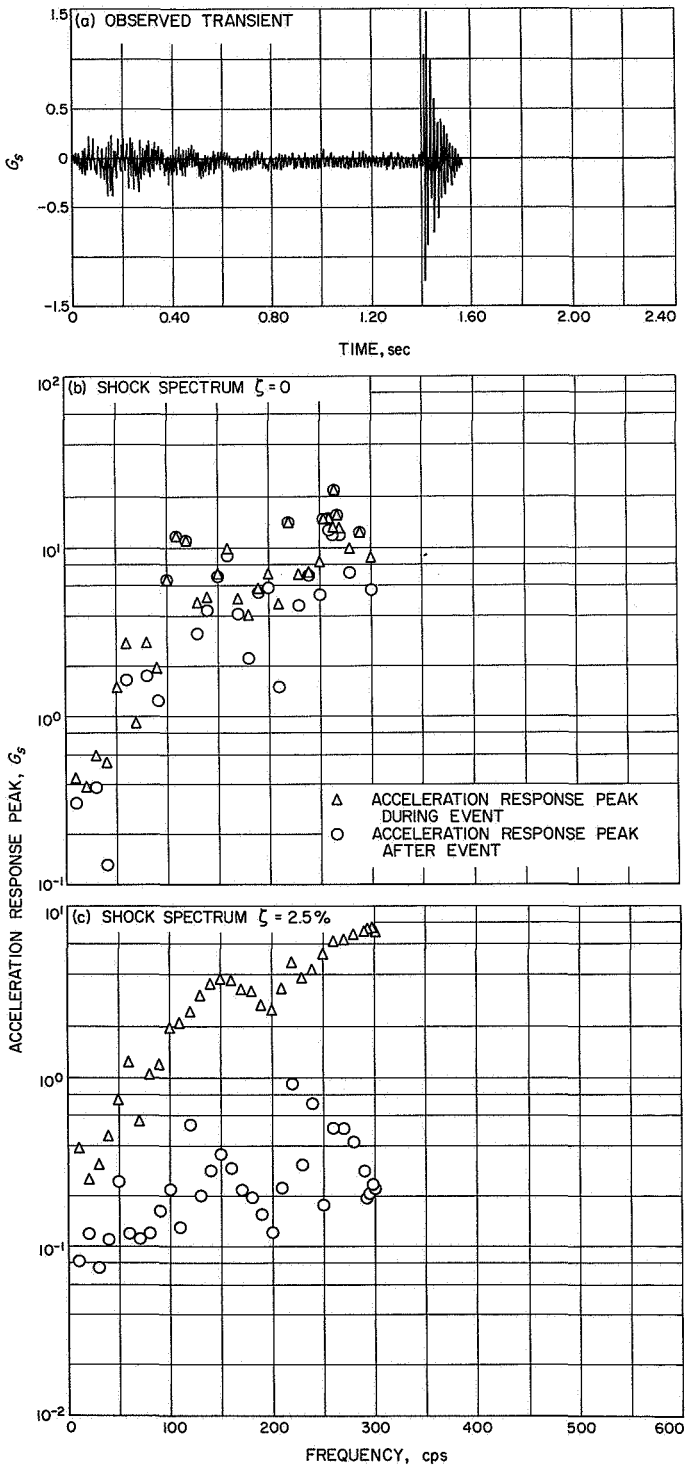


**Fig. 46. Shock spectra for Channel 10 at jettison of horizon sensor fairings**

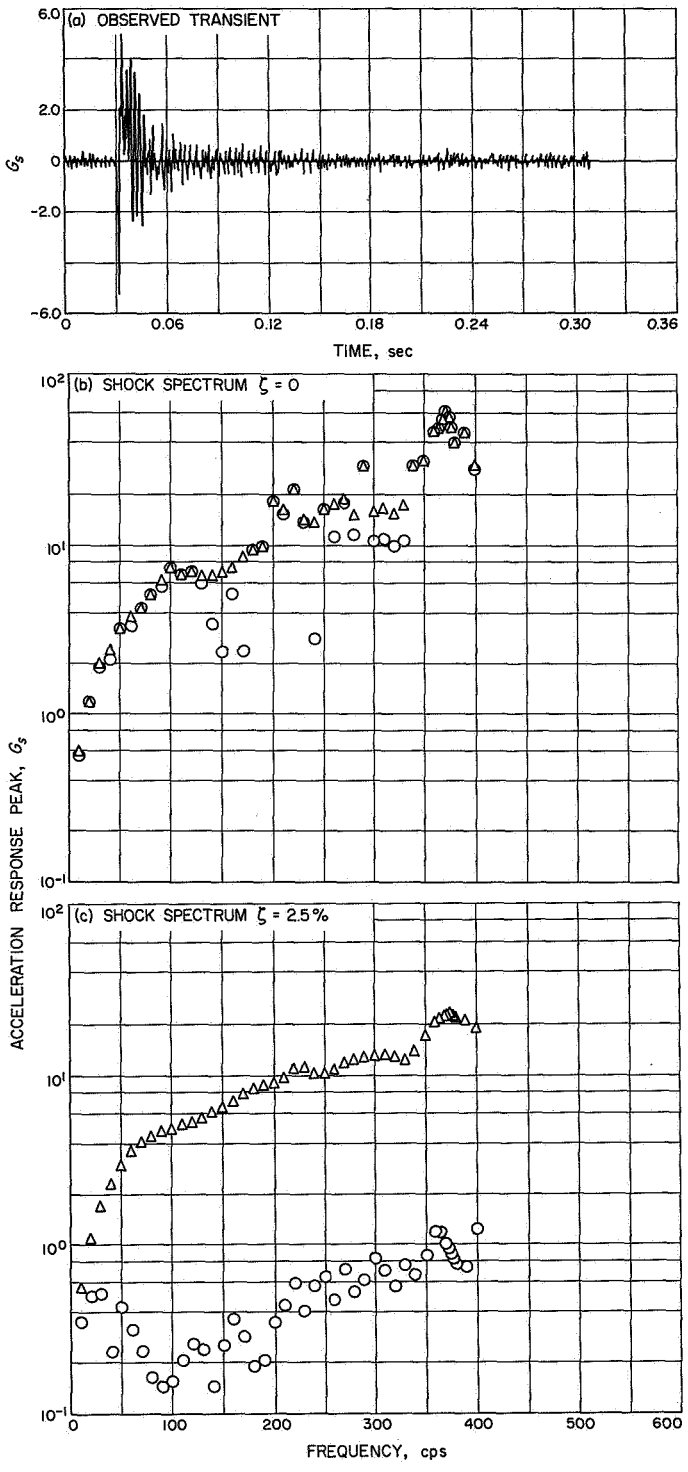


**Fig. 47. Shock spectra for Channel 11 at jettison of horizon sensor fairings**

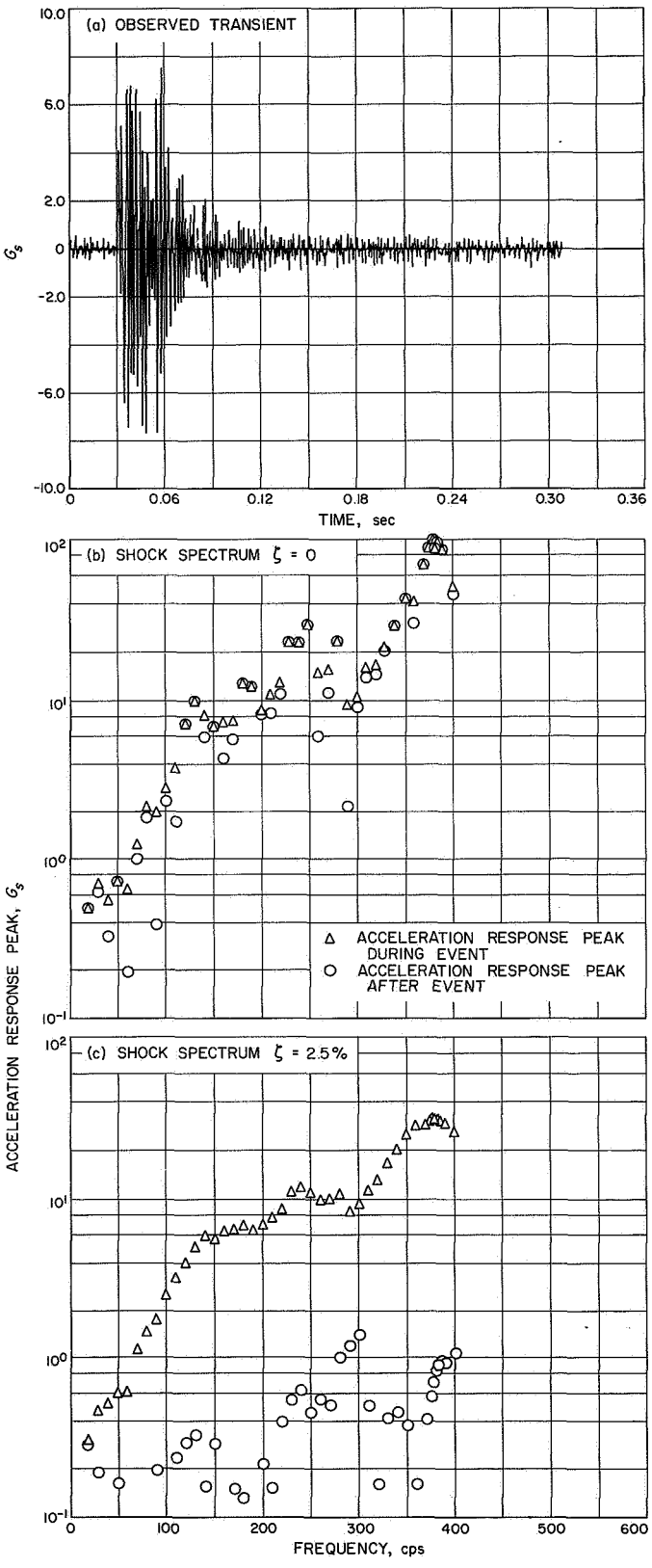


**Fig. 48. Shock spectra for Channel 12 at jettison of horizon sensor fairings**

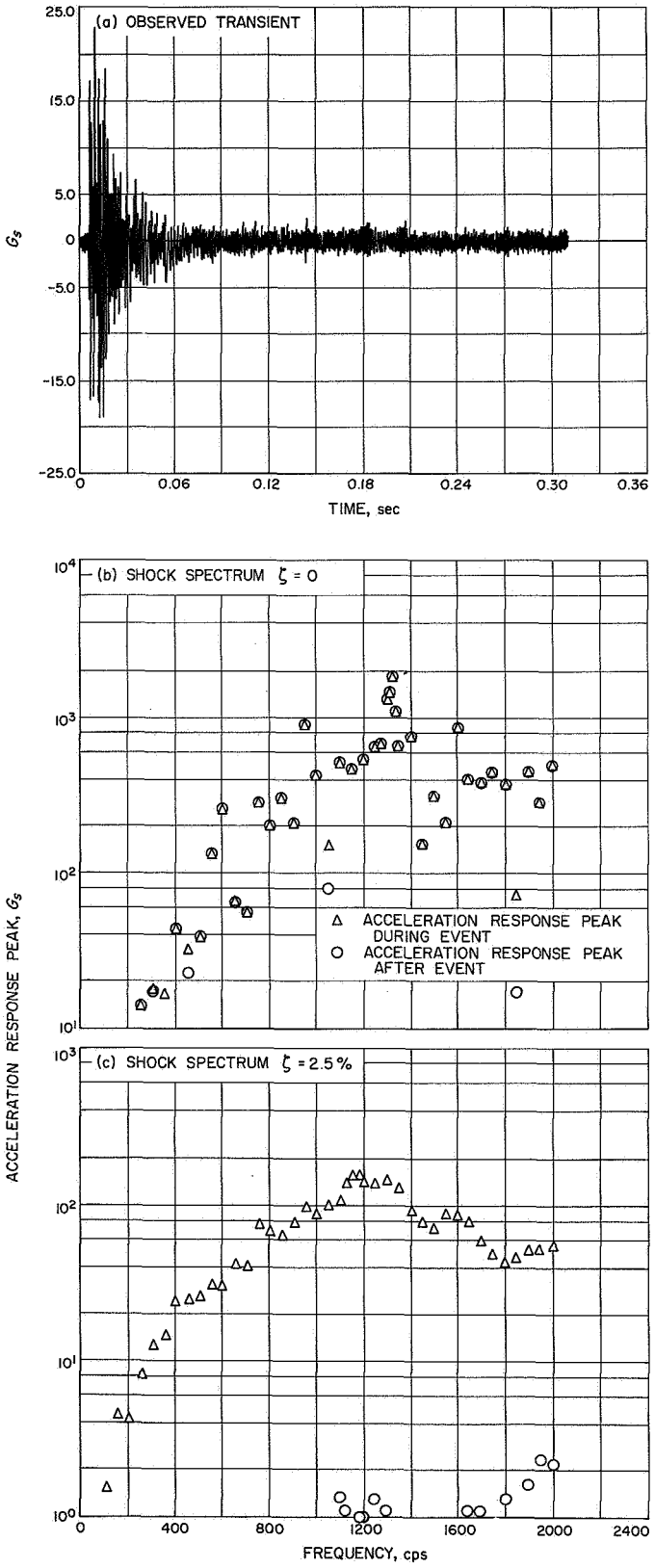


**Fig. 49. Shock spectra for Channel 17 at jettison of horizon sensor fairings**

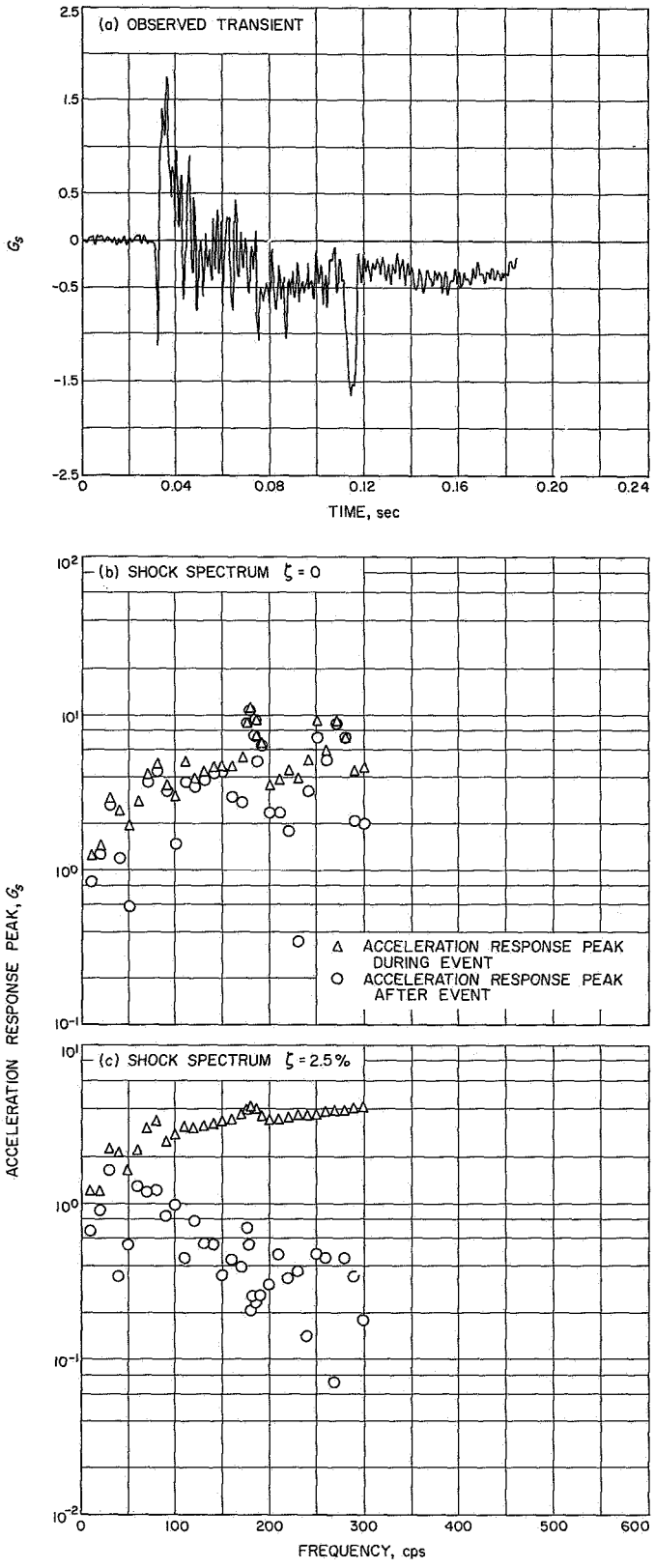
(a) OBSERVED TRANSIENT
$G_s$
TIME, sec
(b) SHOCK SPECTRUM $\zeta = 0$
(c) SHOCK SPECTRUM $\zeta = 2.5\%$
ACCELERATION RESPONSE PEAK, $G_s$
Δ ACCELERATION RESPONSE PEAK DURING EVENT
○ ACCELERATION RESPONSE PEAK AFTER EVENT
FREQUENCY, cps

**Fig. 50. Shock spectra for Channel 10 at shroud ejection**

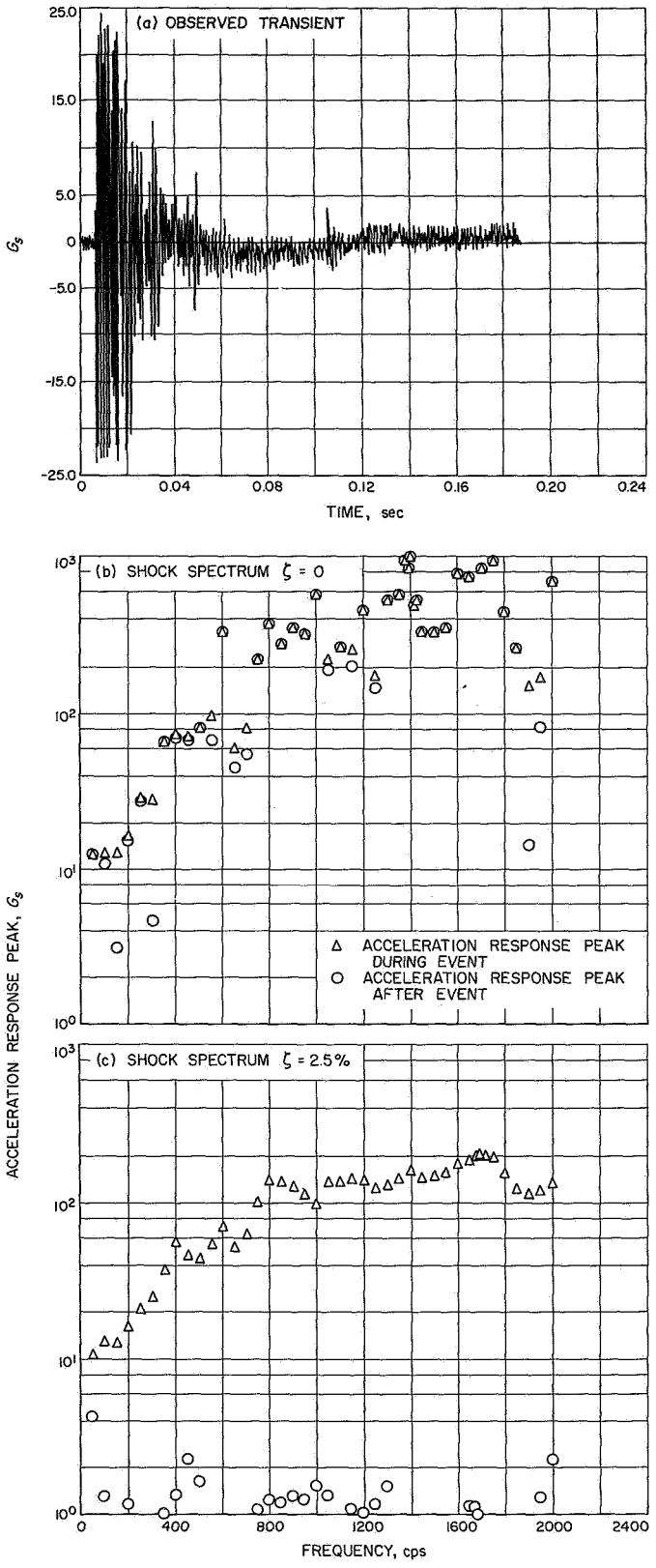
(a) OBSERVED TRANSIENT
$G_s$
TIME, sec
(b) SHOCK SPECTRUM $\zeta = 0$
(c) SHOCK SPECTRUM $\zeta = 2.5\%$
ACCELERATION RESPONSE PEAK, $G_s$
Δ ACCELERATION RESPONSE PEAK DURING EVENT
○ ACCELERATION RESPONSE PEAK AFTER EVENT
FREQUENCY, cps

**Fig. 51. Shock spectra for Channel 17 at shroud ejection**

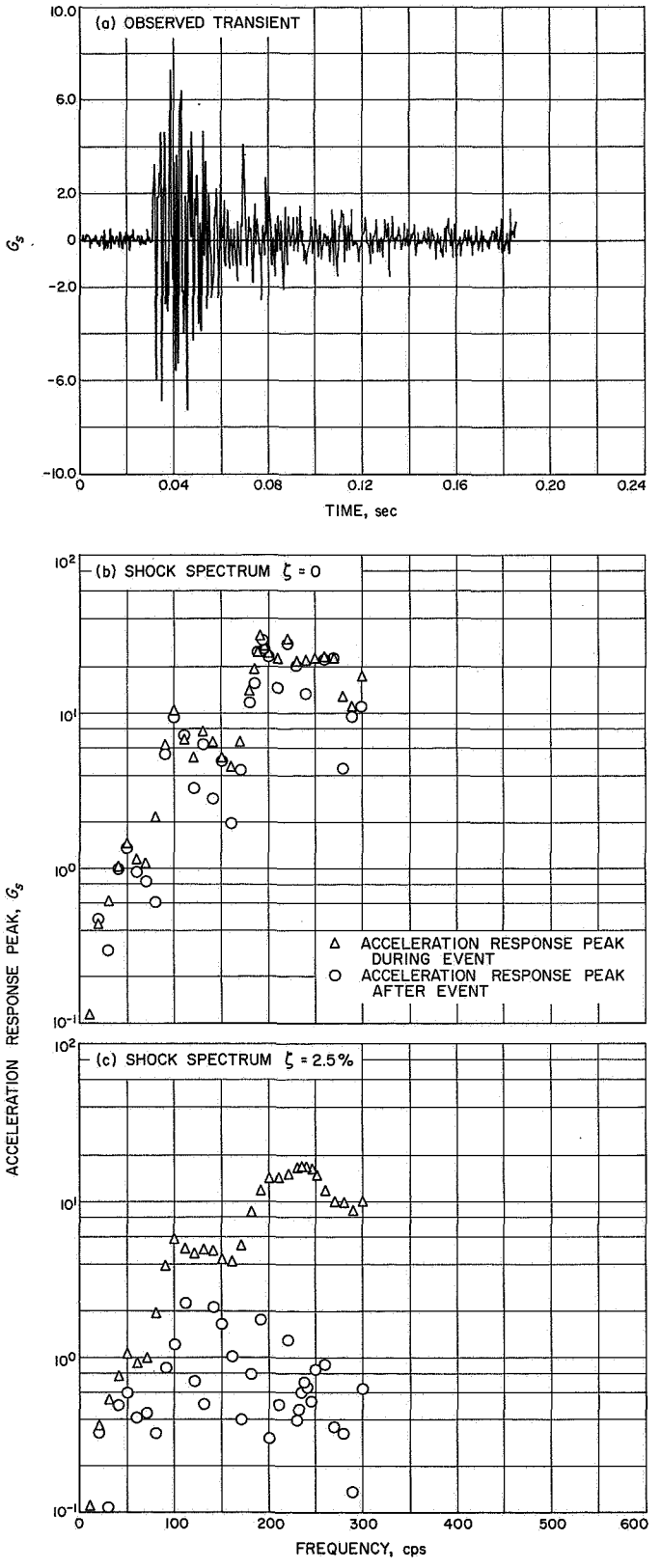


**Fig. 52. Shock spectra for Channel 12 at *Atlas–Agena* separation**

# IV. ACOUSTIC DATA

## A. Flight Microphone

Sound-pressure data was obtained from prior to launch until shroud jettison. The magnetic-tape data were reduced by the following techniques: (1) direct-write, (2) band-pass filters (100-cps band-pass filters with averagers from 10 to 2,000 cps), and (3) tape-loop spectral analyses (using 13.5 or 13.8 and 105 cps analysis filters). Wide-band pressure level (20–2,000 cps) is plotted vs time in Fig. 6. Wide-band sound-pressure levels at significant flight times are shown in Table 2.

Direct-write displays of representative portions of the acoustic data during lift-off and during transonic flight are shown in Figs. 30 and 31. Power spectral-density plots of the Channel 18 data, using an analysis filter bandwidth of about 13.5 cps, are given in Figs. 53 through 58.

The flight times analyzed are: Lift-off, 380-cps vibration, transonic flight, 87.5–89.5 sec, 113.5–115.5 sec, and a pre-flight quiet time. Pressure spectrum-level plots of the same flight times were obtained with a 105-cps analysis filter and are given in Figs. 59 through 64.

## B. Umbilical-Tower Microphones

Sound-pressure measurements during lift-off were obtained from two microphones on the platform of the umbilical tower. These data were recorded on magnetic tape and reduced by use of the band-pass filter and tape-loop spectral analyses. The time sample from 0 to 2 sec (referenced to band-pass data analyses) was reduced by tape-loop analysis. Figures 65 and 66 are PSD analyses of the data using a 13.5-cps analysis filter; Figures 67 and 68 are pressure spectrum-level plots of both microphones using a 105-cps analysis filter.

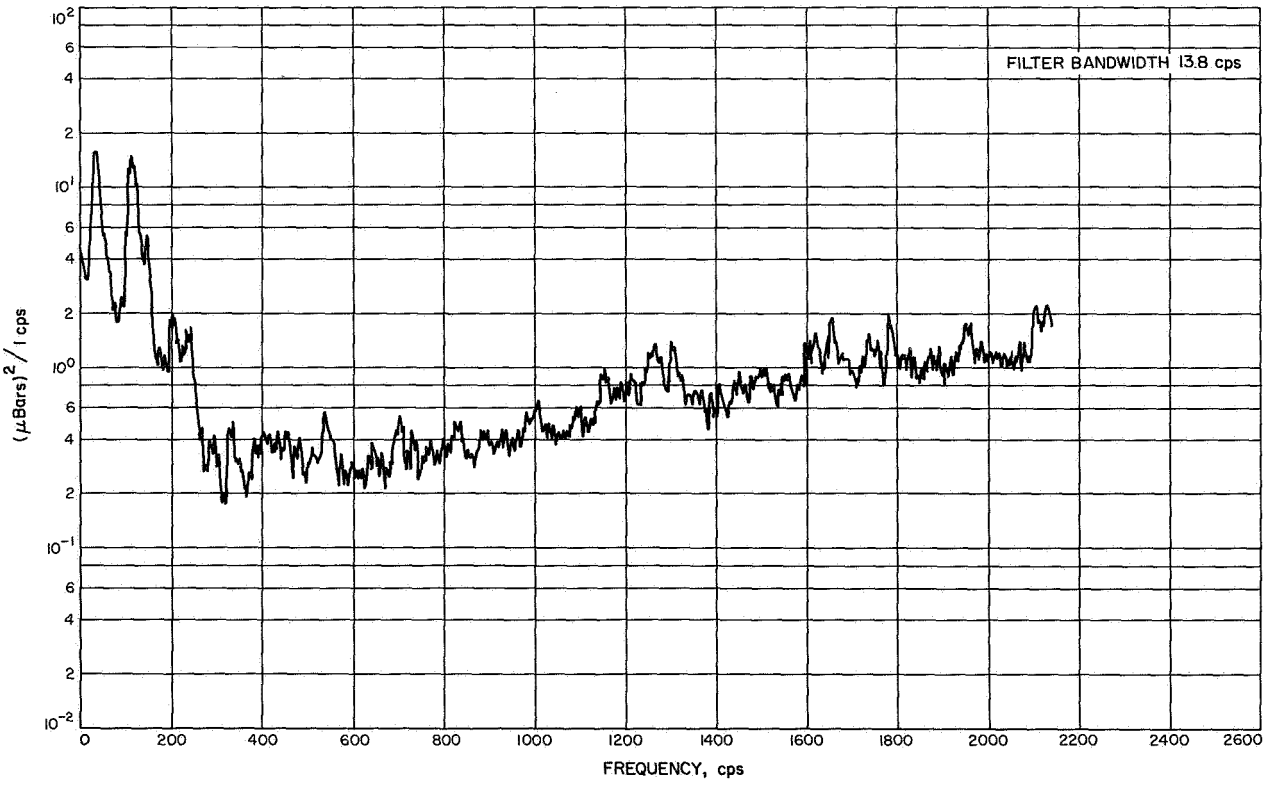


**Fig. 53. Pressure spectral density for flight microphone at pre-flight quiet time**

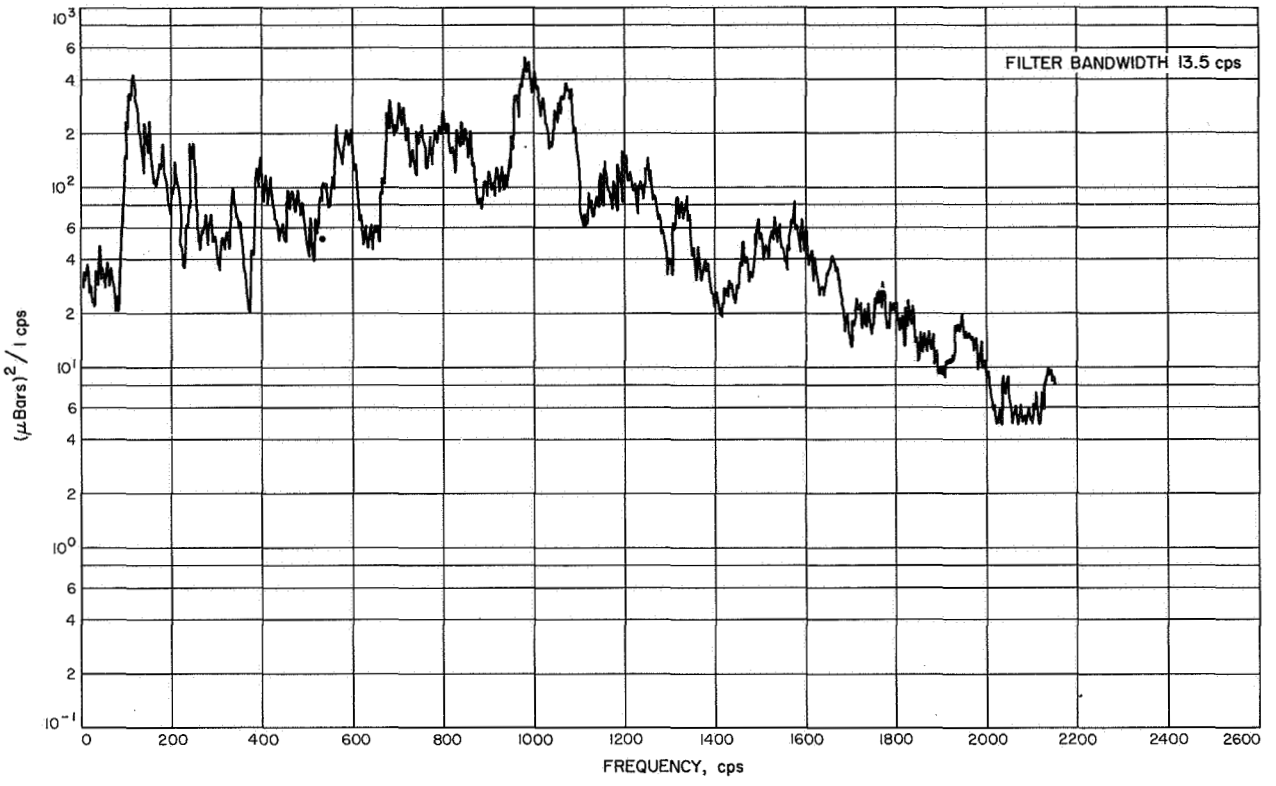


**Fig. 54. Pressure spectral density for flight microphone at lift-off**

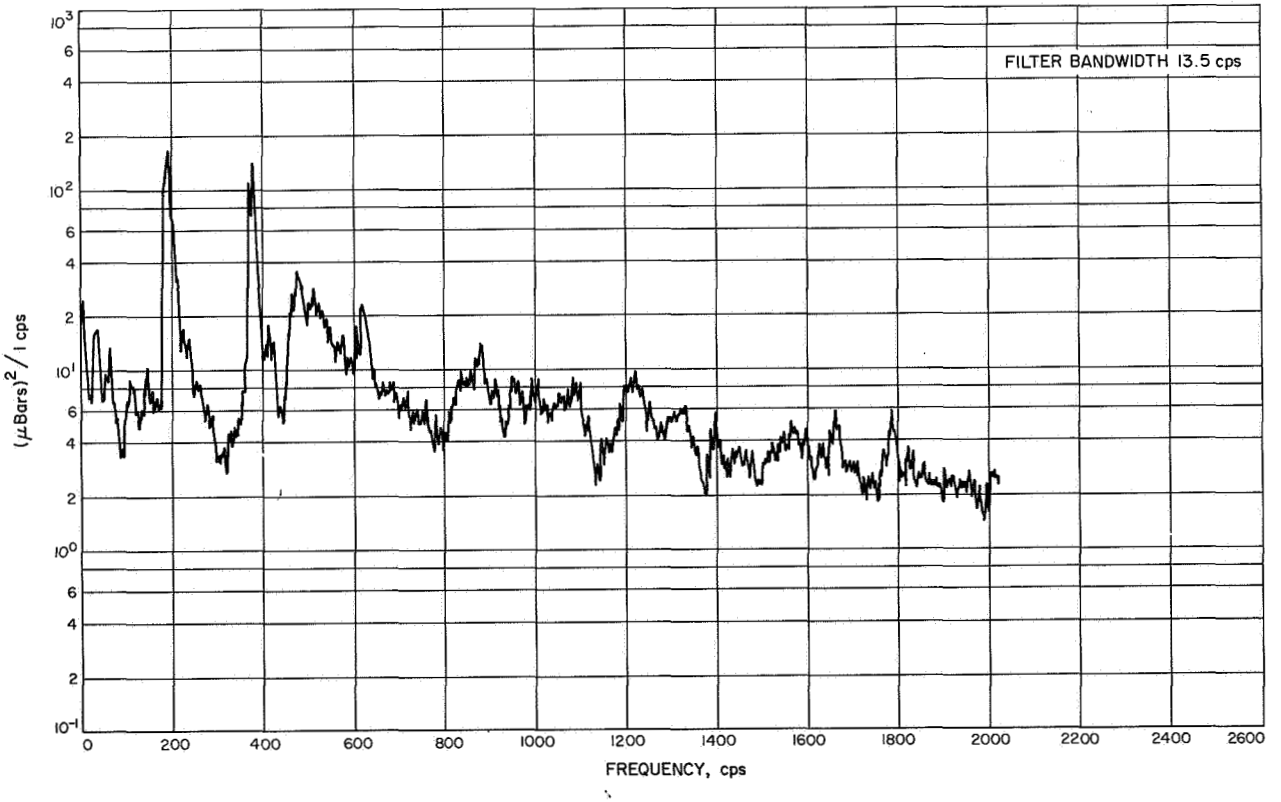


**Fig. 55. Pressure spectral density for flight microphone at 380-cps vibration**

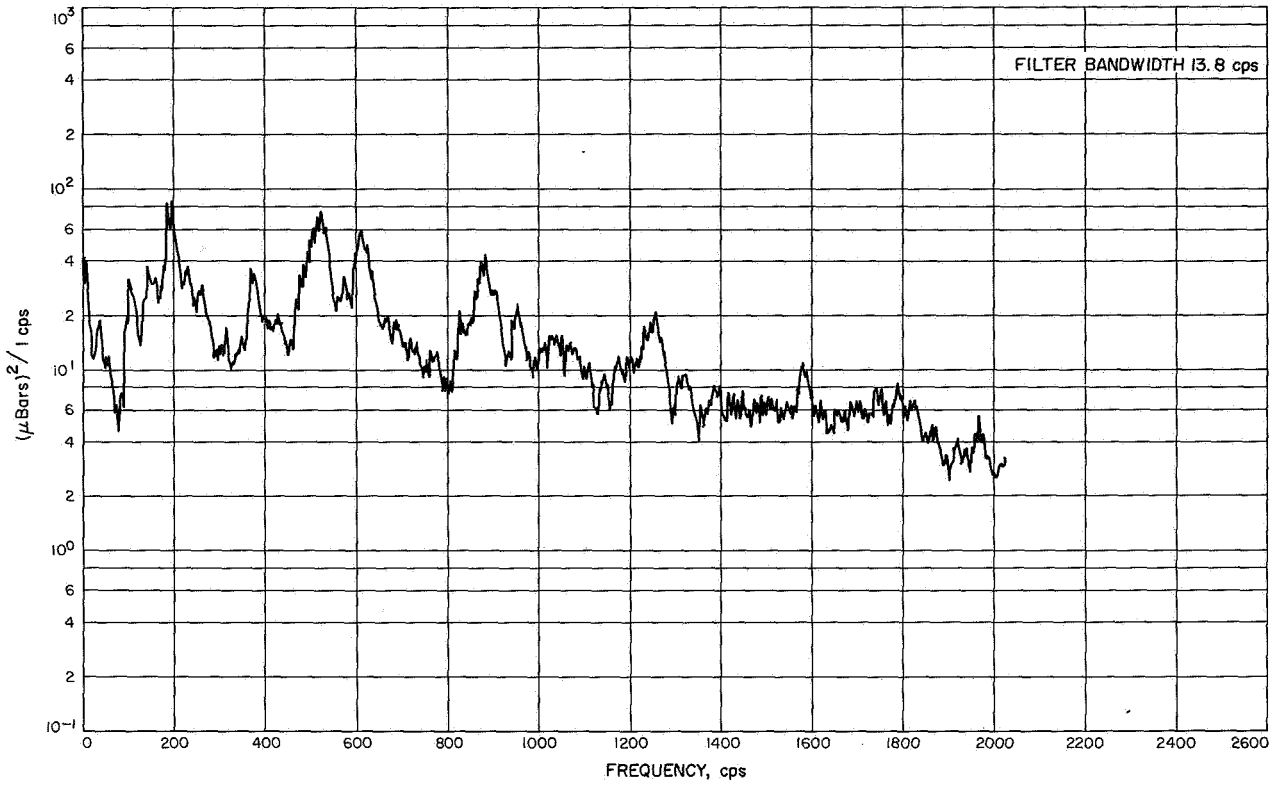


**Fig. 56. Pressure spectral density for flight microphone at transonic flight**

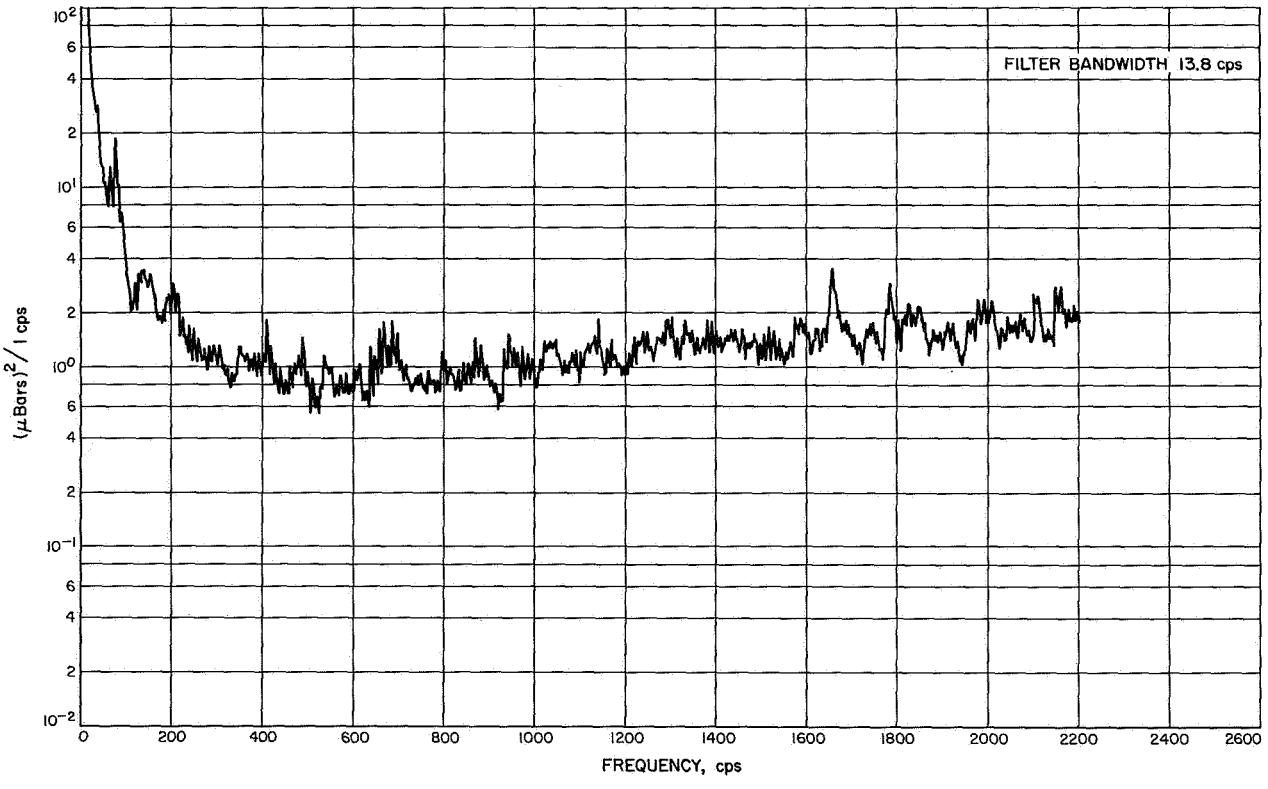


**Fig. 57. Pressure spectral density for flight microphone at 87.5–89.5 sec**

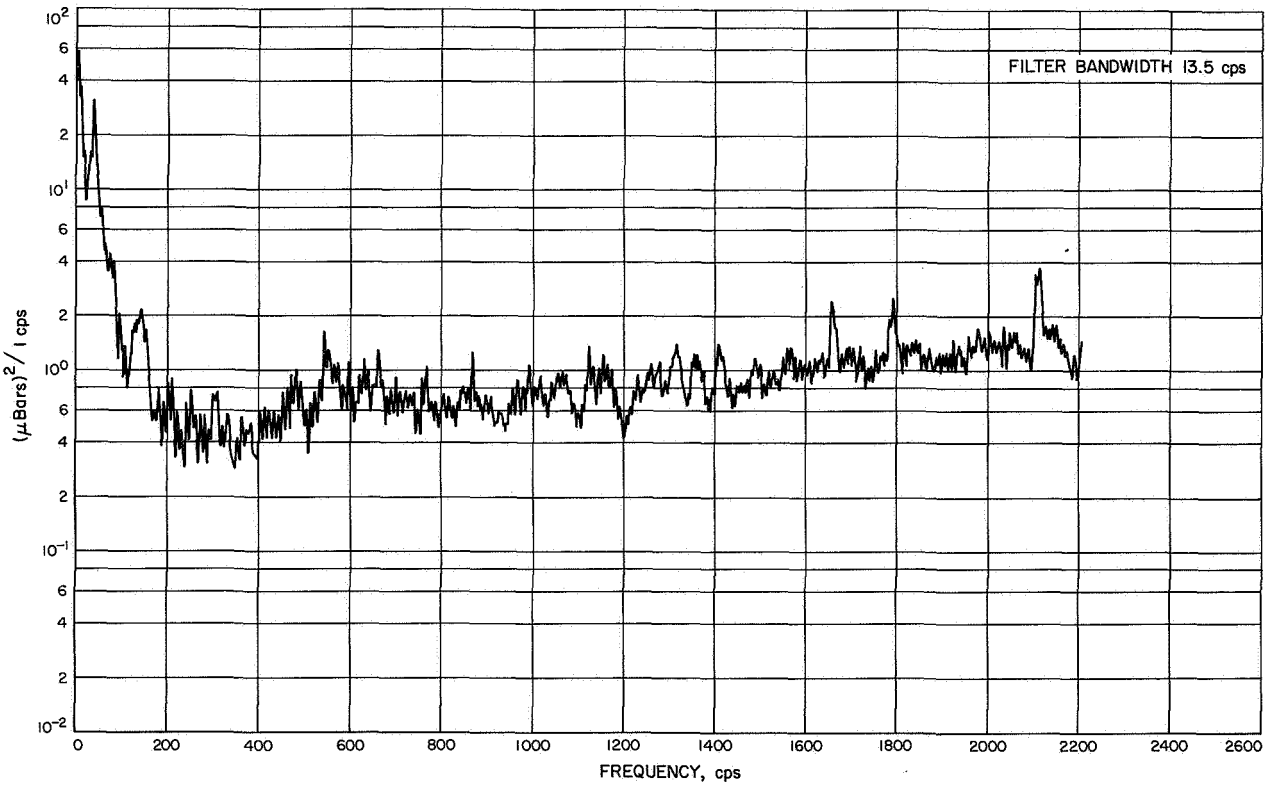


**Fig. 58. Pressure spectral density for flight microphone at 113.5–115.5 sec**

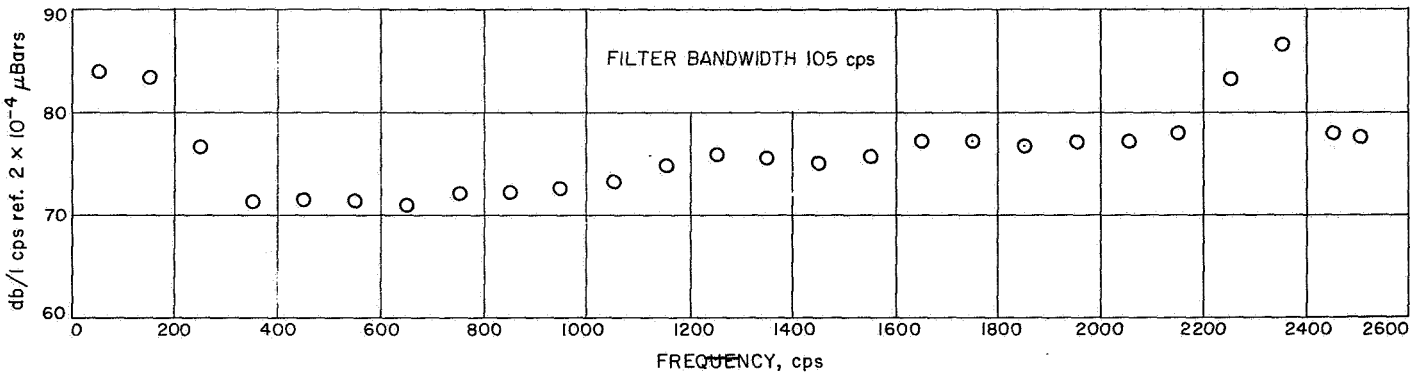


**Fig. 59. Sound-pressure spectrum level for flight microphone at pre-flight quiet time**

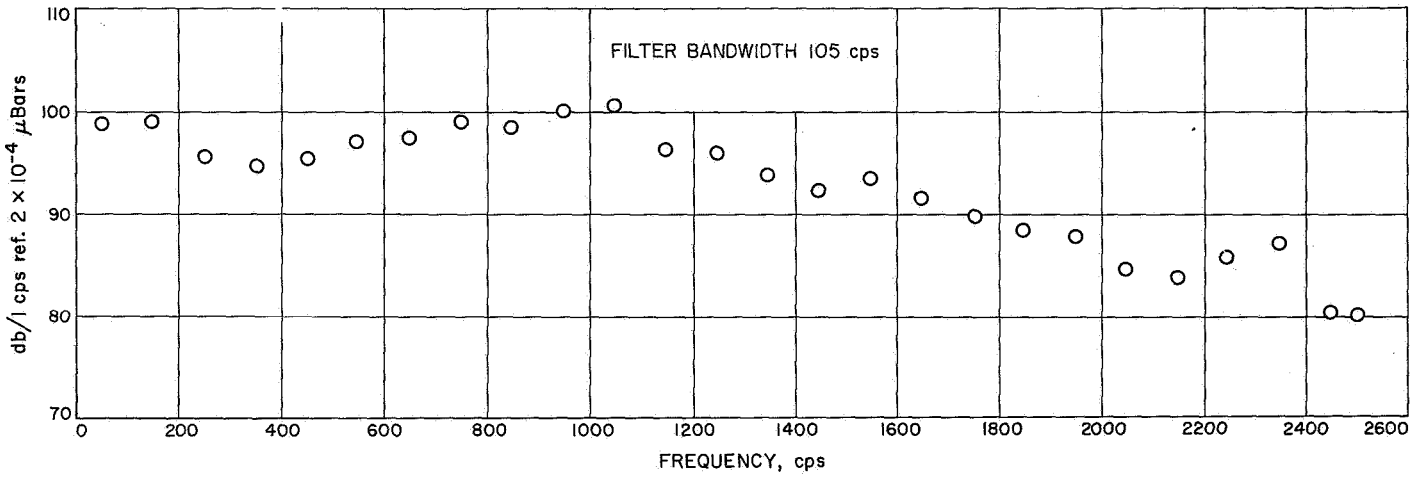


**Fig. 60. Sound-pressure spectrum level for flight microphone at lift-off**

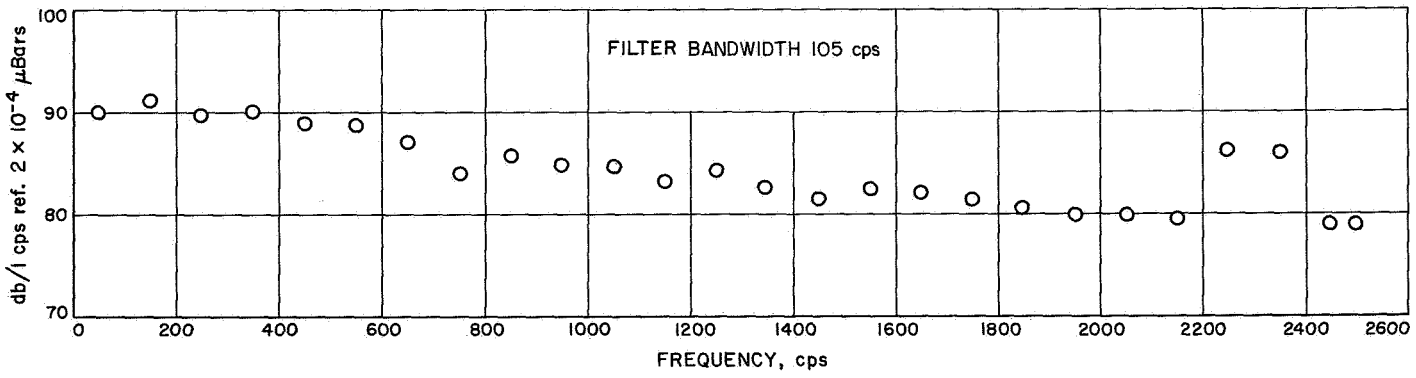


**Fig. 61. Sound-pressure spectrum level for flight microphone at 380-cps vibration**

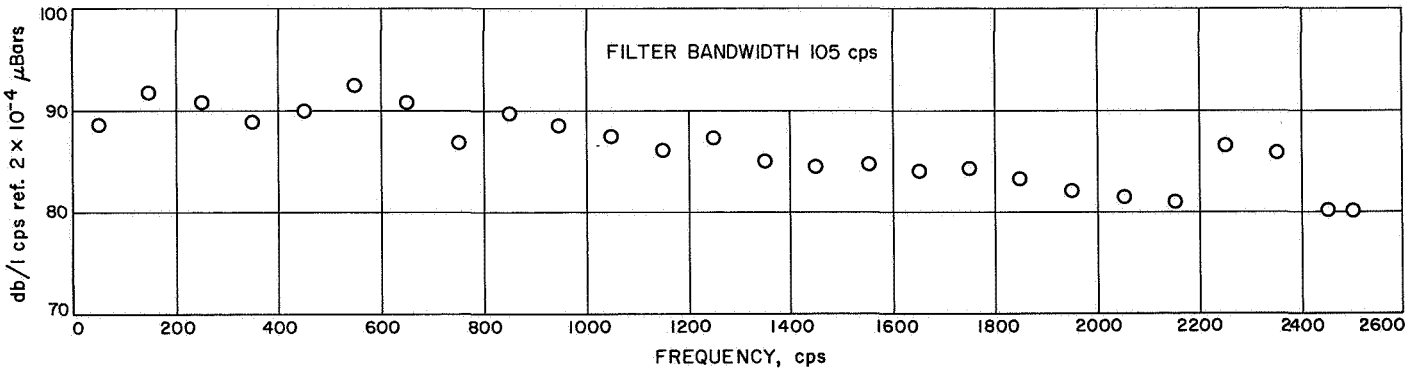


**Fig. 62. Sound-pressure spectrum level for flight microphone at transonic flight**

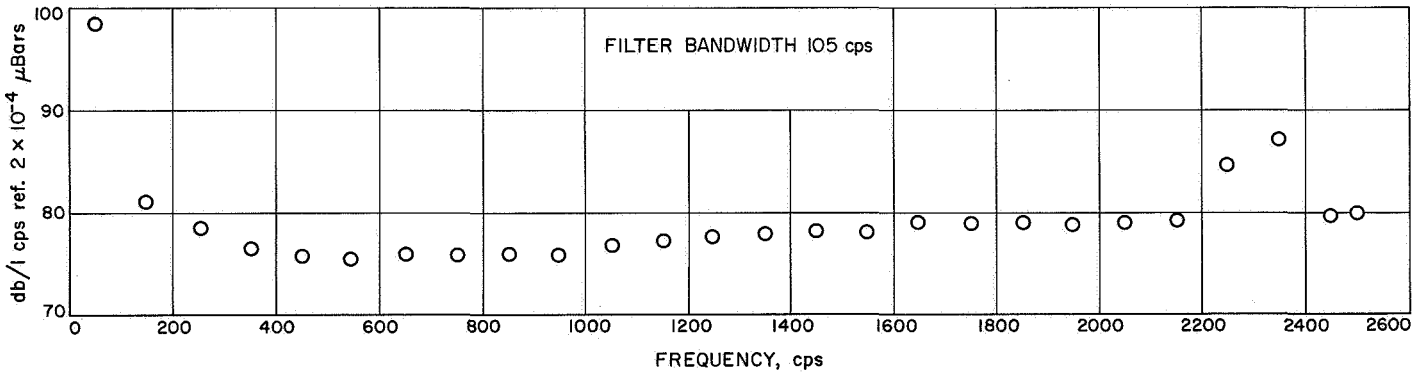


**Fig. 63. Sound-pressure spectrum level for flight microphone at 87.5–89.5 sec**

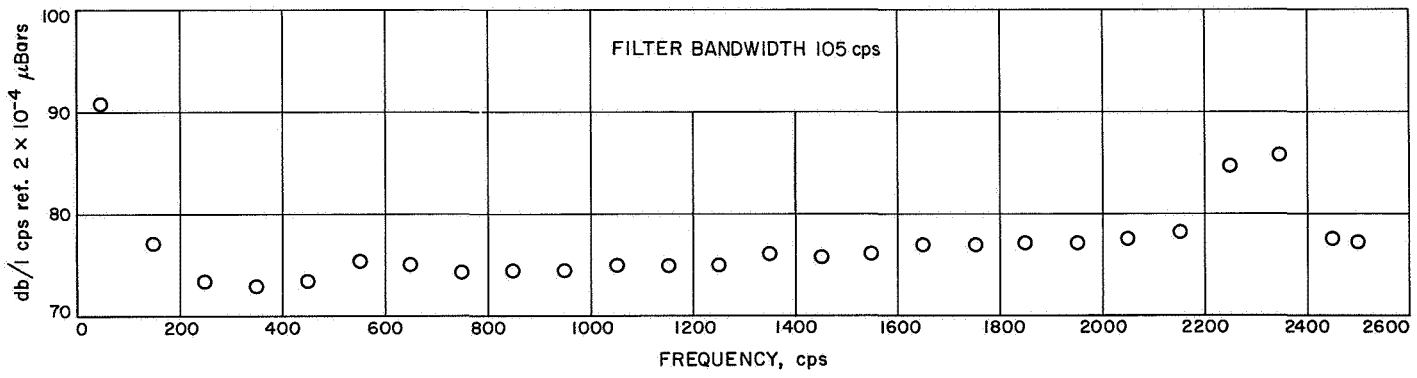


**Fig. 64. Sound-pressure spectrum level for flight microphone at 113.5–115.5 sec**

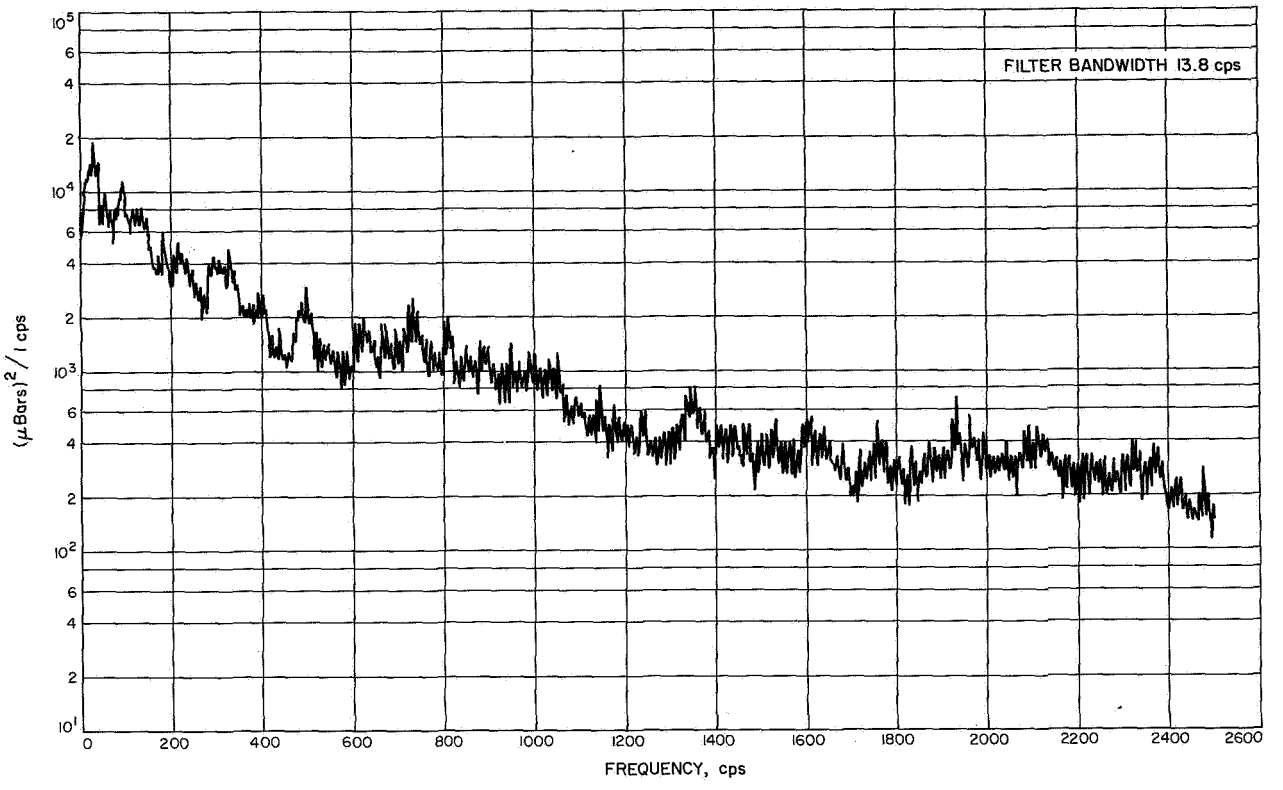


**Fig. 65. Pressure spectral density for umbilical-tower microphone No. 1 at lift-off**

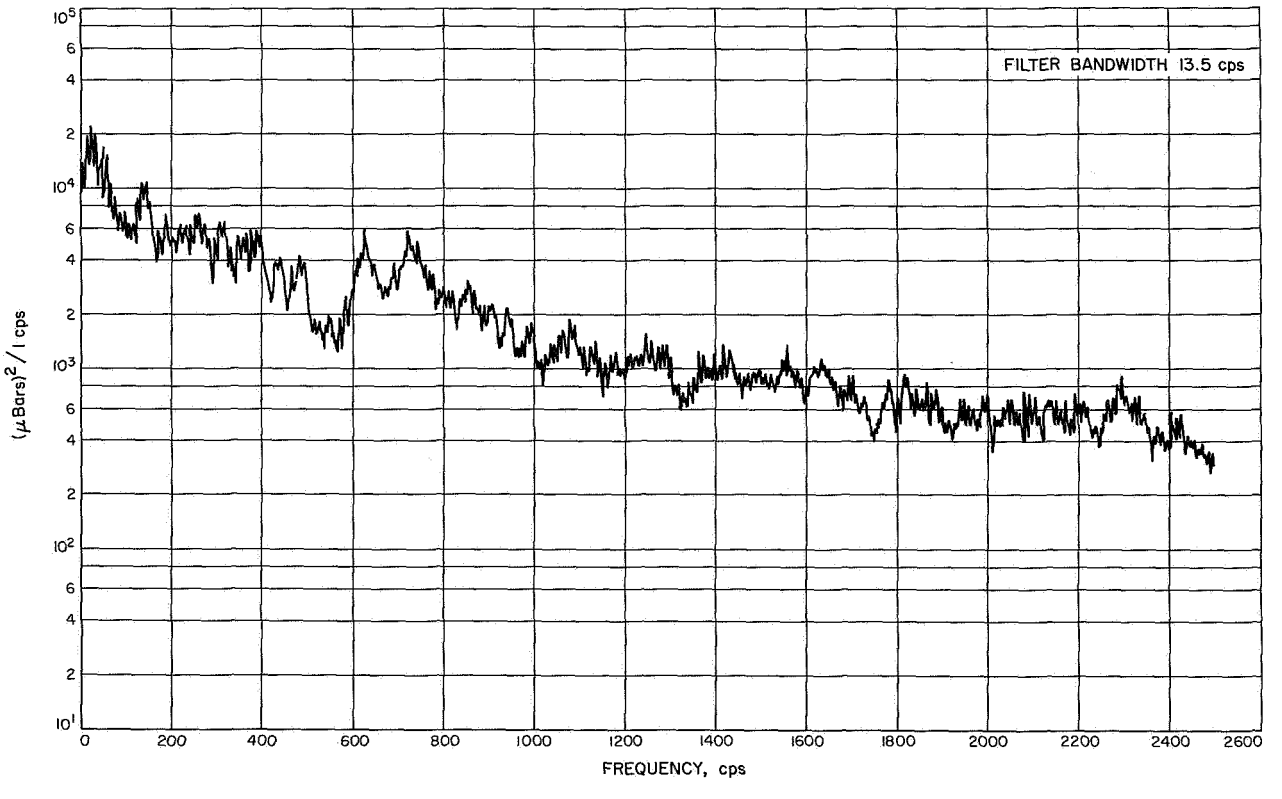


**Fig. 66. Pressure spectral density for umbilical-tower microphone No. 2 at lift-off**

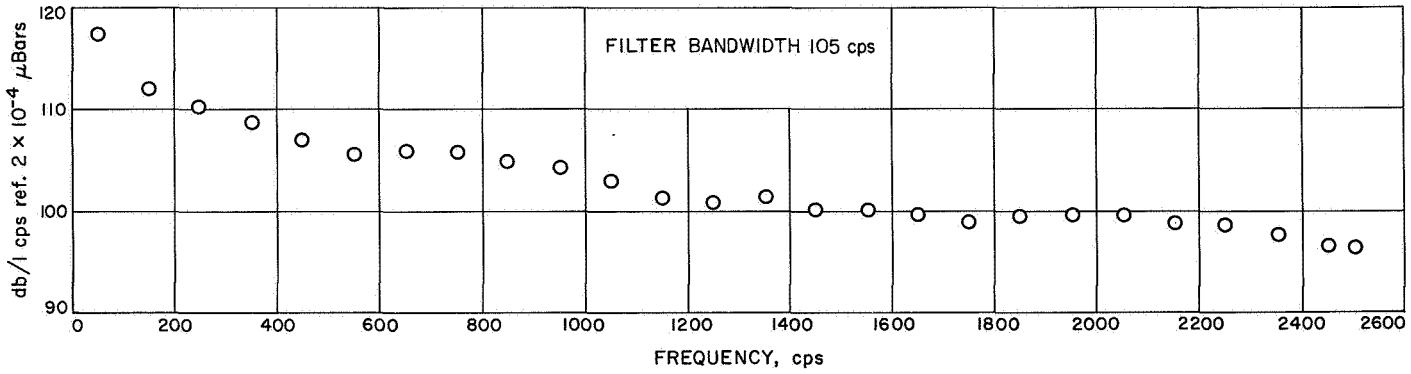


**Fig. 67. Sound-pressure spectrum level for umbilical-tower microphone No. 1 at lift-off**

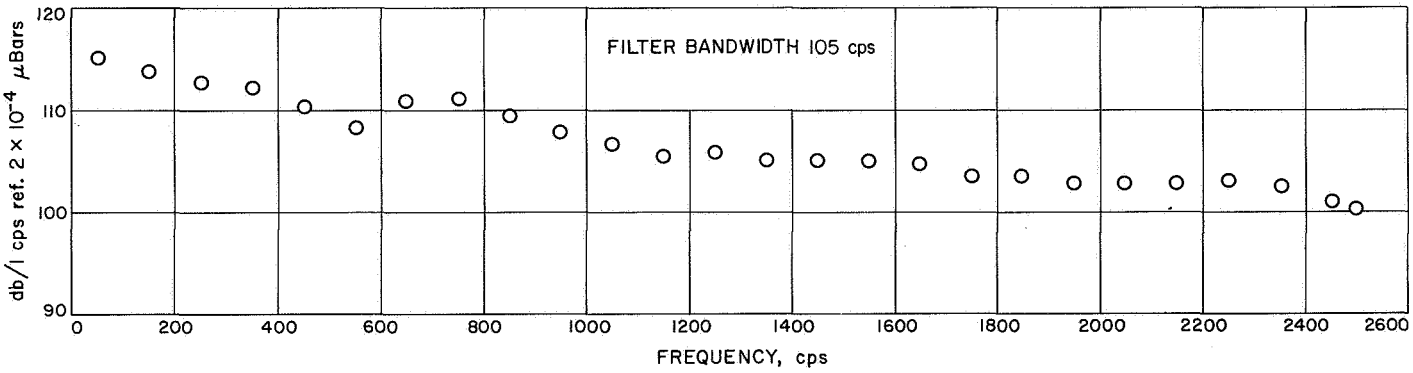


**Fig. 68. Sound-pressure spectrum level for umbilical-tower microphone No. 2 at lift-off**

# V. DISCUSSION

## A. High-Frequency Vibration

Measured flight-vibration levels (Channel 17) on *RA-6* were significantly higher than any similar measurements on *Rangers 1* through *4* (*RA 1–4*). The increase was clearly evident during both the lift-off and the transonic flight periods. The five vibration measurements from *RA 1–4* were almost identical in over-all level; *RA-1* had both an axial and a radial measurement, while *RA 2–4* had only radial measurements. For example, the five lift-off maxima over-all vibration levels ranged from 2.1 to 2.3 $g_{rms}$ and the five transonic levels ranged from 3.3 to 4.0 $g_{rms}$. In contrast, the over-all vibration levels measured during the *RA-6* flight were 3.7 $g_{rms}$ at lift-off and 8.2 $g_{rms}$ at transonic flight (Fig. 6). The PSD at lift-off and transonic flight showed the same gross differences (*RA-6* compared with *RA 1–4*). Unlike the over-all vibration levels, the PSD from the *RA 1–4* flights were not overlays, but showed some variation. The PSD data from *RA-6* (Figs. 26 and 28) at lift-off and transonic flight are compared with a statistical analysis (Ref. 2) of the *RA 1–4* data, and the flight acceptance (FA) vibration test used on the *RA-6* spacecraft (Figs. 69 and 70). It can be seen that the measured transonic vibration greatly exceeds

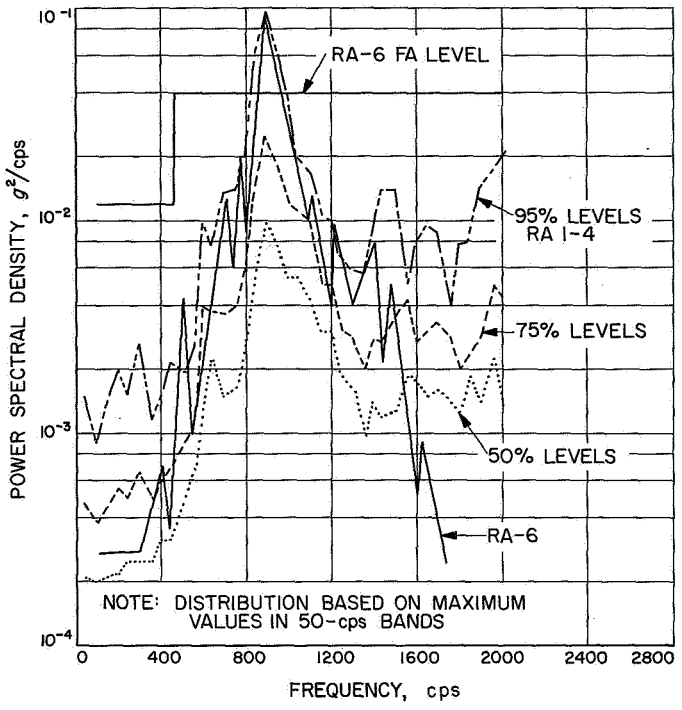


**Fig. 69. Uncorrected *RA-6* flight-vibration data compared with *RA 1–4* flight-vibration data at lift-off**

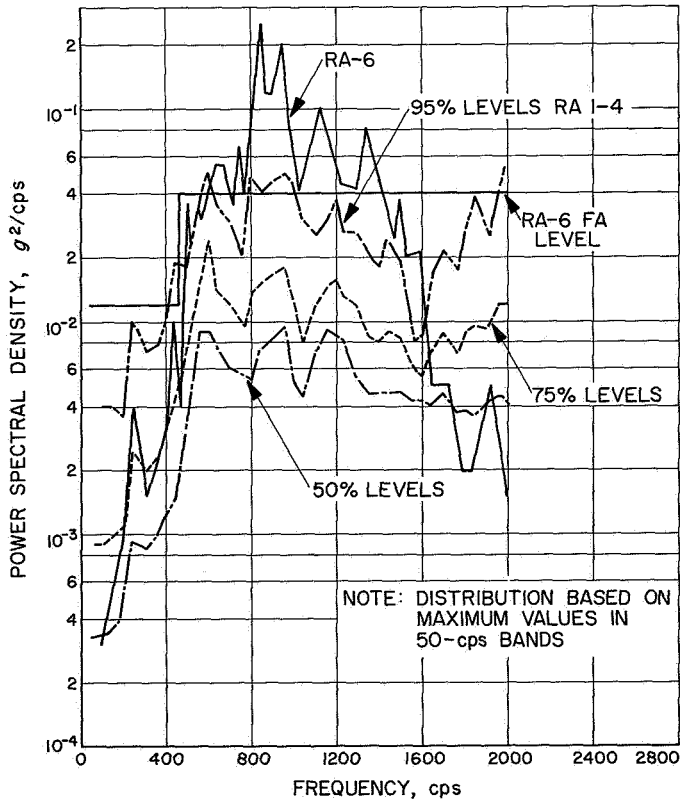


**Fig. 70. Uncorrected *RA-6* flight-vibration data compared with *RA 1–4* flight-vibration data at transonic flight**

both the FA vibration test and the 95% probable vibration levels from the statistical analysis over a large range of frequencies. The lift-off vibration approximates the *RA 1–4* 95% probable vibration levels. This sudden increase in the level of over-all measured vibration and the broad spectral increase in PSD were not anticipated since there should be no gross change in the over-all energy of the basic source of the vibration-excitation mechanism. The acoustic-noise field from rocket motor noise at lift-off and the quasi-acoustic-noise field caused by buffet at transonic flight are the basic sources of the measured flight vibration; neither source should change significantly in energy level, because both the launch-pad characteristics controlling lift-off acoustics (flame deflection, rocket jet-stream power, etc.) and the spacecraft geometry and flight characteristics controlling transonic buffet (external spacecraft geometry, dynamic pressure, etc.) should not have been significantly different on *RA-6*. A large increase in vibration level both at lift-off and at transonic flight emphasizes the fact that some change in the sensitivity of the flight accelerometer to the acoustic excitation must have been responsible for the higher measured vibration, since these phenomena have unrelated sources.

Changes which might have affected measurements on *RA-6* other than structural changes are: (1) that the structure and the location of the mounting block holding the high-frequency flight accelerometer were changed, or (2) that the sterilization diaphragm used on *RA 1–5* was removed on *RA-6*. The mounting block and location for the *RA-6* accelerometer are shown in Fig. 4. The mounting block and location for the *RA 1–4* radial accelerometers (with no diaphragm) are shown in Fig. 71. The differences are evident from the photographs; the *RA-6* block was placed lower on the porkchop fitting, and it carried two cylindrical Statham low-frequency accelerometers (Channels 10 and 12), rather than the rectangular Statham used on *RA 1–4*.

To experimentally evaluate the effect of the mounting block and diaphragm changes on the measured vibration, a special test was conducted. It consisted of placing a 50-in. section of the *Agena* forward-structure with an attached spacecraft adapter into the Jet Propulsion Laboratory (JPL) reverberation chamber. The top of the adapter was plugged with a plywood and fiberglass plate in order to reduce the acoustic field within the adapter—the spacecraft and shroud would do this in flight. The acoustic field within the chamber was then brought up to 142 db (ref. $2 \times 10^{-4}$ $\mu$bar), and the outputs of the flight accelerometer and a microphone on the outside of

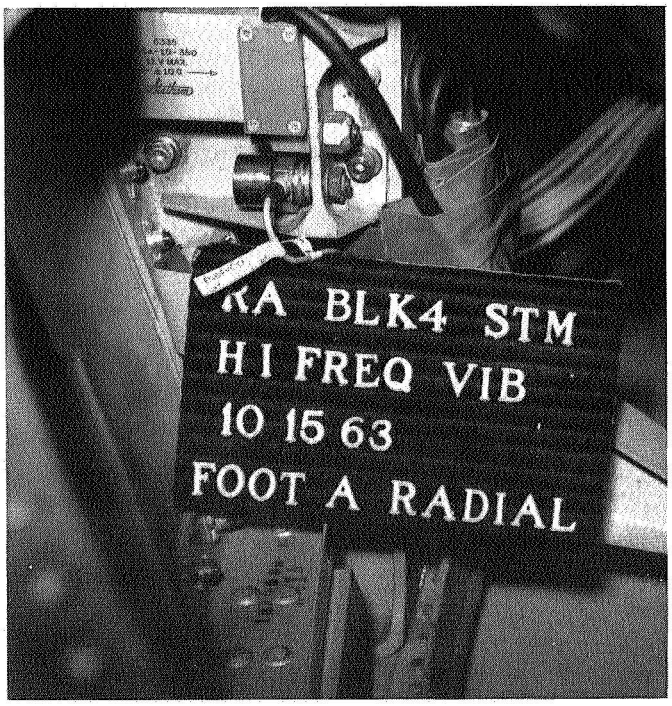


**Fig. 71. *RA 1–4* flight-accelerometer mounting block**

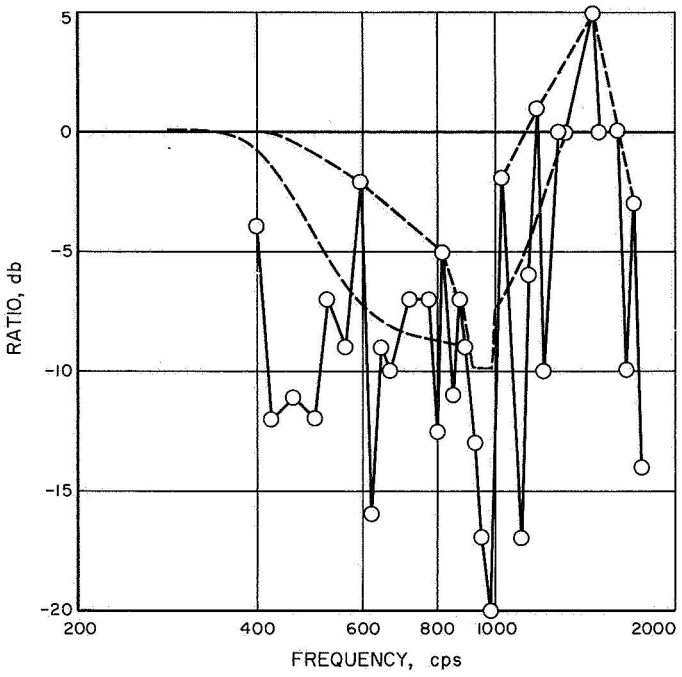


**Fig. 72. Ratio of flight-accelerometer acoustic susceptances, *RA 1–4* to *RA-6***

the adapter, near the flight accelerometer, were recorded. The test was repeated four times with the following mounting-block-diaphragm configuration:

1. *RA 1–4* mounting block, no diaphragm
2. *RA-6* mounting block, no diaphragm
3. *RA 1–4* mounting block, with diaphragm
4. *RA-6* mounting block, with diaphragm

For this test, the flight-accelerometer mounting block was always mounted at the spacecraft *Foot A* location. In order to compare the *RA 1–4* and *RA-6* measured flight vibration, the acoustic susceptances (ratio of vibration level to acoustic pressure level) were calculated for the *RA 1–4* flight configuration (*RA 1–4* mounting block with diaphragm) and the *RA-6* flight configuration. (*RA-6* mounting block, no diaphragm). Figure 72 shows the ratio of these two susceptances plotted vs frequency.

The *RA 1–4* configuration is seen to have a lower susceptance in the 400- to 1,000-cps area and a higher susceptance in the 1,000- to 1,600-cps area. This would indicate that the *RA-6* configuration should measure a higher vibration level in the 400–1,000-cps frequency range than the *RA 1–4* configuration with an identical acoustic excitation. Conversely, the *RA 1–4* configuration would measure a higher value in the 1,000–1,600-cps region. The data from Fig. 72 could then be used to convert the *RA-6* flight data to that which would have been measured if an *RA 1–4* flight accelerometer and diaphragm had been used. The corrected data would then have to be used as a basis for comparison with the *RA-6* vibration test levels, since the basic spacecraft and assembly tests were determined from the *RA 1–4* flight vibration data and transfer functions using the *RA 1–4* flight-accelerometer mount as a reference point.

Two correction curves were used (Fig. 72). The *RA-6* PSD data were corrected by multiplying the measured PSD data by both corrections. The upper correction curve results in the least decrease in *RA-6* data in the 400–1,000-cps region, and the most increase in *RA-6* data in the 1,000–1,600-cps region, and is, therefore, the most conservative correction. The lower curve, drawn through a mean value of the fluctuating curve, is an estimate of a mean correction. The corrected *RA-6* lift-off and transonic data (using both the conservative and mean corrections) are compared with the 95%-probability data from *RA 1–4* (Figs. 73 and 74). The corrected lift-off measurement falls well within the *RA 1–4* 95% level except for the conservative correction between 1,200 and 1,400 cps. The corrected transonic measurement falls within the *RA 1–4* 95% levels up to 1,000 cps, but both the conservative and mean corrections are higher above 1,000 cps.

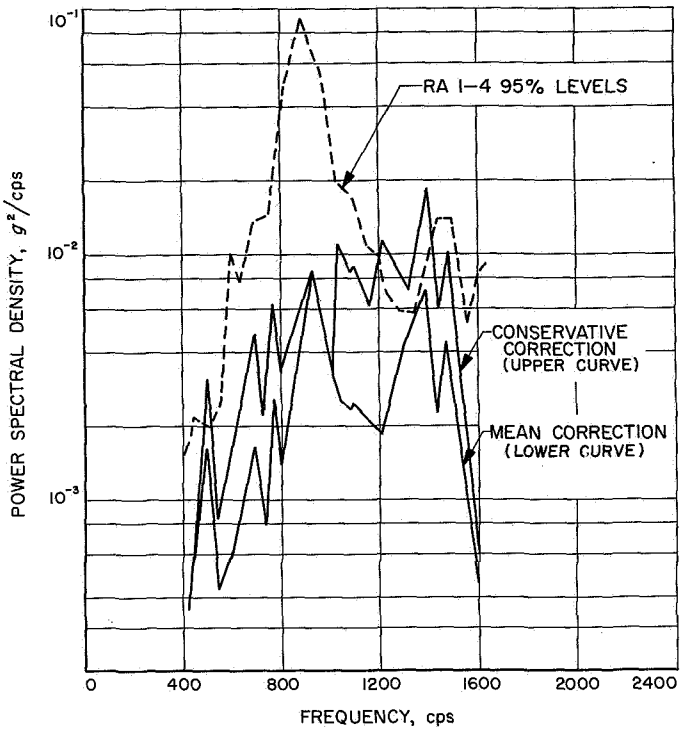


**Fig. 73. Measured *RA-6* flight vibration corrected to *RA 1–4* flight accelerometer at lift-off**

To have a basis for comparison with the actual FA vibration test to which the *RA-6* spacecraft was actually tested, it is further necessary to adjust the *RA-6* flight-location data to the spacecraft feet, since the FA vibration-test input was directly at the feet. Gains from the flight location (*RA 1–4* mounting block) are available (Ref. 2). These are the maximum (least attenuation) results of both vibration tests and acoustic tests. The corrected transonic-flight data (Fig. 74) were adjusted to the spacecraft feet, as shown in Fig. 75. For comparison, the *RA-6* FA specified-test spectrum is also shown. It may be seen that the mean-corrected data are completely covered by the test; two narrow peaks of the conservatively corrected data exceed the test level at 840 and 1,100 cps.

The adequacy of the assembly-test levels is qualified by (1) the comparison of the spacecraft FA test levels with the flight data corrected to the *RA 1–4* mounting block, and adjusted to the spacecraft feet, and (2) comparison of the corrected measured-flight vibration on *RA-6* with the flight data from *RA 1–4*.

Measurements of the actual tests performed on the *RA-6* flight vehicle are compared with the specified-test

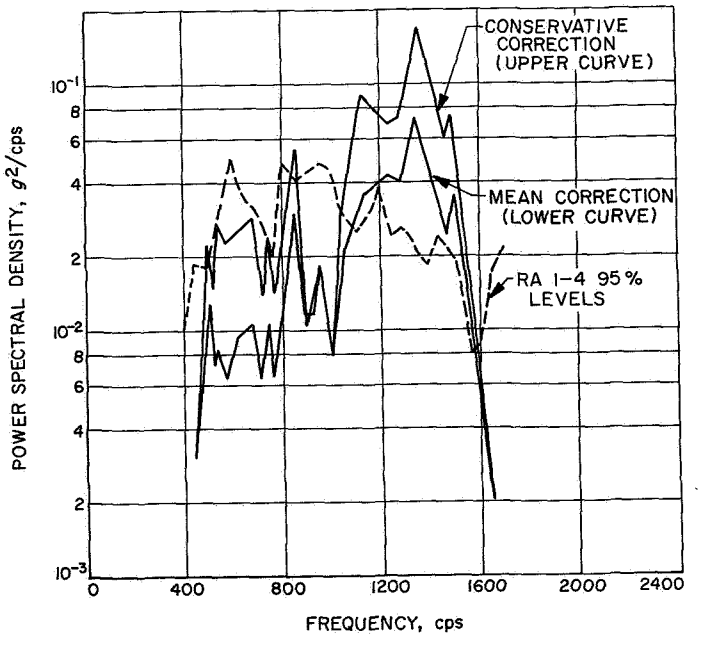


**Fig. 74. Measured *RA-6* flight vibration corrected to *RA 1–4* flight accelerometer at transonic flight**

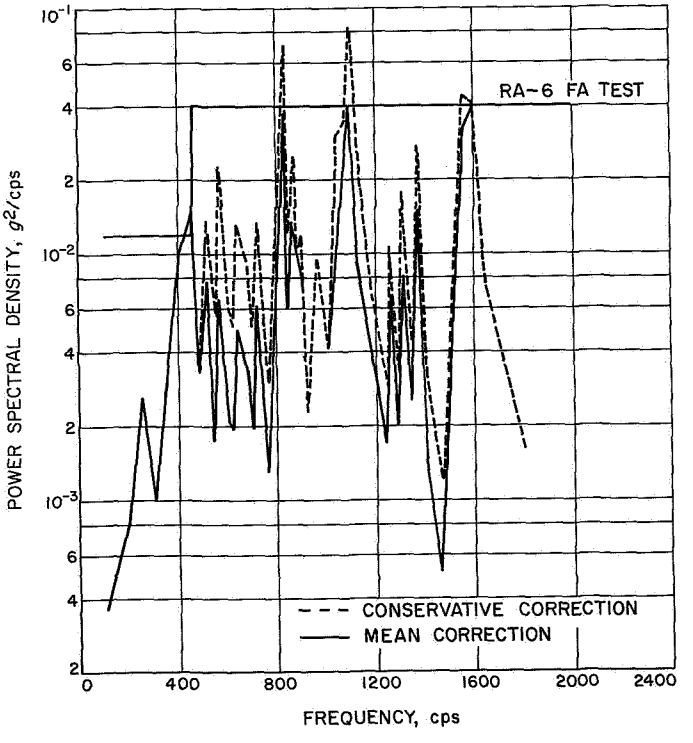


**Fig. 75. Transonic flight vibration adjusted to spacecraft feet**

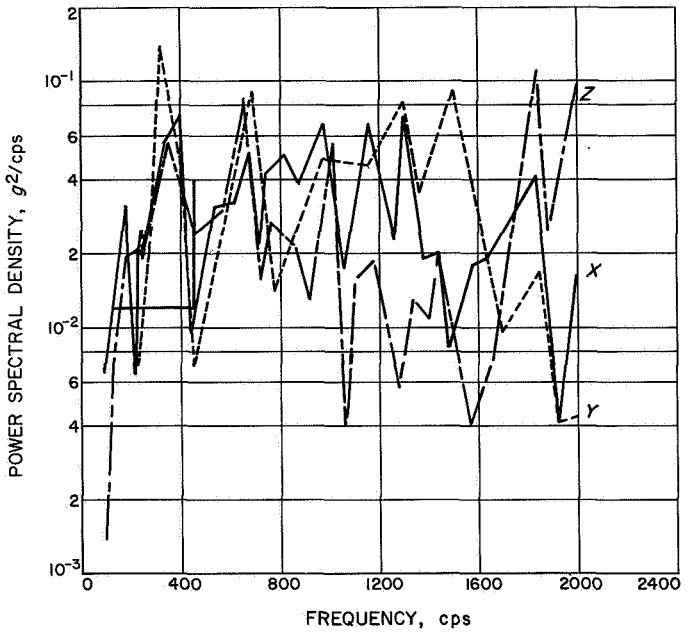


**Fig. 76. *RA-6* specified flight-acceptance test spectrum compared with actual test spectra**

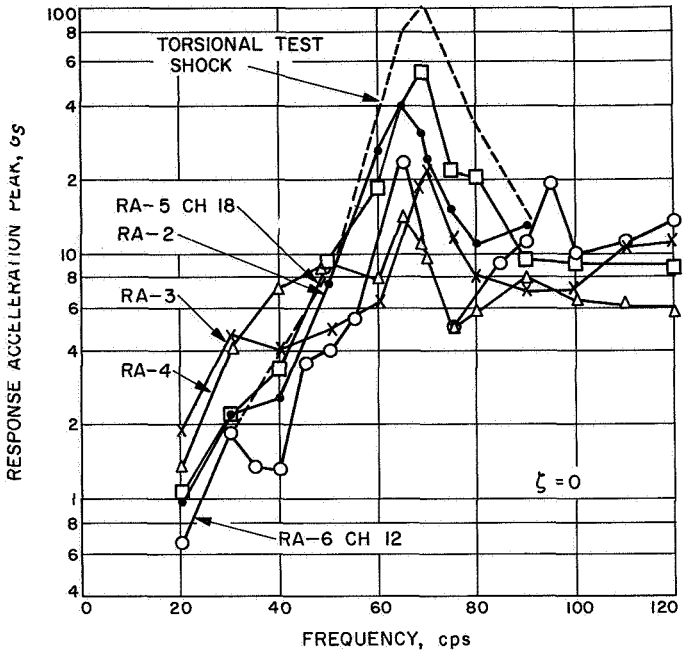


**Fig. 77. Shock spectra of BECO transient for *RA-2, 3, 4, 5, 6***

spectra in Fig. 76. It may be seen that the actual-test spectra in the *X*, *Y* and Z axes vary from the specified test as much as the corrected *RA-6* flight data. The test input on the Figure is actually a composite rms sum of the inputs at the six spacecraft feet, and each foot may therefore also vary from the indicated test input.

## *B. Low-Frequency Vibration*

### 1. Booster Engine Cut-off Transient

On *Ranger* flights *1* through 5, accelerometers measuring tangential motion have indicated an oscillation at 65 to 70 cps lasting for approximately 0.2 sec during booster shut-down. The peak acceleration observed during this pulse has ranged from 1.5 to 5.0 *g* on various flights. On the *RA-5* flight, the phase relation on opposite sides of the vehicle was monitored, and the motion was verified to be torsional.

On *RA-6*, the characteristic pulse was again observed, this time at 65 cps and ±1.4 *g*. Instrumentation on the booster engines indicated the source of this shock to be thrust oscillation during booster shut-down. This thrust oscillation resulted in a longitudinal vibration of ±22 *g* at the booster gimbal block (Ref. 3). As on *RA-5*, the shock was verified to be primarily a torsional motion, rather than a vehicle bending motion. Shock-spectrum analysis of the BECO pulse was made and is presented in Section III (Figs. 42 and 43). A comparison of the *RA-6* BECO shock spectrum with the spectra of previous BECO shocks and with the torsional test shock is shown in Fig. 77[1]. This Figure shows the maximum response of a single degree-of-freedom system having a natural frequency given on the abscissa to each of the shocks. The details of the mechanism whereby the longitudinal oscillation at the booster couples into torsional motion at the spacecraft are not thoroughly understood; however, it appears reasonable that the degree of coupling may vary from flight to flight.

A second consideration resulting in a lower observed torsional pulse is the possibility that the tangential pickups were near a torsional node on the *RA-6* flight. Structural changes stiffened the Block III spacecraft torsionally, and preliminary investigation has indicated that a torsional node at 69 cps shifts from the spacecraft down into the spacecraft adapter. Further study of this topic is under way.

The torsional test used at JPL consisted of a 69-cps amplitude-modulated sine wave applied with two shakers placed to give an input torsional motion. No torsional test was performed on the *RA-6* flight spacecraft; however, the Block III proof test model (PTM) was subjected

[1]Shock amplitude is 6 *g*, zero-to-peak, for the test spectrum. *RA-6* was not torsionally tested. Block III PTM was tested to a shock having 1.8 times the amplitude of the illustrated shock.

to a torsional test in which the levels were 11 *g* zero-to-peak at the spacecraft feet. The expected 95-percentile level based on the *RA 1–5* flight measurements was 6.7 *g* at the flight-measurement location.

### 2. Radial Vibration

Review of Channel 10 transient data, summarized in Table 3, shows a maximum peak reading of 0.8 *g* zero-to-peak occurring at launch and first *Agena* cut-off. This compares with a 95-percentile level of 0.7 *g* zero-to-peak established from previous flight radial acceleration measurements. Sinusoidal sweep tests on the spacecraft include a 0.5 $g_{rms}$ sweep from 10 to 100 cps and a 1.3 $g_{rms}$ sweep from 100 to 425 cps.

## C. *Acoustic Data*

*Ranger 6* was the first of the Ranger spacecraft to be instrumented for sound-pressure measurements by a microphone within the spacecraft shroud cavity. In addition to this internal microphone, two sound-pressure measurements on the umbilical tower were obtained during the early portion of lift-off. The data from these measurements were presented previously in Section IV.

### 1. Internal Sound-Field Measurement

The flight microphone was located at the inner surface of the shroud on the spacecraft $+X$ axis (between *Feet A* and *B)* at JPL Station 457, as shown in Fig. 3. This location is approximately in the center of the $+X$ solar panel. As can be seen also from the Figure, the microphone is on the side opposite the deflected rocket exhaust and almost at the point nearest to the umbilical-tower microphone. However, ground acoustic tests have shown that even with a more one-sided acoustic excitation than is present at lift-off, the sound field within the spacecraft cavity is fairly uniform. Therefore, it is reasonable to compare the measured flight level with the uniform reverberant-field level used in the bare PTM spacecraft reverberant-chamber acoustic test.

The pressure spectral-level data from Figs. 60 and 62 which were taken at the internal microphone at lift-off and transonic flight were replotted as 1/3-octave sound-pressure-level (SPL) spectra on Fig. 78. Shown for comparison is the SPL spectrum used on the *Ranger* Block III PTM acoustic test. It is evident that the actual flight internal-acoustic field has been more than adequately simulated.

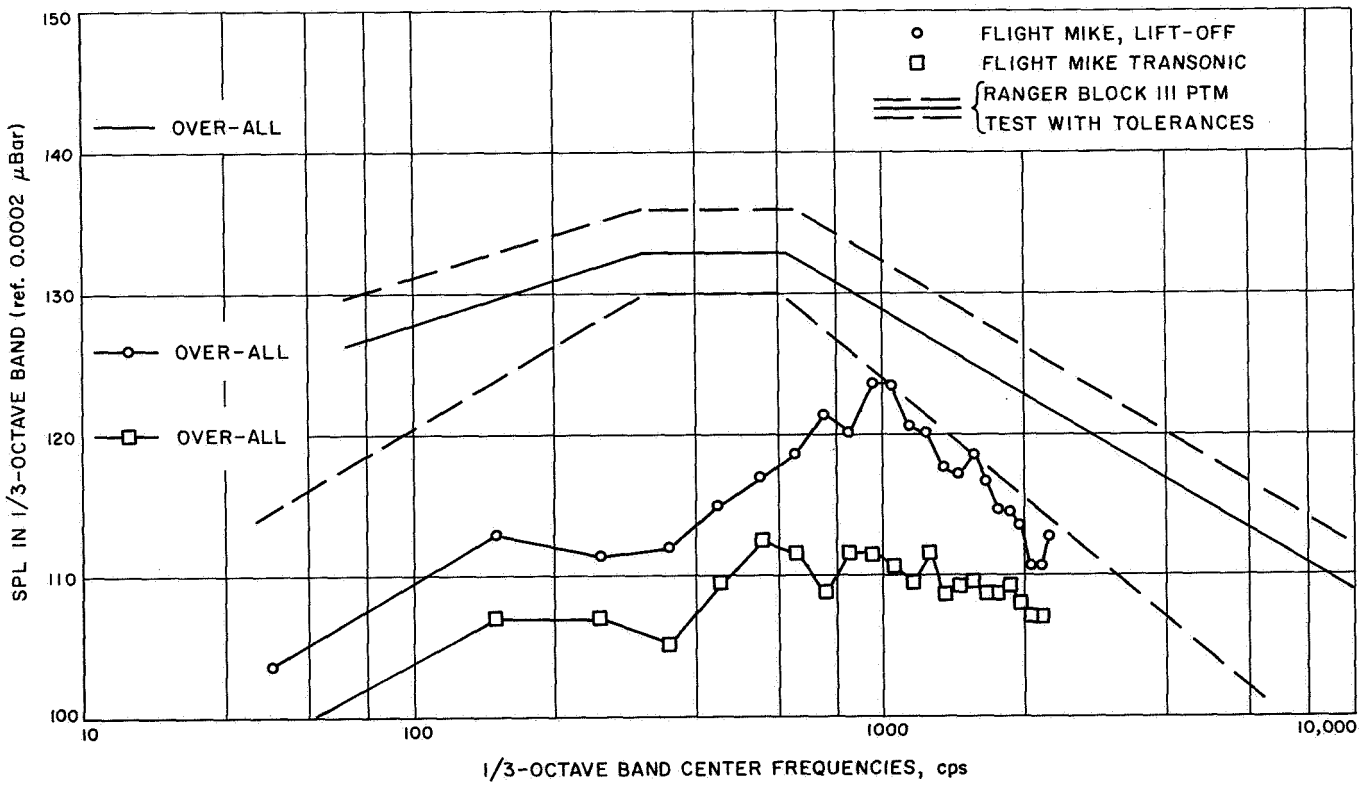


**Fig. 78. Internal acoustic-pressure data at lift-off in 1/3-octave bands compared with reverberant chamber test levels**

Figure 78 also shows the internal-acoustic field at transonic flight to be at a lower level than that at lift-off. The over-all SPL at lift-off is 126 db, which is 6 db higher than the over-all level of 120 db found at transonic flight. This difference runs counter to the vibration measurement; as discussed in Section V, the measured over-all vibration at lift-off is significantly lower than at transonic flight for both *RA 1–4* and *RA-6*. This fact tends to support the assumption that the source of vibration at the transonic period is aerodynamic buffeting resulting from flow separation at the start of area reduction, and is, therefore, localized to the adapter and a portion of the forward part of the *Agena*. Therefore, although the local external-sound field at the adapter near the flight accelerometer is higher at transonic flight than at lift-off (as evidenced by the vibration data), the difference in transmission characteristics caused by the more localized sound field results in a lower internal SPL at transonic flight than at lift-off.

### 2. Umbilical-Tower Microphone Data

The 100-cps spectral analyses of the umbilical-tower data (Figs. 67 and 68) were replotted as 1/3-octave SPL plots in Fig. 79. For comparison, a pre-flight estimate (Ref. 2) of the external-sound field and of the measured internal-sound field at lift-off (Fig. 78) is also shown. The measured sound field is significantly lower than the estimate. This may only partially be accounted for by the closer proximity of the spacecraft to the noise source. A

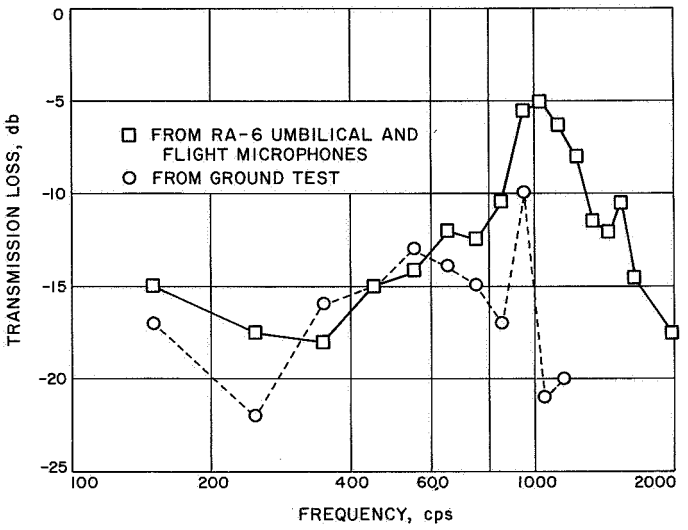


**Fig. 80. Ratio of internal to external sound pressure at lift-off compared with a ground test**

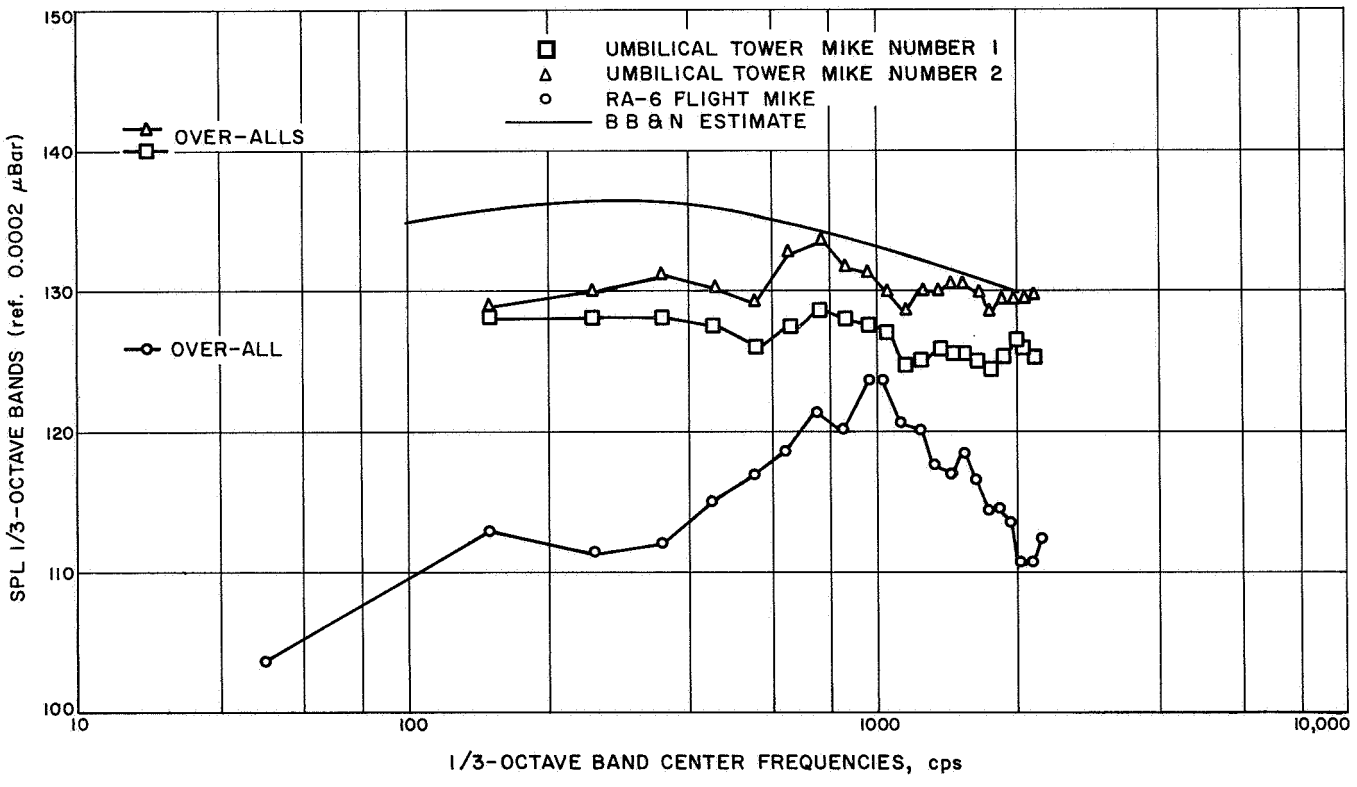


**Fig. 79. Umbilical-tower microphone data at lift-off in 1/3-octave bands**

ratio of the measured internal-sound field from the flight measurement to the umbilical-tower measurement would represent a measure of the shroud transmissibility. Figure 80 is the ratio of the internal-sound field at lift-off to the average of the two umbilical-tower measurements of the external-sound field. Shown for comparison is a transmissibility curve measured from ground acoustic tests. There is fair agreement up to about 750 cps; above this, the transmissibility from *RA-6* flight is lower than the ground test.

# VI. CONCLUSIONS

Final evaluation of the *RA-6* flight data shows that the dynamic environment was within nominal limits. The flight vibration levels were within predicted statistical limits based on previous flight data. Also, the vibration levels were within test-specification levels for both low-frequency periodic motion and for wide-band random motion.

## A. Wide-Band Vibration

Power spectral density analysis of Channel 17 data (wide-band, radial) at launch and at the transonic period shows a significantly higher level (8.2 $g_{rms}$ at transonic flight) than previously observed. Post-flight investigation showed that changes in the accelerometer mounting block and mounting-block locations on *RA-6* were a primary contributor to the increased measured levels. Acoustic tests utilizing both the old and the new mounting systems indicated that the new mounting system was more susceptible to acoustic excitation in the 600–1,000-cps range. It was in this frequency range that flight levels appeared to be significantly higher on *RA-6*. Utilizing an empirically derived correction factor, the *RA-6* measurement was adjusted for comparison with previous flight measurements. Such adjustment brought the observed levels within the 95-percentile levels predicted from previous flight data, therefore showing reasonable statistical agreement with the previous flights. It is concluded that actual vibration levels experienced by the spacecraft at the launch and the transonic periods may not have been higher than on previous flights; although the post-flight empirically determined correction may only be used to bring the data within 95-percentile limits of the *RA 1–4* flights. It is believed that an exact correction factor, if obtainable, would bring the *RA-6* data much closer to the previous flight data. All other measurements which are considered valid indications of the dynamic environment were within the bounds established by previous flight data. That is, where direct comparison can be made to previous flights, the *RA-6* vibration levels were below previously observed maxima. It is also concluded that the spacecraft had been adequately tested to withstand the observed dynamic environment.

## B. TV Subsystem Turn-On

An event of considerable investigation was the turn-on of Channel-8 power during booster engine jettison. Oscillograph records of all vibration channels (Figs. 33 and 34) show nominal transient-vibration levels during booster jettison, and no indication of any dynamic event at Channel-8 turn-off.

A post-flight investigation of vibration effects on *Ranger* Block III command-decoder relays showed that observed flight-vibration levels could not be independently responsible for any relay closure causing actuation of the TV subsystem.

## C. BECO Transient

The characteristic torsional oscillation was observed on the *RA-6* flight; however, the levels were lower than previously observed. Instrumentation on the booster verified that the source of the motion was thrust oscillation during booster shut-down. The low level of torsional motion might possibly be attributed to a small degree of coupling between longitudinal vibration and torsional

vibration, or to the presence of a torsional node near the flight-instrumentation location. The latter topic is presently under further investigation.

### D. Acoustic Measurements

Both internal spacecraft measurements and external umbilical-tower measurements were lower than expected. The ratio of these internal and external measurements showed reasonable agreement with ground tests. The measured acoustic-pressure levels within the spacecraft at transonic flight were 6 db lower than those at lift-off. Coupled with the vibration measurement (higher at transonic flight than at lift-off), this phenomenon could be explained by the localized pseudo-sound field caused by buffet.

## REFERENCES

1. Lockheed Missiles and Space Company, *LMSC Final Calibration Report for Vehicle 6008*, LMSC/657744, Sunnyvale, California.

2. Bolt, Beranek & Newman, Inc., *Noise and Noise-Induced Structural Vibration of the Ranger Spacecraft*, BBN Report No. 1038, Cambridge, Massachusetts, December 20, 1963.

3. General Dynamics/Astronautics, *Atlas Space Launch Vehicle Flight Test Evaluation Report 199D*, Report No. GDA/BKF64-002, San Diego, California. Prepared by SLV Test Evaluation Group under Contract AF 04(694)-196, March 30, 1964. SECRET.